Evaluation of the Reliability of Nondestructive Ultrasonic Inspection Methods for the Detection and the Characterization of Defects in Hydroelectric Turbine Welded Joints

by

Hamid HABIBZADEH BOUKANI

MANUSCRIPT-BASED THESIS PRESENTED TO ÉCOLE DE TECHNOLOGIE SUPÉRIEURE IN PARTIAL FULFILLMENT FOR THE DEGREE OF DOCTOR OF PHILOSOPHY
Ph.D.

MONTREAL, MARCH 15TH, 2018

ÉCOLE DE TECHNOLOGIE SUPÉRIEURE
UNIVERSITÉ DU QUÉBEC

BOARD OF EXAMINERS

THIS THESIS HAS BEEN EVALUATED

BY THE FOLLOWING BOARD OF EXAMINERS

Mr. Martin Viens, Thesis Supervisor
Departement of Mechanical Engineering at École de technologie supérieure

Mr. Souheil-Antoine Tahan, Thesis Co-supervisor
Departement of Mechanical Engineering at École de technologie supérieure

Mr. Michel Rioux, Chair, Board of Examiners
Departement of Automated Manufacturing Engineering at École de technologie supérieure

Mr. Mohammad Jahazi, Member of the jury
Departement of Mechanical Engineering at École de technologie supérieure

Mr. Denis Thibault, External Evaluator
Research Institute of Hydro-Quebec (IREQ)

Mr. André Moreau, External Evaluator
National Research Council Canada (NRC)

THIS THESIS WAS PRENSENTED AND DEFENDED

IN THE PRESENCE OF A BOARD OF EXAMINERS AND THE PUBLIC

ON MARCH 02ND, 2018

AT ÉCOLE DE TECHNOLOGIE SUPÉRIEURE

ACKNOWLEDGMENTS

After a period of several years, today is the day to write this appreciation to finish the writing of my thesis. It has been an intense period of learning during which I developed and improved my scientific and personal capabilities. Pursuing my PhD studies has had a big impact on me and my life. This impact reflects on the people who have significantly helped and supported me.

First and foremost, I wish to thank my advisor, Professor Martin Viens, for giving me moral support and intellectual freedom throughout my PhD studies, supporting my attendance at several conferences and scientific events, and helping me in generating and developing new ideas. My graduate experience was also enriched by the opportunity that he offered me to work as a teaching assistant.

I would like to express my sincere gratitude to my co-advisor, Prof. Antoine Tahan, for all his scientific contributions and financial support to make my PhD experience productive. His trust, guidance and patience throughout the course of this thesis are greatly appreciated. Undoubtedly, he is and will be one of the most influential people in my professional life.

I would like to extend my special thanks to Dr. Martin Gagnon for his great contribution to this project. He is definitely a great professional mentor who taught me how to choose the right tools and direction in order to successfully complete my thesis. Whenever I felt disappointed during my PhD pursuit, his enthusiasm for the research turned it into motivation and drive to go forward. This project could not have progressed without his considerable collaboration.

Additionally, I would like to thank my thesis committee members Professor Mohammad Jahazi, Professor Michel Rioux, Dr. André Moreau and Dr. Denis Thibault for taking the time to read my thesis and offering their insightful comments, suggestions, and encouragement.

I am extremely grateful to the Natural Sciences and Engineering Research Council of Canada (NSERC), Fonds de recherche du Québec - Nature et technologies (FRQNT), ANDRITZ Hydro Ltd., Institut de recherche d'Hydro-Québec (IREQ), the MITACS accelerate program, and École de technologie supérieure (ÉTS) for providing me with the funding sources that allowed me to pursue my graduate studies. I would particularly like to single out ANDRITZ Hydro Ltd. and IREQ for their excellent cooperation and for giving me the opportunity to do internships at their facilities and to benefit from their technical supports.

I am thankful for the help and support of fellow lab-mates and collaborators in every step of this thesis. I had the opportunity to work on some phases of my thesis with Dr. Demartonne Ramos França who helped me with his great ability to express the most complicated ideas in easy words. In regards to the experimental phase of this project, I wish to thank Mario Corbin and the IREQ's staff for providing me with technical support and trainings. I am especially grateful for the conversations with Stéphane Godin and his constructive suggestions as I was working on the effect of reformed austenite. The initial inspections of this project would not have been possible without the help of Vincent Houle and his colleagues at Les Inspections Atlas Quebec Inc. In the very first steps of this thesis, I had the opportunity to do my internship under the supervision of Mr. André Coutu who helped me to improve my understanding of professionalism.

I would like to thank all my friends who made my good times better and my hard times easier throughout my studies at ÉTS. I would like to address my special thanks to my office mate, Ehsan Mohseni, who has been an amazing friend since the very first moments we started working together.

Finally, I would like express my very special thanks and appreciation to my family for all the support and love they offered: first and foremost to my great parents, Nahid and Saeid, who brought me up with a passion for learning and backed me up in every stage of my life; to my brothers, Vahid and Navid, for being so inspirational and encouraging; and to my devoted,

supportive, and patient wife, Sorour, who has been a wonderful friend and companion throughout this journey.

Hamid Habibzadeh Boukani

ÉVALUATION DE LA FIABILITÉ DES MÉTHODES DE CONTRÔLE NON DESTRUCTIVES PAR ULTRASONS POUR LA DÉTECTION ET LA CARACTÉRISATION DE DÉFAUTS DANS DES JOINTS SOUDÉS DE TURBINES HYDROÉLECTRIQUES

Hamid HABIBZADEH BOUKANI

RÉSUMÉ

Dans un environnement industriel compétitif, les fabricants tentent en permanence d'optimiser leurs processus de production et de bénéficier de leurs installations aussi efficacement que possible. Leurs efforts se concentrent sur la maximisation de l'efficacité globale des équipements de production et leur durée de vie. Par ailleurs, dans le domaine de la production d'électricité, la demande croissante pousse les producteurs à prolonger l'utilisation de leurs installations de production et à éviter les arrêts inutiles dus à des défaillances prématurées. Dans les centrales hydroélectriques, où les roues de turbine tournent sous des charges variables et cycliques, la fatigue est l'un des principaux processus de dégradation qui limitent la durée de vie des équipements de production. Par conséquent, l'utilisation de modèles (basés sur la mécanique de la rupture) pour estimer la durée de vie de ces équipements est de plus en plus populaire. Puisque les arrêts de production causés par des défaillances prématurées ou le remplacement inutile de composants de production majeurs sont assez coûteux en termes de temps et d'argent, il est essentiel d'estimer précisément leur durée de vie résiduelle.

Dans les cas qui nous intéressent, la durée de vie d'un composant est basée sur l'approche de la tolérance aux dommages dans lequel la durée de vie déclarée est une fraction du nombre de cycles qui, suivant des modèles basés sur la mécanique de la rupture, sont nécessaires pour propager une fissure à partir d'une taille initiale déterminée par inspection (ou par le seuil de détection) jusqu'à la rupture. En conséquence, la dimension des défauts existants dans la structure est l'une des principales entrées de ces modèles. Cette entrée est généralement caractérisée en utilisant les résultats des essais non destructifs (END) qui, par conséquent, doivent être fiables afin d'avoir une image factuelle de l'intégrité des composants. Dans ce contexte, il est crucial d'avoir des connaissances détaillées sur les défauts qui se produisent fréquemment, ainsi que sur les propriétés des matériaux inspectés car ceux-ci affectent l'efficacité et la fiabilité des essais non destructifs utilisés.

Dans ce projet de recherche, nous allons d'abord étudier en profondeur les propriétés acoustiques des matériaux les plus fréquemment utilisés pour les roues de turbine. En effet, le contrôle par ultrasons est la méthode END la plus couramment utilisée pour l'inspection pour les défauts internes de telles roues. Dans la seconde étape, l'effet de traitements thermiques sur les propriétés acoustiques de l'acier inoxydable martensitique, un des matériaux les plus largement utilisés pour la fabrication des roues, est évalué. Enfin, une évaluation des caractéristiques des défauts communément détectés dans les joints soudés des roues est réalisée. Le résultat de cette recherche pourrait être utilisé pour étudier la probabilité

d'occurrence (POO) et la probabilité de détection (POD) des défauts de soudage lors de l'inspection des joints des roues de turbine.

Mots-clés: essais non destructifs (END), fiabilité d'une inspection, évaluation non destructive quantitative (QNDE), probabilité de détection (POD), inspection ultrasonore (UT), modélisation et simulation des UTs, défauts, fissures, turbine hydroélectrique.

EVALUATION OF THE RELIABILITY OF NONDESTRUCTIVE ULTRASONIC INSPECTION METHODS FOR DETECTION AND CHARACTERIZATION OF DEFECTS IN HYDROELECTRIC TURBINE WELDED JOINTS

Hamid HABIBZADEH BOUKANI

ABSTRACT

Due to the competitive environment of the industrial world, manufacturers continuously try to optimize their production processes and to benefit their facilities as efficiently as possible. Their efforts concentrate on maximizing the overall effectiveness of production equipment and their service life. As an example, in the electricity generation field, the growing need for electricity pushes producers to extend the use of their production facility and to avoid unnecessary downtime due to premature failures. In hydroelectric power plants, where turbine runners spin under cyclically varying loads, the fatigue phenomenon is one of the main degradation processes limiting the service life of generation equipment. Therefore, the use of fracture mechanics based models to estimate the fatigue life of this equipment is increasingly growing. Since unplanned production halts due to premature failure or unnecessary replacement of major production parts is fairly costly in terms of time and money, it is essential to more precisely specify their estimated fatigue life.

In our case of interest, the life of a part is based on damage tolerance approach in which a fraction of the number of cycles that, based on fracture mechanics, are required to grow a crack from an initial size determined by inspection (or by the detection threshold) to failure. Accordingly, the dimension of existing flaws in the structure is one of the main inputs of these models. This input is generally characterized using the results of nondestructive testing (NDT) methods which, therefore, should be reliable in order to have a factual picture of the integrity of components. In this context, it is crucial to have detailed knowledge on the commonly occurring flaws as well as on the inspected material properties because they impact NDT efficiency and reliability.

In the proposed research, we will first try to thoroughly study the acoustic properties of the most frequently used materials in turbine runners. Indeed, ultrasonic testing is the most widely used NDT method for runner inspection for internal flaws. In the second step, the effect of heat treatment on the acoustic properties of martensitic stainless steel, one of the most extensively used steel grades for runner manufacturing, is assessed. Finally, an evaluation of the characteristics of flaws commonly detected in the welded joints of runners is carried out. The outcome of this research could be employed for studying the probability of occurrence (POO) and the probability of detection (POD) of welding flaws while inspecting turbine runner joints.

Keywords: Nondestructive testing (NDT), Inspection reliability, Quantitative nondestructive evaluation (QNDE), Probability of detection (POD), Ultrasonic inspection (UT), UT modelling and simulation, Defects, Cracks, Hydroelectric turbine runner.

TABLE OF CONTENTS

Page

LIST OF TABLES

Page

LIST OF FIGURES

Page

LIST OF ABREVIATIONS

AP	Application Parameters
AISI	American Iron and Steel Institute
ASTM	American Society for Testing and Materials
BCC	Body-Centered Cubic
BCT	Body-Centered Tetragonal
CT	Computed Tomography
EDS	Energy Dispersive X-ray Spectroscopy
FCAW	Flux-Cored Arc Welding
FSH	Full Screen Height
GDS	Glow Discharge Spectroscopy
GMAW	Gas-Metal Arc Welding
HF	Human and Environmental Factors
HT HAZ	High Temperature Heat Affected Zone
IREQ	Institut de Recherche d'Hydro-Québec
LEFM	Linear Elastic Fracture Mechanics
LOP	Lack of Penetration
MPI	Magnetic Particles Inspection
NDT	Nondestructive Testing
OM	Optical Microscopy
PA	Phased-Array
PAUT	Phased-Array Ultrasonic Testing
POD	Probability of Detection

POFI	Probability of False Indication
POO	Probability of Occurrence
QNDE	Quantitative Nondestructive Evaluation
RMS	Root Mean Square
SAE	Society of Automotive Engineers
SAFT	Synthetic Aperture Focusing Technique
SDH	Side Drilled Hole
SEM	Scanning Electron Microscopy
SMAW	Shielded-Metal Arc Welding
SNR	Signal-to-Noise Ratio
SOV	Separation of Variables
STD	Standard Deviation
TOF	Time of Flight
UNS	Unified Numbering System
UT	Ultrasonic Testing
XRD	X-ray Diffraction

LIST OF SYMBOLS AND UNITS OF MEASUREMENTS

α	Ultrasonic Attenuation Coefficient
β_0 , β_1	Linear Regression Coefficients in $\hat{a}$ vs. a Correlation
δ	Random Error of Linear Regression of $\hat{a}$ vs. a
$\Phi(x)$	Cumulative Distribution Function of Random Variable x
γ	Austenite
$\mu(a)$	Mean Value of Signal Amplitude for Flaw Size of a
ρ	Density
σ	Standard Deviation of Error of Linear Regression (δ)
a	Flaw Size
a_{50}	Flaw Size Having 50% Probability of Detection
$a_{90/95}$	Flaw Size Having 90% Probability of Detection in 95% POD Experiments
$\hat{a}$	Signal Amplitude
$\hat{a}_{decision}$	Decision Threshold
A_1	Signal amplitude in S41500
A_2	Signal Amplitude in A27
Ac_1	Austenitic Start Transformation Temperature During Heating
dB	Decibel
HV	Hardness Vickers
HRC	Rockwell C Hardness
M	Martensite

N_1	Backscattering Noise Level in S41500
N_2	Backscattering Noise Level in A27
R	Reflection Coefficient
R_a	Roughness Average (Arithmetic Average)
T	Transmission Coefficient
V	Ultrasonic Wave Velocity
V_L	Longitudinal Wave Velocity
W_1	Standard Deviation of Backscattering Noise Distribution in S41500
W_2	Standard Deviation of Backscattering Noise Distribution in A27
wt%	Percentage by Weight

INTRODUCTION

Problem statement

As the civilian infrastructure, the transportation equipment and the military platforms remain in-service for longer times, application of reliable inspection methods are becoming increasingly necessary (Achenbach, 2000). Some of these structures are designed to remain in service for a long period of time without any plan to be replaced. This long service life is fulfilled only if appropriate actions are considered so that any performance and safety issues as well as increasingly costly repairs are prevented. In order to extend the life expectancy of these aging industrial structures, critical defects should be detected and characterized before catastrophic failures occur; a process which involves several technical challenges (Achenbach, 2000). When structural systems are in service, defects develop in the material; their propagation rate is governed by fatigue, corrosion, or other deterioration mechanisms. Fatigue is the dominant degrading mechanism for steel components working below 650°C (Boyd-Lee, Harrison, & Henderson, 2001). Since all defects with various situations, dimensions, and orientations do not show the same tendency to propagate and degrade the material under the service conditions, allowable limits for defects should be determined. These limits are specified by studies of material behaviour and fracture analysis. Nondestructive testing (NDT) methods, whose results are among the essential parameters for degradation mechanism monitorings, play a significant role in characterizing the imperfections and discontinuities present in the material.

Therefore, the NDT outcome, including detection and sizing of flaws, should be reliable enough to be used as the base of decisions leading us to keep a component in service for a specified time without encountering risks. Quantitative Nondestructive Evaluation (QNDE) methods provide us with tools to know how reliable the results of a specific NDT technique are and how close the technique pictures the conditions of the component.

Hydro-Québec, one of the largest hydroelectric producers in the world, is in its seventh decade of life. As the structures and facilities of this company (such as hydroelectric turbines) are getting older, efforts are increased to keep them in a reliable condition and to extend their life (Thibault, Gagnon, & Godin, 2014). This is important since an unexpected failure is accompanied with costly and time-consuming electricity production halts and maintenance process. In the current study, the focus is on the Francis turbine runners employed at the Beauharnois hydroelectric station. As shown in Figure 0.1 and Figure 0.2, Francis runners are spinning wheels with fixed blades welded on their top and bottom ends to the crown and band, respectively. The flow of water with large kinetic energy is directed toward these blades and makes the runner spin which consequently leads to the rotation of the turbine shaft and the coupled rotor. The loading condition of these blades resembles a beam which is fixed at both ends. The force applied by the water flow is accompanied by the reaction forces and torques in the joints. The cyclic nature of the forces causes in-service defects to develop through fatigue in highly stressed areas. According to some previous researches (Coutu, Proulx, Coulson, & Demers, 2004; Huth, 2005), the transitional welded areas between the blade and band or crown are identified as the critical areas of stress concentration for high head Francis runners. Huth also indicates that once the runner is put in service, fatigue cracks start propagating from flaws and inclusion which were not undetected. Therefore in order to estimate the fatigue life of these runners, a model has been developed by the Institut de recherche d'Hydro-Québec (IREQ). This model is based on the Kitagawa diagram which requires several inputs including the characteristics of flaws in the structure (Gagnon, Tahan, Bocher, & Thibault, 2014).

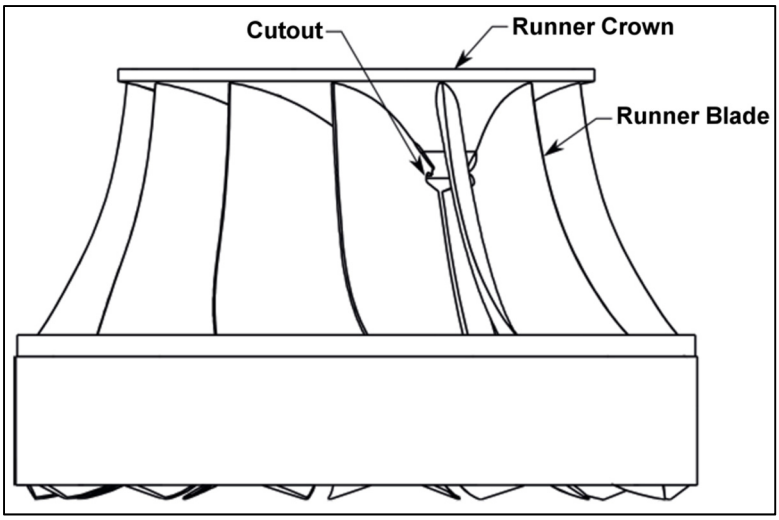

Figure 0.1 Overall overview of Francis turbine runner
Taken from Gagnon *et al*. (2013)

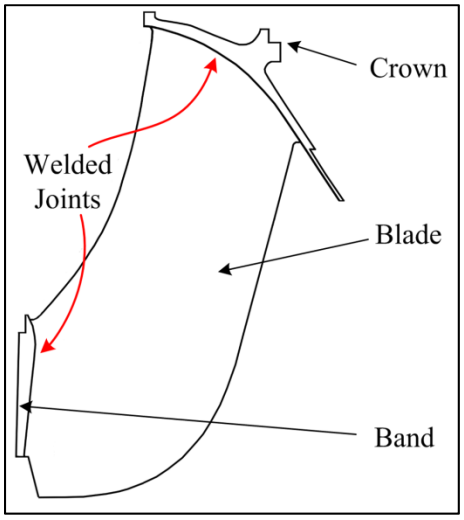

Figure 0.2 Schematic of the runner blade

The aforementioned facts highlights the importance of using highly reliable NDT techniques possessing more precise detection capability which provides us with more realistic description of the flaws as well as lower uncertainty in sizing and characterizing them. Therefore, quantitative measures are required to make comparisons among different NDT methods and to select the best one for the current application.

The process of creation of these quantitative means requires establishing a reasonable combination of modelling and practical approaches to make a trade-off between costs and quality of the results. In order to obtain results which best represent the reality, efforts should be focused on designing and simulating the required tests that closely mimic those that could be performed on real runner's welded joints. To this end, the properties of the materials used for runner production as well as the characteristics and the origin of the most regularly occurring welding defects should be identified. In addition, the capability of the currently used NDT methods as well as their limitations should be known.

Research objectives

The final objective of the project is to obtain precise fatigue life estimations for Francis turbine runners in order to avoid either premature failure or production halts for unnecessary maintenance. This research, as a part of a large project, sheds light on the detection and the characterization of flaws in the welded joints of hydroelectric turbine runners as they are located in the most critical zones in terms of fatigue failure. In fact, loading conditions and fatigue related material properties, as two inputs of life estimation models, have been previously studied in details (Gagnon *et al.*, 2014; Gagnon, Tahan, Bocher, & Thibault, 2010; Gagnon, Tahan, Bocher, & Thibault, 2012b; Thibault, Bocher, Thomas, Gharghouri, & Côté, 2010; Thibault *et al.*, 2014) while the flaw characteristics, as the third input, are still fed into the developed models as assumptive values (Gagnon, Tahan, Bocher, & Thibault, 2012a; Gagnon *et al.*, 2014). On the other hand, the loading conditions could be measured using industrial methods (e.g. strain gauges) while the runner is in service (Arpin-Pont, Gagnon, Tahan, Coutu, & Thibault, 2012; Gagnon, Tahan, & Coutu, 2009) and furthermore the material properties could be evaluated using small scale laboratory experiments. However, there is no industrial solution for characterizing the existing flaws in the runners; in other words, costly electricity production halts and subsequent inspections processes should be followed to assess the characteristics of existing flaws. Even worse, the materials should undergo destructive processes in order to confirm the validity of the inspections as well as the characteristics of existing flaws. Moreover, there is no quantitative measure

defining the reliability of different NDT methods applied on hydraulic runner joints in the industry. By focusing on the welding flaw characteristics and detectability, we are facing the following questions:

- What are the most expected flaw characteristics in the critical welded joints of Francis runners?
- What are the best NDT methods to detect and characterize these flaws?
- What are the inconsistencies of the currently used NDT methods?
- How reliable are the recommended NDTs?

In order to answer the preceding questions, some preliminary steps should be taken. First, it is necessary to find and compare the material properties affecting the outcome of the currently used ultrasonic testing (UT). In this context, the ASTM (American Society for Testing and Materials) A27 and CA6NM steel grades which are the two commonly used steels for hydraulic runner production are investigated in terms of their acoustic properties. Note that, in order to remove the effect of casting defects from ultrasonic measurements, UNS (Unified Numbering System) S41500, the rolled version of CA6NM steel, is considered throughout this work rather than its cast version. Thus, a qualitative comparison between the capabilities of UT of these two steels could be made. In addition, the required parameters for modelling the ultrasonic inspection of these two grades are obtained.

Second, a more detailed study on the variation of acoustic properties of 13Cr-4Ni material, UNS (Unified numbering system) S41500, caused by different tempering heat treatments is carried out. This step is required to find out how the reformed austenite content in the microstructure of this martensitic stainless steel influences the ultrasonic wave attenuation and signal-to-noise ratio (SNR) which are the main parameters of an ultrasonic inspection. Moreover, this will be helpful for future model-based studies of ultrasonic inspection where the acoustic properties of materials are among the critical inputs.

Third, it is essential to identify the flaws most likely occurring in the runner joints due to the fact that several principal factors of inspection reliability are affected by the flaws'

characteristics (nature, location, size, orientation, geometry, …). First of all, by determining these characteristics, chances will be higher to diagnose the manufacturing process and remove the deficiencies causing the formation of such flaws. In addition, the shortcomings and the blind zones of the currently applied NDT methods in the detection of such flaws will be recognized. Furthermore based on the capabilities of available NDT methods, the inspection techniques and parameters best suited for detection of these common characteristics will be determined.

Finally by employing the characteristics of the real welding flaws, the capability of different NDT methods could be more accurately modelled and then quantitatively compared for this specific application. Hence, characterizing the common welding flaws and the properties of frequently used materials will provide the required data for evaluating the reliability of the applied and recommended NDT methods for runner joint inspection.

State of the art

In this research, the specimens are produced according to the real manufacturing procedure. The advantage is that the thickness of the joint components is selected to be in the same scale as the most critical part of real runners. Moreover after being tested by several commercially available NDT methods, the joints are sliced and subsequently the slices undergo a new set of destructive and nondestructive evaluations to check the integrity of the joint and to characterize any significant welding flaw present in the slices. Next, a point by point comparison is realized between the slices and the outcome of some of the used NDT methods in order to find out how appropriate they detect, picture and characterize the principal anomalies in the welded joints. This large-scale study connecting the real flaws' characteristics with the outcome of different NDT methods and evaluating the capability of phased-array ultrasonic testing (PAUT) method on real components is one of the first researches of this type in the hydroelectricity industry. On the other hand, this research is the first of its kind trying (a) to study the acoustic properties of martensitic stainless steels and (b) to detect and characterize the most common welding flaws in Francis runner joints in

terms of type, size, geometry, and position. The latter will be useful to find out if the welding flaws are located either in the covered or in the blind zone of the applied NDT methods. This information will help to determine if in the fatigue life estimation models, the flaw size input should be determined by using either the probability of detection (POD) data - where the flaw's position is covered - or the probability of occurrence (POO) data - where the flaw is located in the inspection blind zone. Last but not least, in the literature the effect of heat treatment on the acoustic properties of materials have always been evaluated at rather high frequencies and mostly in terms of metallurgical effects but this research looks into the impact of heat treatment on the inspection outcome.

Thesis structure

The thesis content is structured in 4 chapters. The first chapter reviews the related researches previously published in the literature. In chapters 2 and 3, the effect of microstructure of commonly used materials for runner production and the influence of tempering heat treatment on the parameters of ultrasonic inspection is evaluated. The final chapter provides an assessment on the detection capability of different NDT methods and also a destructive process for the characterization of common welding flaws in hydraulic runner joints. As represented in Figure 0.3, each chapter is dedicated to answering one of the following questions:

- Chapter 2: How do the different microstructures of the mostly used steel grades in runner production, ASTM A27 and UNS S41500, affect the ultrasonic inspection?
- Chapter 3: What is the effect of tempering heat treatment on the acoustic properties of UNS S41500 martensitic steel and on the resulting POD of ultrasonic inspection?
- Chapter 4: How are different NDT methods compared in terms of detecting welding flaws in runner joints? What are the most common welding flaws in runners?

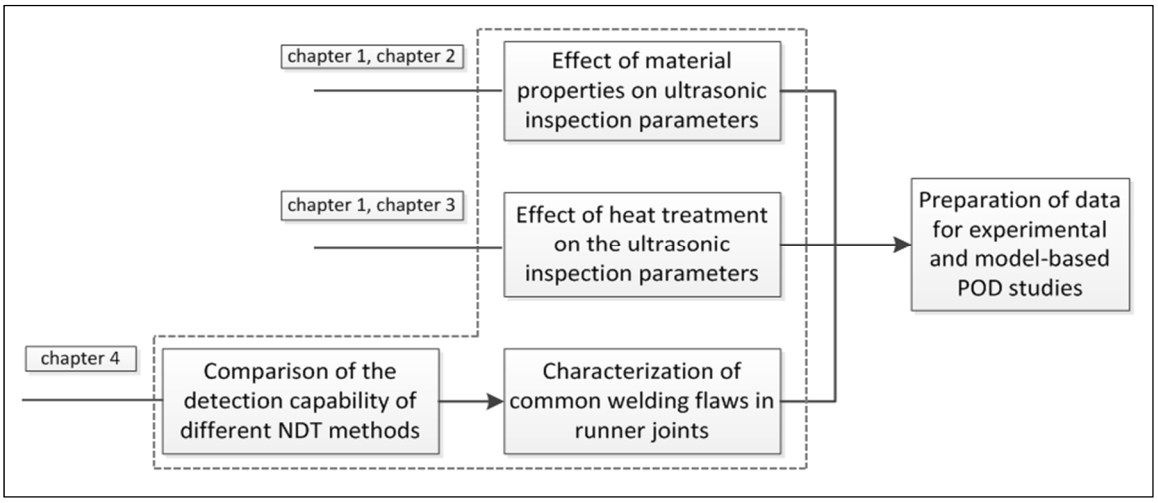

Figure 0.3 Required steps to prepare the data for POD studies and thesis structure

CHAPTER 1

LITERATURE REVIEW

1.1 Introduction

As the civilian infrastructure, transportation equipment, power generation facilities and military platforms remain in-service for longer times, application of reliable inspection methods becomes increasingly necessary (Achenbach, 2000). Some of these structures are not expected to be replaced in a near future; therefore, we have to keep these aging systems functional for several years. This is fulfilled only if appropriate actions are considered so that any performance and safety issues as well as increasingly costly repairs are prevented. We have to detect and characterize defects before failures occur in order to extend the life expectancy of industrial structures; a process which involves technical challenges (Achenbach, 2000).

Operating conditions of in service structural systems causes defects to develop and propagate in the material. The propagation rate of these defects could be estimated according to the effect of fatigue, corrosion, and other deterioration mechanisms. Fatigue is the dominant degrading mechanism for steel components working below 650°C (Boyd-Lee *et al.*, 2001). Since all defects, with various situations, dimensions and orientations, do not show the same tendency to propagate and degrade the material under the service conditions, allowable limits are specified by studies of material behaviour and fracture modes. In these studies, it is assumed that materials fail due to either the initiation and growth of cracks under cyclic loading or the propagation of cracks from existing flaws in the material (Boyd-Lee *et al.*, 2001). The theoretical life of a component is finished when the crack propagates and a critical crack dimension is reached after a number of fatigue cycles (Hakl, Bielak, & Vlasák, 2001). This critical size of fatigue crack is a function of the material and the stress field (Bray & Stanley, 1997; Suresh, 1998).

Damage tolerance approach is one of the fracture mechanics based approaches to estimate the remaining life of critical structures. Hydro-Québec has selected this approach to predict the effects of fatigue damage on the lifetime of hydroelectric turbine runners (Sabourin, Thibault, Bouffard, & Levesque, 2010). In this approach, it is assumed that all components, even the new ones, contain some form of initial flaws. Therefore, the service life of a component is considered to be equal to the time taken for a proven NDT detection size to grow to the critical size (Boyd-Lee *et al.*, 2001). Fracture mechanics experts, in their life estimation models, face three types of uncertainty (material properties, stress field condition, and flaw detection and sizing capability of the inspection system) upon which life assessment calculations are converted into a probabilistic process (Ginzel, Thomson, & Ginzel, 2011; Thibault *et al.*, 2014). Probabilistic failure assessment is considered to be an N-dimensional random vector in which the defect size uncertainty is the most critical parameter (Gagnon *et al.*, 2014; Gagnon *et al.*, 2012b). In such assessment, it is recommended that the defect size is characterized as a random variable possessing a typical probability distribution for a particular NDT method (Altamura & Beretta, 2012; Bagaviev & Ulbrich, 2004).

NDT methods refer to all evaluation techniques which do not alter mechanical and, usually, physical properties of components; besides, they do not affect the future application of the parts. The application of NDT methods in different industries has been increasing as a reliable means of post-manufacturing quality control, structural health monitoring and in-service maintenance. These methods are supposed to detect mechanical and physical discontinuities in materials and make intelligible indications of them. Due to the fact that hydraulic turbine runners are generally inspected using different techniques of ultrasonic inspection method (Habibzadeh Boukani, Viens, Tahan, & Gagnon, 2014; Katchadjian, 2004), the principal focus of this study will be on the UT.

As mentioned earlier, a proven NDT detection size is typically used in the life estimation (damage tolerance) calculations as the initial crack size. Generally, this initial value is considered to be a size of flaw that is almost always detected using a particular NDT method. In order to characterize this size, quantitative studies are carried out on the reliability of the

applied NDT methods leading to the generation of probability of detection (POD) curves. POD is usually expressed as a function of flaw size (length or height) but, in reality, it is a function of more: factors related to the material (microstructure, geometry), to the flaw itself (flaw type, orientation, shape, and density), and to the inspection system (NDT method, testing conditions, and NDT personnel) (Georgiou, 2006; Jenson, Mahaut, Calmon, & Poidevin, 2010; Matzkanin & Yolken, 2001; Wang, 2006). Therefore, repeated inspections on the same flaw sizes and types may not lead to consistent indications; the inconsistency of indications is due to the uncertainty introduced in inspection outcome as a result of ignoring the factors other than flaw size. The statistical approaches, used to create POD curves, characterize this uncertainty and variability. As compared to the other parts of the Retirement for Cause/Damage Tolerance approach, obtaining and characterizing POD curves has been less investigated in the literature (Tryon, Cruse, & Mahadevan, 1996). As shown in Figure 1.1(a), there is an area of uncertainty occurring between the smallest detectable flaw size (where POD rises from zero) and the largest missed flaw size (where POD reaches unity); this uncertainty is referred to the confidence level. As an example, one of the most important output of POD curves is the $a_{90/95}$ value which is a flaw size having 90 percent probability of detection in 95 percent of the POD evaluations. In case, there is no POD data for a given inspection condition, the resolution of the flaw detection technique replaces $a_{90/95}$ in the fatigue life assessment and accordingly more uncertainty is incorporated in the calculations.

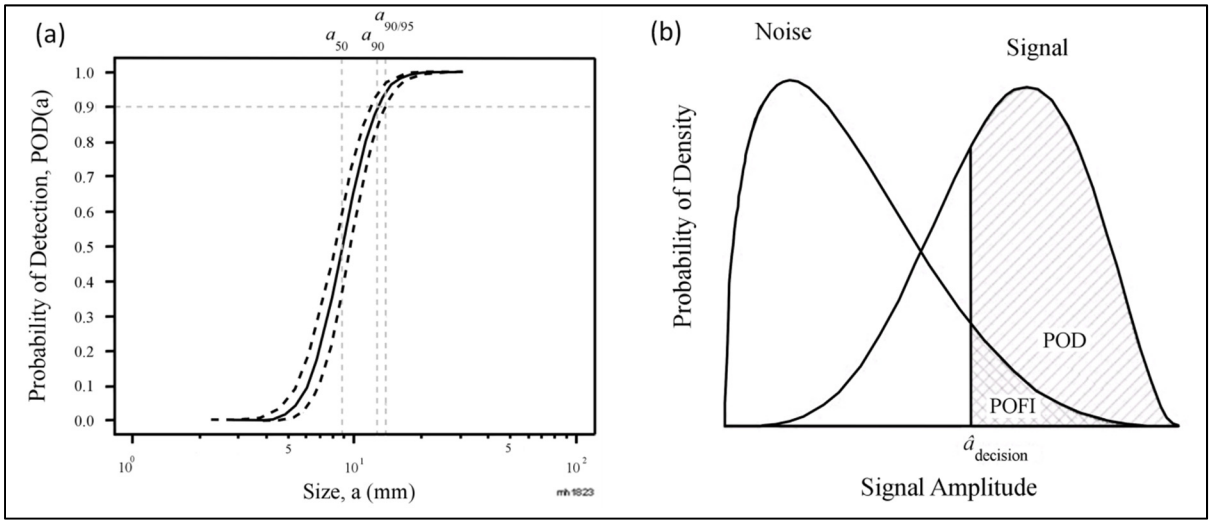

Figure 1.1 (a) POD curve and 95% confidence bounds of signal response data; (b) relation of POD and POFI with the noise and signal probability densities
Adapted from Annis (2009)

As depicted in Figure 1.1(b), POD value for a fixed flaw size depends on the probability distribution of the received signal from this particular flaw size as well as the amplitude of the decision threshold ($\hat{a}_{decision}$) above which the indications are considered as detected (hit). The decision threshold is normally selected relative to the noise distribution (Annis, 2009; Georgiou, 2006; Matzkanin & Yolken, 2001). Therefore, any parameter affecting the noise and signal distributions could alter the POD and consequently the $a_{90/95}$ value. Microstructural features affecting the mechanical and physical properties of materials (including acoustic properties) are among the key parameters influencing the distribution of NDT signals (Gür & Tuncer, 2005; Lin, Li, & Zhang, 2003). So, it is crucial to investigate and understand the correlation of these properties with microstructure of the materials of interest and hence to specify how the POD will be affected by the variations in the microstructure. A better understanding allows for more precisely interpreting the inspection outcome as well as more accurately modelling the ultrasonic inspection process. In addition, since POD is a function of defect type, geometry and position, it is necessary to characterize the most common flaws occurring in the components under study in order to have a relevant POD study to the reality of the case. Figure 1.2 illustrates the main parameters affecting the capability of NDT methods. In short, the actual reliability of NDT methods could be

expressed as a function of the intrinsic POD, application parameters (AP), and human and environmental factors (HF) (Carvalho, Rebello, Silva, & Sagrilo, 2006; Carvalho, Rebello, Souza, Sagrilo, & Soares, 2008; Wall, Burch, & Lilley, 2009):

$$POD\ actual = POD\ intrinsic - g(AP) - h(HF) \tag{1.1}$$

Taken from Wall, Wedgwood and Burch (1998)

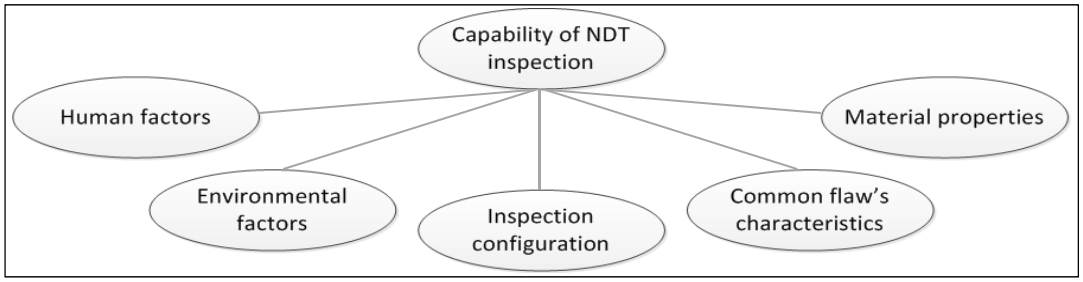

Figure 1.2 Factors affecting the capability of NDT inspection

Modelling approach allows for characterization of the intrinsic capability of NDT method by isolating the application, human and environmental factors. This will be helpful in order to compare the capability of NDT methods regardless of external effects (Da Silva & De Padua; Wall & Burch, 2000; Wall *et al.*, 2009). Since further research in this area could include the generation of model-based POD curves for runner inspection, it is primarily required to assess the factors concerning the intrinsic POD. Accordingly, a study mainly focusing on the material properties and common welding flaws in hydraulic runners should be realized. At the same time a qualitative comparison between the capabilities of the frequently used NDT methods is required in order to find the advantages and disadvantages of different available methods. The focus will be on the reliability of the currently applied methods.

1.2 Impact of material properties on ultrasonic waves

Although several researches in the literature (Carreón, Barrera, Natividad, Salazar, & Contreras, 2016; Freitas, Albuquerque, Silva, Silva, & Tavares, 2010; Gür & Tuncer, 2005; Mutlu, Oktay, & Ekinci, 2009; 2013; Palanichamy, Vasudevan, Jayakumar, Venugopal, &

Raj, 2000; Stella, Cerezo, & Rodríguez, 2009; Vijayalakshmi, Muthupandi, & Jayachitra, 2011) cover the impact of microstructure of polycrystalline metals on ultrasonic wave propagation, their focus principally remains on metallurgical evaluations where the main targets include grain sizing and microstructural characterization. Generally for grain sizing, the tests are carried out in the Rayleigh region of scattering where the wavelength of ultrasonic waves is significantly larger than the mean size of grain diameter and hence the ultrasonic wave scattering is a function of the third power of grain size. Furthermore, most of the aforementioned studies employ longitudinal waves due to the simpler generation and application of this wave mode. In brief, further research is essential to explore the effect of microstructural evolutions on the outcome of longitudinal and transversal ultrasonic inspections and their capability in flaw characterization. It is also noteworthy that the ultrasonic properties of each material grade (more specifically each steel grade) are affected differently by its characteristic microstructure. Therefore, each steel grade should be studied individually and the effect of variations in the ultrasonic properties of these materials on the inspection outcome should be assessed.

Ultrasonic velocity, attenuation and backscattering noise characteristics are the most important parameters studied in the literature. As discussed by several researchers (Papadakis, 1965; Ploix, 2006), the intrinsic attenuation of materials is due to scattering and absorption. The latter is negligible in polycrystalline materials as compared to the scattering effect which results from deviation and reflection of the propagating wave at acoustic impedance discontinuities. Scattering not only decays the travelling wave energy, but it also causes grass noise via the random reflection of a small percentage of wave energy back to the receiver (Shull, 2002). This noise can be captured in the pulse/echo ultrasonic inspections where it can easily mask the signals from small flaws. Thus, it is believed that the combined effect of scattering induced attenuation and grass noise adversely affects the detection capability (Feuilly, Dupond, Chassignole, Moysan, & Comeloup, 2009; Guo, 2003).

Papadakis (Papadakis, 1970), who is one of the main researchers in the ultrasonic field, evaluates the effect of austenitization temperature of quenched SAE 52100 steel on the

longitudinal and transversal wave attenuation. The author mentions that the scattering phenomenon is the main contributor to the ultrasonic attenuation in steel. It is also added that the attenuation principally depends on the grain size as well as the elastic moduli of the substructures of the grains. As also reported by Feuilly *et al.* (Feuilly *et al.*, 2009), the attenuation increases monotonically with the grain size and frequency in the Inconel® 600 alloy. In duplex stainless steels, the ultrasonic velocity is found to be a function of both the phase content and the grain size in different heat treated samples while the attenuation is reported to be directly correlated with the grain size (Vijayalakshmi *et al.*, 2011). Palanichamy *et al.* (Palanichamy, Joseph, Jayakumar, & Raj, 1995) indicate that transversal waves are more sensitive than longitudinal waves in terms of dependency on the grain size of austenitic stainless steels. They also observe that ultrasonic velocity shows lower sensitivity than attenuation to the variations in the microstructural features and residual stresses.

Apart from the grain size, the attenuation and the velocity of both longitudinal and transversal waves are found to change as a function of phase transformation induced by different heat treatments (Freitas *et al.*, 2010; Gür & Cam, 2007). Both of these studies mention that due to the lower crystal lattice distortion and dislocation density, the ultrasonic waves propagate more rapidly in the ferrite-pearlite microstructure than in the martensitic one. In contrast to Freitas *et al.* (Freitas *et al.*, 2010), Papadakis (Papadakis, 1970) indicates that lamellar pearlite and tempered martensite are considered to be the most and the least attenuating phases among all. This is confirmed by Kumar *et al.* (Kumar, Laha, Jayakumar, Rao, & Raj, 2002) who affirm that the martensitic microstructure possesses low elastic anisotropy as a consequence of randomly oriented martensite laths breaking the prior grain volume into fine regions. In both of these studies, the prior austenite grain size is found to be the main contributor to the attenuation. Additionally, the presence of ferrite phases in a martensitic microstructure is reported to induce a significant increase in the attenuation (Papadakis, 1970). The results obtained by Stella *et al.* (Stella *et al.*, 2009) also imply that heat treatment processes can affect the acoustic properties of materials through the change in the fraction of phases present in the microstructure. According to their conclusions, the variations in the microstructure of specific steel alloys may not be observed by only

evaluating the ultrasonic velocity; however, the attenuation and power spectrum of reflected ultrasonic waves could convey useful information concerning microstructural changes. In another study, Kruger and Damm (Kruger & Damm, 2006) propose that since the longitudinal wave in austenite travels in a noticeably lower velocity (approximately 5600 m/s at room temperature) than in martensitic and ferritic structures (approximately 5900 m/s), so the variations of ultrasonic velocity could be employed for online estimation of the volume fraction of austenite in the microstructure during the cooling of low alloy steels.

Other researchers concentrated on establishing correlations between the mechanical properties and ultrasonic parameters. In some references (El Rayes, El-Danaf, & Almajid, 2015; Kumar *et al.*, 2002; Lin *et al.*, 2003), hardness was reported to be inversely correlated with ultrasonic velocity in low alloy, ferritic, and martensitic steels whereas in another study (Bouda, Benchaala, & Alem, 2000) on medium carbon steels, ultrasonic velocity changes proportionally with hardness. However, Hsu *et al.* (Hsu, Teng, & Chen, 2004) were not able to demonstrate a particular relationship between ultrasonic velocity and hardness of tempered CA-15 martensitic stainless steel. These authors reveal that ultrasonic attenuation directly rises with hardness and tensile strength due to the fact that these mechanical properties are enhanced as a consequence of the presence of carbides (scatterers) at the martensite grain boundaries. More recently (El Rayes *et al.*, 2015) indicate that, in the 9-12% Cr martensitic-ferritic steel, ultrasonic attenuation increases with hardness because hardness elevation is caused by the higher content of martensite and dispersed carbide in the microstructure; the latter promotes more scattering interfaces and higher anisotropy resulting in ultrasonic waves to be further attenuated.

1.3 Microstructural evolution of 13Cr-4Ni martensitic stainless steel

Martensitic stainless steel grade is widely used in the manufacturing of hydraulic turbine runners due to its favorable properties including corrosion resistance, good weldability, high strength and toughness (Amrei, Monajati, Thibault, Verreman, & Bocher, 2016; Amrei, Verreman, Bridier, Thibault, & Bocher, 2015; Mirakhorli, Cao, Pham, Wanjara, & Fihey,

2016; Sarafan, Wanjara, Champliaud, & Thibault, 2015). Hydraulic runners should be tempered before putting in-service in order to retrieve their mechanical properties, especially the toughness and ductility, after welding (Ma, Wang, Liu, & Subramanian, 2012). Bilmes *et al.* (Bilmes, Solari, & Llorente, 2001) demonstrate that the tempering heat treatment of 13Cr-NiMo steel causes the martensite phase to soften, and at the same time, promotes the precipitation of fine austenite particles along with the boundaries of martensite laths, blocks and packets as well as prior austenite grains. The martensite to austenite transformation could also cause a slight decline in the carbide and carbonitride particles in the microstructure as a consequence of refinement and dissolution in the austenite regions (Bilmes, Llorente, Méndez, & Gervasi, 2009). Double tempering produces higher reformed austenite content with a more uniform distribution in the microstructure since the austenite/martensite interfaces created in the first tempering process assist the precipitation of new austenite particles (Bilmes *et al.*, 2001). Although the reformed austenite impact on the mechanical properties and its thermal and mechanical stability are studied in the literature (Bilmes, Llorente, & Ipiña, 2000; Bilmes *et al.*, 2009; Bilmes *et al.*, 2001; Godin, 2014; Thibault *et al.*, 2011), its influence on the acoustic properties and the NDT outcome needs to be discovered.

1.4 Welding flaws in hydraulic turbine runner joints

The assembly and joining of the thick sections of hydraulic turbine runners require multiple welding passes which is generally achieved using conventional welding processes (Amrei *et al.*, 2016; Amrei *et al.*, 2015; Mirakhorli *et al.*, 2016; Sarafan *et al.*, 2015). Due to its high deposition rate combined with its flexibility in using shielding gasses and fluxing materials with continuous metal wires, flux cored arc welding (FCAW) is a favorable method for this application as compared to gas metal arc welding (GMAW) and shielded metal arc welding (SMAW) (Kou, 2003; Starling, Modenesi, & Borba, 2011; Tümer & Yılmaz, 2016). Moreover considering the non-flat welding positions as well as considerable amount of metal required for joining the components in hydraulic turbines, FCAW is found to be a quite efficient and productive method.

This joining process, similar to other welding methods, is vulnerable to introduce discontinues originated from several sources including welding thermal cycles, impurities in the weld zone, technical and human factors. In FCAW, one of the roles of the fluxing material (oxide compounds in the core of electrodes) is to form a slag layer protecting the weld metal from oxidation during the post-weld cooling process. Moreover, shielding gases are used during welding to prevent the molten weld pool from being exposed principally to the nitrogen and oxygen of the ambient air. As reported in the literature (Bauné, Bonnet, & Liu, 2000; Tümer & Yılmaz, 2016), the presence of a certain amount of CO_2 in FCAW shielding gases promotes higher arc stability, welding speed, and penetration as well as a desired mode of metal transfer (spray transfer). Even though CO_2 is an inert gas at room temperature, it could decompose in the arc heat and introduce a certain amount of oxygen to the welding zone which reacts with some of the elements and hence forms oxide compounds tending to float on the weld metal. The perturbations in the welding zone may cause the floating slag layer to drown in the weld pool, get entrapped, and generate inclusions (Bauné *et al.*, 2000; Pamnani, Jayakumar, Vasudevan, & Sakthivel, 2016; Quintana, Mclane, Babu, & David, 2001; Tümer & Yılmaz, 2016; Zhu, Fan, Liu, & Ma, 2016). Furthermore according to several studies (Caron & Sowards, 2014; Guo, Lin, Gao, Fan, & Yang, 2013; Habibzadeh Boukani *et al.*, 2014; Salvador & Antunes, 2016), incomplete interpass cleaning and undesirable surface profile of weld bead may also contribute to the formation of slag inclusions in multipass welding processes. This inclusion type may promote the formation of interpass lack of fusion due to the fact that the uncleaned oxide layer may not be melted by the subsequent weld pass as a result of its higher melting point (Habibzadeh Boukani *et al.*, 2014; Rihar & Uran, 2006). The results of residual stress measurements in the 13Cr-4Ni martensitic stainless steel joints (Thibault, Bocher, & Thomas, 2009; Thibault *et al.*, 2010) reveal the existence of a zone, just below the last weld layer, which is under a longitudinal stress close to the yield strength of the material. So, formation of lateral cold cracks is likely to occur in this subsurface zone owing to the coexistence of elevated residual stress and high hardness. It is also noteworthy that the out-of-position welding of runner joints as well as their complex geometry could lead to accessibility limitations intensifying instabilities in the

arc manipulation and hence raising the probability of occurrence of porosities, lack of penetrations, toe cracking, and lack of fusions (Habibzadeh Boukani *et al.*, 2014; Xiao, Shi, Ma, Zhang, & Li, 2013). A part of the current study is dedicated to the characterization of some common welding flaws in the joints of hydraulic runners using nondestructive and destructive methods; the flaws will be characterized in terms of their geometry, position, orientation, type, and dimensions.

1.5 Nondestructive inspections and flaw detection/characterization on runner joints

Although different aspects of hydraulic turbine runner design, manufacturing and productivity are thoroughly investigated in the literature, nondestructive inspection and flaw characterization of these runners are rarely studied. Therefore in the recent studies on the fatigue life estimation of hydraulic runners (Gagnon *et al.*, 2012a; 2014), the flaw characteristics and their detectability are the least developed part. As reported by (Xiao *et al.*, 2013), surface inspection methods are the most frequently used practices for the quality control of runners. Yicheng *et al.* (Yicheng, Xiaohong, Jun, & Hui, 2011) and Xiao *et al.* (Xiao *et al.*, 2013) believe that conventional ultrasonic methods are associated with some limitations deriving from the need to use several transducers for different beam angles, the complex geometry of runners, the variation in the thickness of runner components, and the necessity to manually manipulate the transducers to cover the whole weld region. Yicheng *et al.* (Yicheng *et al.*, 2011) also concludes that, in all ultrasonic techniques, the access to the joint on the second-half skip is complicated since the complex shape of blades reflects the ultrasonic waves to various directions. In spite of the fact that only some regions in the runner joint experience higher in-service stresses, Zhang *et al.* (Zhang, Li, Shi, & Liang, 2014) propose to cover the whole welded area in the inspection process considering the combined effect of in-service and welding residual stresses. Some researchers (Xiao *et al.*, 2013; Yicheng *et al.*, 2011) tried to model the PAUT process and to optimize the scanning path of inspection without considering a real distribution of flaw's position, orientation and geometry. In addition in (Yicheng *et al.*, 2011), only the Kirchhoff diffraction theory is used for modelling the beam/defect interaction while the authors inserted several flaws

unfavorably oriented relative to the PA transducer. For the aforementioned flaws which are far from the specular observation direction, the ultrasonic response is predominantly generated by the tip diffraction effect which could not be accurately calculated using only the Kirchhoff diffraction theory. On the other hand in their POD calculations, the variable parameters which are the core of a POD study are not identified and the effect of material properties is neglected.

Inspection outcome and flaw detection in runner joints suffer from some microstructural evolutions. Due to the non-equilibrium cooling conditions after welding, a fraction of δ-ferrite remains in the microstructure of the martensitic stainless runners joints (Amrei *et al.*, 2015; Thibault *et al.*, 2014). Therefore, it could be concluded that these BCC islands in the BCT background matrix can contribute to an increase in the ultrasonic attenuation (Papadakis, 1970). In addition, the mandatory tempering heat treatment on the runner promotes a fraction of reformed austenite content; the reformed austenite content could further grow in case of double or multiple tempering effects caused by the thermal cycles of multipass welding process. So, it is necessary to evaluate the impact of the tempering heat treatment and the reformed austenite content on the ultrasonic properties.

On the other hand, the previous investigations on the application of NDT in hydraulic turbine industry mainly consist of using intentionally seeded flaws in the samples and inspection models (Xiao *et al.*, 2013; Yicheng *et al.*, 2011; Zhang *et al.*, 2014). These flaws are not always appropriate representatives of the real welding flaws and thus the POD study will not be applicable to the real conditions. Moreover as the use of life estimation models and fracture mechanics concept in hydroelectric industry becomes increasingly important, a thorough study on the common flaw types in runner joints as well as the optimal NDT methods to characterize them seems to be necessary. This study aims to investigate some real welding defects in the runner joints so that to evaluate their characteristics and detectability.

In conclusion, due to the tendency of the hydro-turbine industry to move toward the damage tolerance approach, despite all the previous studies, there is an essential need to extend the

knowledge on the characteristics and detectability of the common welding flaws in the runner joints. In addition, the variability in the result of previous researches concerning the effect of metallic microstructure on the ultrasonic properties necessitates the need for this study which is specifically dedicated to the influence of heat treatment and microstructure of widely used materials in the hydro-turbine industry on the reliability of NDT methods. Furthermore, in a few earlier studies on the reliability of NDT methods in the runner inspection field, the authors neglected some significant parameters in order to remove certain constraints on their studies and their corresponding models; therefore, comprehensive analytical model-based studies are required in the future to accurately characterize and quantify the POD of welding flaws in the turbine runner joints. The outcome of this research is an important source for the preparation of the input data for such studies.

CHAPTER 2

INFLUENCE OF THE MICROSTRUCTURE OF HYDRAULIC TURBINE RUNNER ON ULTRASONIC INSPECTION

Hamid Habibzadeh Boukani[a], Demartonne Ramos França[b], Martin Viens[a], Souheil-Antoine Tahan[a], and Martin Gagnon[c]

[a] Department of Mechanical Engineering, École de technologie supérieure (ÉTS), Montréal (Québec), H3C 1K3, Canada
[b] John Abbott College, Montréal (Québec), H9X 3L9 Canada
[c] Institut de recherche d'Hydro-Québec (IREQ), Varennes (Québec), J3X 1S1, Canada

Paper submitted to the International Journal of Microstructure and Materials Properties, November 2017

Abstract

Considering the time and money required to manufacture and replace in-service hydro-turbine runners, appropriate fatigue models are required to make accurate life estimations of these runners. These models need several inputs including the flaw size distribution near stressed zones. Since ultrasonic testing (UT) is principally used to detect and characterize flaws in those components, reliable UT results are required to reduce the uncertainty in flaw characterization and hence the life estimations. This uncertainty depends on the acoustic properties in the material which in turn are functions of the microstructure. Therefore, we investigated the influence of microstructure on the acoustic properties of two widely used steels for manufacturing of runners. Of these, the S41500 grade demonstrates lower attenuation and backscattering noise as well as higher signal-to-noise ratio. As a result, the reliability of UT outcome on runners made of S41500 is higher due to superior probability of detection and better sensitivity.

2.1 Introduction

Owing to good mechanical properties as well as high cavitation and corrosion resistance, martensitic stainless steels are now widely used in the production of hydraulic turbine

runners. However, before the advent and domination of these steels in the hydroelectricity industry, runners used to be produced using other materials like ASTM A27 steel.

The application of nondestructive testing (NDT) methods in different industries has increased because it represents a reliable method for post-manufacturing quality control, structural health monitoring, and in-service maintenance scheduling. In these cases, the accuracy in positioning and sizing of any potential flaw is a crucial issue. This accuracy is mainly influenced by different features of the material, inspection method, and human factors (Carvalho *et al.*, 2006; Carvalho *et al.*, 2008; Wall *et al.*, 2009). Generally, hydro-turbine runners are inspected using ultrasonic inspection methods for which microstructural features of materials are important parameters affecting the sound wave properties (Gür & Tuncer, 2005; Habibzadeh Boukani *et al.*, 2014; Lin *et al.*, 2003). These properties include sound wave velocity, attenuation, and noise spectrum. Therefore, in order to be able to either precisely interpret the inspection outcome or accurately simulate the inspection process, the acoustic properties of the material of interest are required. Notice that attenuation diminishes the amplitude of the wave as it is traveling by removing energy from it, and hence it most likely decreases the probability of detection (POD) of a flaw hidden in the material. Hence, relative attenuation is a good metric for the comparison of different materials in terms of inspectability. For normal wave inspection, sound wave velocity directly impacts the localization of discontinuities buried within the thickness of the component. For refracted waves, this issue needs to be studied more meticulously because any significant variation in velocity results in a deviation in wave direction which would in turn lead to erroneous positioning of flaws in the component. Noise level is another acoustic feature which affects the POD of an inspection system because it can modulate the threshold amplitude value above which the signal is considered as a hit. In welded joints, where the microstructure (and hence the acoustic properties) varies between the weld and the base metal, positioning and sizing of discontinuities will be further complicated.

Hydro-Québec, a major hydro-power producer in North America, has developed a method to predict the probability of fatigue damage to avoid unexpected maintenance. This model,

based on the damage tolerance approach, considers the fatigue life of runners as the time taken for an existing flaw to grow and reach its critical size. To be effective, this life estimation model requires several inputs such as flaw size which should be characterized as accurately as possible (Gagnon *et al.*, 2012a) using information available from ultrasonic inspection. Inaccuracy in sizing and positioning of welding flaws in these hydraulic runners might lead to unexpected fatigue cracking and failure under normal in-service dynamic loading.

We notice that the use of numerical methods for simulating nondestructive inspection processes is becoming more common in the industry (Dib *et al.*, 2016; Renshaw, Thigpen, & Breza, 2013; Zhao & Rudlin, 2014). Precise definition of the acoustic parameters of the materials under study is thus becoming essential. In fact, accurate simulation parameters lead to more realistic and practical results (Chatillon, Poidevin, Gengembre, & Lhémery, 2003). To this end, this study wishes to establish, as accurately as possible, the basic parameters for common materials used for producing hydraulic runners. For the microstructures under study, ultrasonic noise has been characterized using the distribution of noise amplitude in time domain. This distribution is an important asset allowing the computation of probability of detection (POD) and probability of false indications (POFI) (Sarkar, Meeker, Thompson, Gray, & Junker, 1998).

The current study will focus specifically on the acoustic properties of the steel grades used for the manufacturing of hydraulic turbine runners in order to assess the influence of signal and noise distributions on POD and POFI. We have noticed that even if many grades of steel have been studied in the literature in terms of acoustic properties (Freitas *et al.*, 2010; Gür & Tuncer, 2005; Hsu *et al.*, 2004; Lin *et al.*, 2003; Palanichamy *et al.*, 2000; Vijayalakshmi *et al.*, 2011), limited information is available for the acoustic properties of the steel grades used for the manufacturing of hydraulic turbine runners. Of these, in a study on the relative attenuation coefficient of low alloy steels, Lin et al. (Lin *et al.*, 2003) showed that the microstructure created by various heat treatments can be differentiated by their acoustic properties. Based on their findings, the attenuation was the lowest for quench-tempered

martensite and the highest for pearlite-ferrite microstructure. Gur and Tuncer (Gür & Tuncer, 2005) conducted a research on AISI 4140 and AISI 5140 steels. They reported that the grain size, degree of lattice distortion, and dislocation density have an inverse effect on the sound velocity. As a conclusion, the sound velocity in martensitic microstructures is lower than in fine ferrite-pearlite microstructure while coarse ferrite-pearlite has the highest velocity value. Freitas et al. (Freitas *et al.*, 2010) presented similar behaviour in plain carbon steels. In addition, they found the residual stresses to be another reason for the sound velocity to decrease in materials. Palanichamy et al. (Palanichamy *et al.*, 2000) have arrived at the same conclusion for austenitic stainless steels where they found that the velocity of longitudinal and transverse waves drops as a result of the presence of point defects and dislocations. According to Kupperman and Reimann (Kupperman & Reimann, 1980), the direction of propagation and the crystallographic orientation of grains in austenitic stainless steel cause variations in the velocity of longitudinal and transverse waves. Furthermore, experiments conducted by Palanichamy et al. (Palanichamy *et al.*, 1995) focussed on the effect of the grain size of austenitic stainless steel on the ultrasonic velocity. They demonstrate that the velocity of transverse waves decreases more steeply with the grain size. The authors also explain that the velocity is sensitive to the changes in the microstructure, residual stress and dislocation density. Hirone and Kamigaki (Hirone & Kamigaki, 1958) proposed to inspect coarse-grained austenitic stainless steel components using lower frequencies because as the grain size increases, the attenuation rises due to higher grain scattering. In a research on duplex stainless steel (Vijayalakshmi *et al.*, 2011), it is shown that both ultrasonic attenuation and velocity vary with the grain size, while the velocity is affected by the ferrite content as well. Hsu et al. (Hsu *et al.*, 2004) concluded that the scattering and attenuation in tempered CA-15 martensitic stainless steel rise as a function of the ultrasonic frequency and the precipitated carbides on the martensite/ferrite boundary. Papadakis (Papadakis, 1970), in his study on the acoustic properties of plain carbon steel, points out that although martensite laths are much smaller than the size of parent austenite grains, they can still scatter sound waves individually due to their high anisotropy. Martensitic microstructure consists of parent austenite grains which contain packets and blocks of martensite as well as laths (Thibault *et al.*, 2014). These martensitic features can contribute to the scattering individually.

This study is structured as follows: first, we look at the composition and microstructure of the studied materials in section 2. Then, in section 3, we present an overview on the methods used for ultrasonic data acquisition and processing. Next, we discuss the results of the metallurgical and ultrasonic evaluations obtained to extract ultrasonic properties which influence the inspection reliability. We devote the final section to conclude on the impact of microstructure of these steel grades on the ultrasonic inspection outcome.

2.2 Materials composition and microstructure

2.2.1 Chemical composition

In this study, two different grades of steel are investigated: a martensitic stainless steel (UNS S41500) and a carbon steel (ASTM A27). These grades are both used in the hydropower industry for the production of turbine runners. In order to determine the chemical composition of our specimens, optical emission spectroscopy was performed. Furthermore, carbon/sulfur (C/S) analysis was carried out, by combustion, to accurately determine the content of these two elements in the composition. The results of optical emission spectroscopy and C/S analyses are presented in Table 2.1.

Table 2.1 Chemical composition (wt.%)

Material	%C	%S	%Mn	%P	%Si	%Ni	%Cr	%Cu	%Mo	%Fe
S41500	0.031	0.001	0,71	0,018	0,43	3,89	12,75	0,078	0,57	balance
A27	0.25	0.022	0,70	0,022	0,33	0,12	0,37	0,14	0,050	balance

2.2.2 Steel microstructure

Based on the metallographic evaluations, the microstructure of ASTM A27 steel consists of ferrite and pearlite phases; however, UNS S41500 has a martensitic microstructure which

includes a small amount of reformed austenite inside the parent austenite grains and at their boundaries. Figure 2.1 illustrates the micrographs of the two materials under study. The figure also shows both the optical and scanning electron microscopy (SEM) results. The white zones in Figure 2.1(a) are ferrite particles while the black zones represent the pearlites. In Figure 2.1(b), the martensitic microstructure of S41500 is depicted. In the SEM image of Figure 2.1(c), the pearlitic zones (identified by letter "P") are seen as lamellar structures separated from the ferrite particles by two white dashed lines. Martensite laths are illustrated in more details in Figure 2.1(d) which is taken at 7000X magnification. The grain size measurement was performed according to ASTM E112. For the martensitic stainless grade, revealing the parent austenite grain boundaries was the main challenge; therefore, several combinations of etching agents and duration were used in order to find the optimal processing parameters.

In addition, microhardness measurements have been carried out in order to verify the metallographic results. Measured microhardness values are presented in Table 2.2. The displayed results are the average of measurements performed at five different locations using a force of 98.07 N for 15 seconds. These results of hardness measurements match the outcome of metallographic evaluations. We believe that the internal stresses and lattice distortion, caused by the expansion during the martensitic transformation, as well as high density of dislocations developed in martensite are the main reasons for the elevated hardness observed in the S41500 microstructure as compared to the A27 sample (Nishiyama, 2012).

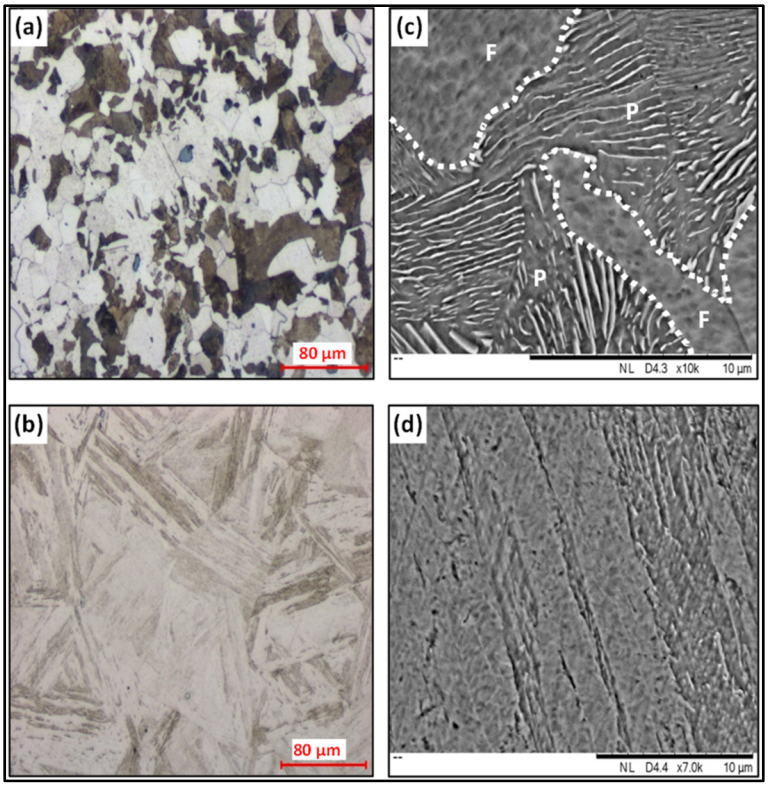

Figure 2.1 Macrographs of (a) A27 and (b) S41500, and SEM images of (c) A27 and (d) S41500

Table 2.2 Hardness and metallographic evaluations

Material	Grain Size (µm)	Hardness (HV10)
UNS S41500	101	300-350
ASTM A27	21	131 ferrite 242 pearlite

2.3 Ultrasonic inspections

2.3.1 Experimental procedure

Samples were cut from as-received materials and they were machined to the final dimensions; subsequently, the surfaces were polished to eliminate the effect of surface roughness. The ultrasonic measurements were accomplished using a 2-axis TecScan

immersion system, as illustrated in Figure 2.2. Encoded immersion testing was used to eliminate the effect of coupling variations on the received signals. Flat transducers of 2.25 MHz (13 mm dia) and 5 MHz (10 mm dia) were employed using pulse-echo method. The transducers were aligned along the normal to the blocks' surface. The excitation voltage and the pulse width were set at 260 V and 30 ns, respectively. In order to have enough time resolution, a sampling rate of 250 MHz was used in the tests. The tank was filled with tap water 24 hours before the beginning of the experiments so as to let any dissolved gas and air bubbles get out of the coupling fluid. Although the diffraction effect on the attenuation was accounted for, the water path was kept constant during all the experiments in order to avoid the deviations in the attenuation measurement caused by beam divergence.

The results were recorded in the form of A-scans. In order to decrease the effect of white noise, an average of 30 records at each location was used. The final values were then calculated by averaging the results obtained for 20 different locations.

2.3.2 Signal acquisition and processing

Referring again to Figure 2.2, the immersion ultrasonic tank is coupled to a computer where the acquired data are displayed and recorded in order to be post-processed using a custom-made code. For the wave velocity, the calculation is straightforward using normal incident waves along with successive backwall reverberations. Therefore, the round-trip distance is divided by the time of flight (TOF) of received signals. In order to find the TOF, zero crossing and cross correlation methods were both applied. Results show that both methods yield similar results.

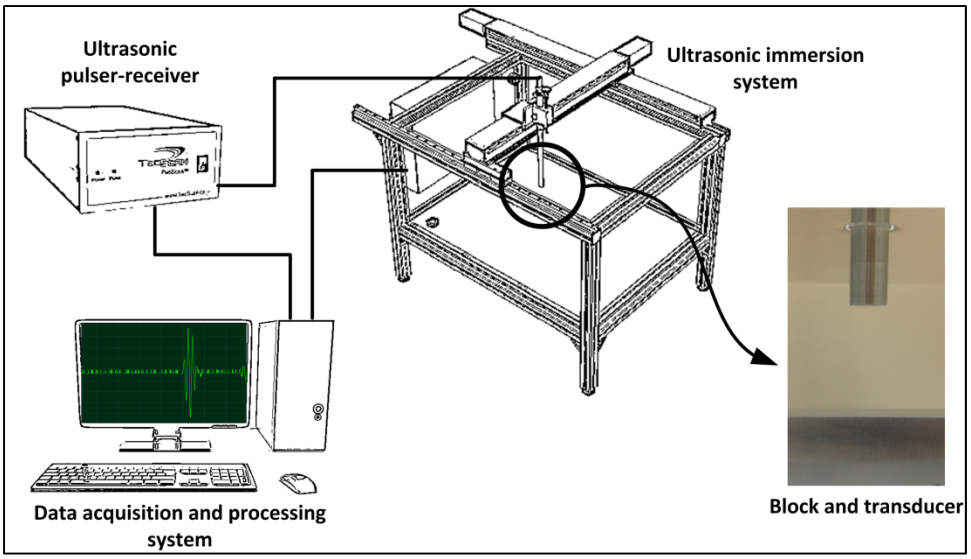

Figure 2.2 The configuration of ultrasonic immersion testing

For the attenuation measurement, the peak amplitude of each backwall reverberation and the traveling distance of wave were used to quantify the decay of ultrasound beam amplitude in these microstructures. It is also noteworthy that the effect of energy loss at each reflection in the steel (due to the wave transmission into water) is incorporated in the calculations by obtaining the acoustic pressure reflection and transmission coefficient which is a function of the density (ρ) and velocity (V) of the neighbouring materials, as shown in equations (1) and (2). The subscripts i and t represent, respectively, the media in which the incident and transmitted ultrasonic waves travel. We used the values available in the literature for the density of water, A27, and S41500, (1.0, 7.8, and 7.8 g/cm3 respectively) while the ultrasonic velocity in the steels was assessed per the previously described method. The wave velocity in water was measured to be 1485 m/s. Figure 2.3 shows the reflection and transmissions occurring at the water/steel interface.

$$R = (\rho_2.V_2 - \rho_1.V_1)/(\rho_2.V_2 + \rho_1.V_1) \tag{2.1}$$

$$T = (2.\rho_2.V_2)/(\rho_2.V_2 + \rho_1.V_1) \tag{2.2}$$

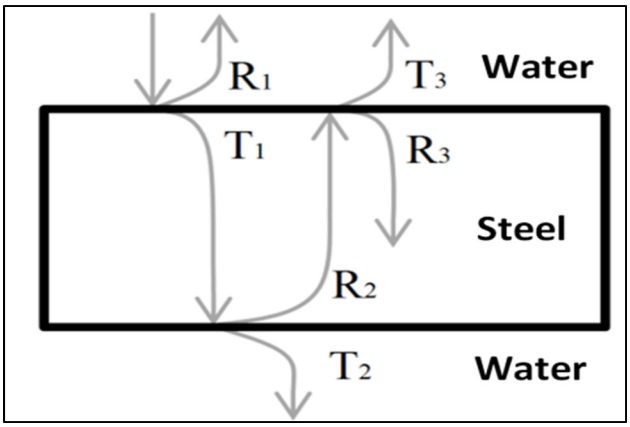

Figure 2.3 Reflections and transmissions occurring at each wave/material interface interaction

As represented in equation (3), travelling ultrasonic waves are attenuated because of different phenomena, including scattering, absorption, and diffraction (Kumar *et al.*, 2002; Vijayalakshmi *et al.*, 2011):

$$\alpha_{measured} = \alpha_{scattering} + \alpha_{diffraction} + \alpha_{absorption} \tag{2.3}$$

In a polycrystalline steel, grain scattering is the most important contributor to the attenuation while absorption has a negligible effect (Palanichamy *et al.*, 1995; Papadakis, 1965; 1981). The effect of diffraction on the attenuation and phase retardation can be compensated using the equations presented by Kino (Kino, 1987).

In order to analyze the noise content of these materials, 10 different locations on each material were studied at 2.25 and 5 MHz. In order to eliminate the effect of system parameters, the noise samples were recorded at a constant system gain for each working frequency. The distribution of peak amplitudes of the backscattering noise within 35 mm of the material thickness was computed and evaluated. In addition, the root mean square (RMS) of the noise was calculated and then analyzed in terms of average and standard deviation for each material and for both frequencies used. Moreover, signal to noise ratio (SNR) was

estimated using the method proposed by Blitz and Simpson (Blitz & Simpson, 1995). The signal level is considered to be the maximum amplitude received from a side-drilled hole (SDH) reflector of 3.18 mm dia at a depth of 60 mm in the material. Then, the transducer is displaced to a location on the specimen far from the reflectors to capture the noise level which is the largest noise amplitude occurring within the same time frame as the SDH's signal.

2.4 Results and discussion

As depicted in the box-plot diagrams of Figure 2.4, longitudinal ultrasonic waves travel with lower velocity in the martensitic microstructure of UNS S41500 as compared to the ferritic-pearlitic microstructure of ASTM A27. Analogous behaviour was reported for the transverse wave velocity in these materials by Boukani et al. (Habibzadeh Boukani, Chentouf, Viens, Tahan, & Gagnon, 2015). This behaviour was also seen in the literature (Freitas *et al.*, 2010; Gür & Tuncer, 2005; Papadakis, 1970) for plain carbon and low alloy steels. This can mainly be attributed to martensitic transformation which is a diffusionless process promoting high levels of distortion, dislocation density, and internal stresses.

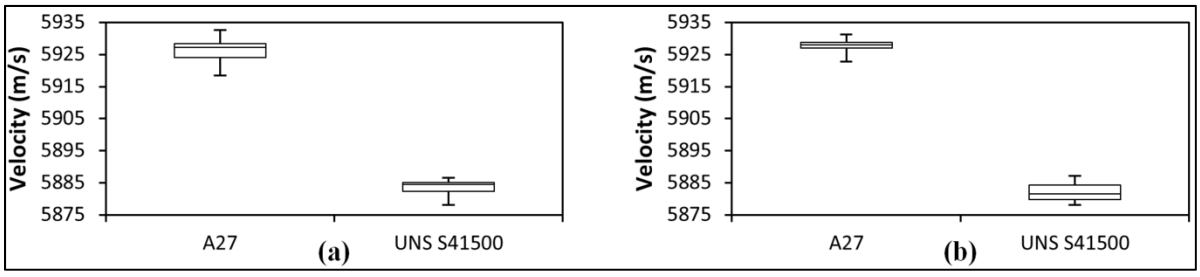

Figure 2.4 Box plot diagram of longitudinal wave velocity in materials at (a) 2.25 and (b) 5 MHz

Furthermore, the presence of a small amount of reformed austenite in the UNS S41500 microstructure can further decrease the velocity owing to lower speed of sound waves in this phase (Kruger & Damm, 2006). We notice that for longitudinal wave velocity (V_L) the

inspection frequency does not play an important role because V_L does not change significantly when the frequency increases from 2.25 to 5 MHz.

Ultrasonic attenuation for longitudinal waves was measured at 20 locations. The average values for both materials at both frequencies are presented in Figure 2.5. It is worth mentioning that the surface roughness of the blocks was controlled in order to ensure that it would not affect the results. According to Isleyici (İşleyici, 2005), the effect of scattering-induced attenuation, caused by surface roughness, is negligible once the roughness is below 1/10 of the ultrasonic wavelength. The measured roughness average (R_a=3.3 μm) was far smaller than the longitudinal beam wavelength (297 μm) in water which is itself smaller than the one in steel; thus, it is assumed that the surface finish has an insignificant impact on the current attenuation measurements. The presence of pearlite and ferrite, possessing different acoustic impedance values, in the A27 microstructure leads to higher acoustic mismatch at the phase interfaces. This in turn causes more scattering attenuation in this material. In other words, due to the high crystallographic mismatch between the pure bcc crystals of ferrite with the anisotropic lamellar structure of pearlite (Bhadeshia & Honeycombe, 2006), the reflection coefficient at the boundary of phases is so high that it allows less energy to be transferred to the adjacent phase along the propagation direction. As presented in Table 2.2, the difference between the microhardness of ferrite and pearlite phases is an indicator of their difference in terms of mechanical properties. For martensitic microstructure, the prior austenite grains are partitioned into a finer microstructure by the martensite laths, blocks, and packets which in turn decreases their elastic anisotropy (El Rayes *et al.*, 2015) and hence the acoustic impedance contrast between adjacent grains. The preceding fact leads to the lower scattering attenuation in the martensitic microstructure. Although there exists some reformed austenite content in the S41500 microstructure, the austenite particle sizes are not large enough (Thibault *et al.*, 2014) compared to the wavelength at the inspection frequency range to make a large scattering effect and to have a remarkable impact on attenuation.

The attenuation for longitudinal waves increases with the frequency in both materials. This occurs because of higher level of scattering at high frequencies caused by larger amount of interactions between the ultrasonic waves and the microstructural features (e.g. grains,

precipitates). This is in accordance with the literature (Ensminger & Bond, 2011; Papadakis, 1981), where the ultrasonic attenuation (α) should change as a function of the frequency.

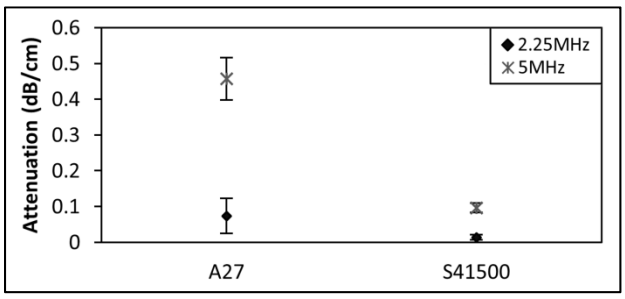

Figure 2.5 Attenuation coefficient for longitudinal waves at 2.25 and 5 MHz with 95% confidence

The effect of attenuation on the amplitude and distribution of the ultrasonic field in these materials was simulated using CIVA software (Calmon, Mahaut, Chatillon, & Raillon, 2006) for a 5 MHz immersion transducer with 45 mm water path, as illustrated in Figure 2.6. The general shape of the amplitude curves, representing the field amplitude on the central axis of the transducer, is due to the effect of divergence; however, the difference between the two curves is caused by scattering. The amplitude ratio of AMP(S41500)/AMP(A27) rises from 1.19 to 1.41 when the path in the material increases from 40 mm to 80 mm. The results show that a reflector located at a given depth in the S41500 grade is exposed to a field possessing higher intensity which brings about stronger reflection. Moreover, due to the effect of higher attenuation in A27, the reflected wave also experiences more energy loss when it travels back to the transducer, which consequently leads to signals with lower amplitude.

In a previous study on the transverse wave properties in these two materials (Habibzadeh Boukani *et al.*, 2015), relative attenuation was measured in order to have a metric to compare the trend of decay of transverse wave amplitude. As presented in Table 2.3, the results of that study demonstrate that transverse wave attenuation follows the same trend as the longitudinal wave attenuation. It is worth mentioning that the effect of diffraction was not isolated and removed from the values obtained in (Habibzadeh Boukani *et al.*, 2015). Accordingly, the

attenuation can only be compared at similar frequencies where the divergence of the beam can be considered as equal.

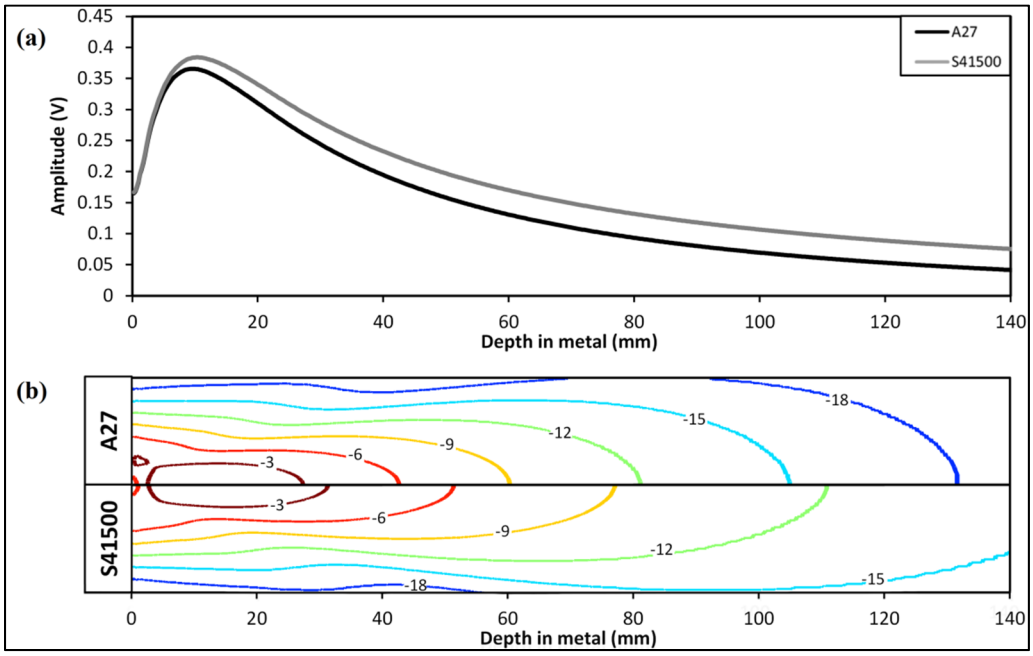

Figure 2.6 (a) Ultrasonic field amplitude on the central axis of transducer and (b) Map of ultrasonic field amplitude (dB) in S41500 and A27

Table 2.3 Relative attenuation coefficient for transverse waves at 2.25 and 5 MHz Adapted from Habibzadeh Boukani *et al.* (2015)

	UNS S41500		**ASTM A27**	
Frequency (MHz)	2.25	5	2.25	5
Transducer Diameter (mm)	13	10	13	10
Relative attenuation (NP/mm)	9.40×10^{-3}	11.19×10^{-3}	11.87×10^{-3}	15.25×10^{-3}
Standard deviation (NP/mm)	0.17×10^{-3}	0.17×10^{-3}	0.45×10^{-3}	0.68×10^{-3}

In addition to the reduced signal energy due to attenuation, ultrasonic inspection of polycrystalline media is also influenced by the backscattered noise generated by the microstructure (Papadakis, 1965). RMS amplitude of noise and SNR were used in this study as parameters for characterizing the ultrasonic noise. By looking at the normalized distribution of noise amplitudes in Figure 2.7(a), it is observed that the noise content in A27

material is distributed over a wider range of amplitudes. Using the RMS values, it can be found that the noise amplitude for the A27 sample is significantly higher than for the martensitic stainless steel sample. Similar to the attenuation, this effect shall to be generated by the high acoustic mismatch at the phase interfaces. The RMS values, presented in Figure 2.7(b), show that the ratio of RMS(A27)/RMS(S41500) increases from 1.2 to 1.83 as frequency goes from 2.25 to 5 MHz because, at higher frequencies, the ultrasonic wave interacts more with the smaller scatterers of A27 material. Note that in Figure 2.7(b), the RMS values for the 2.25 MHz transducer show higher values than for the 5 MHz; this could be due to its larger diameter which is sensitive to a wider scattered wave cone beam angle (Howard, Copley, & Gilmore, 1995). Figure 2.7(c) shows the noise influence on the inspection results in which low-amplitude reflections of flaws could be buried in the noisy A-scan of A27. The presence of two phases with a large acoustic mismatch in the A27 microstructure as well as higher attenuation in this material is believed to be the main reason for the observed SNR behaviour in Figure 2.7(d).

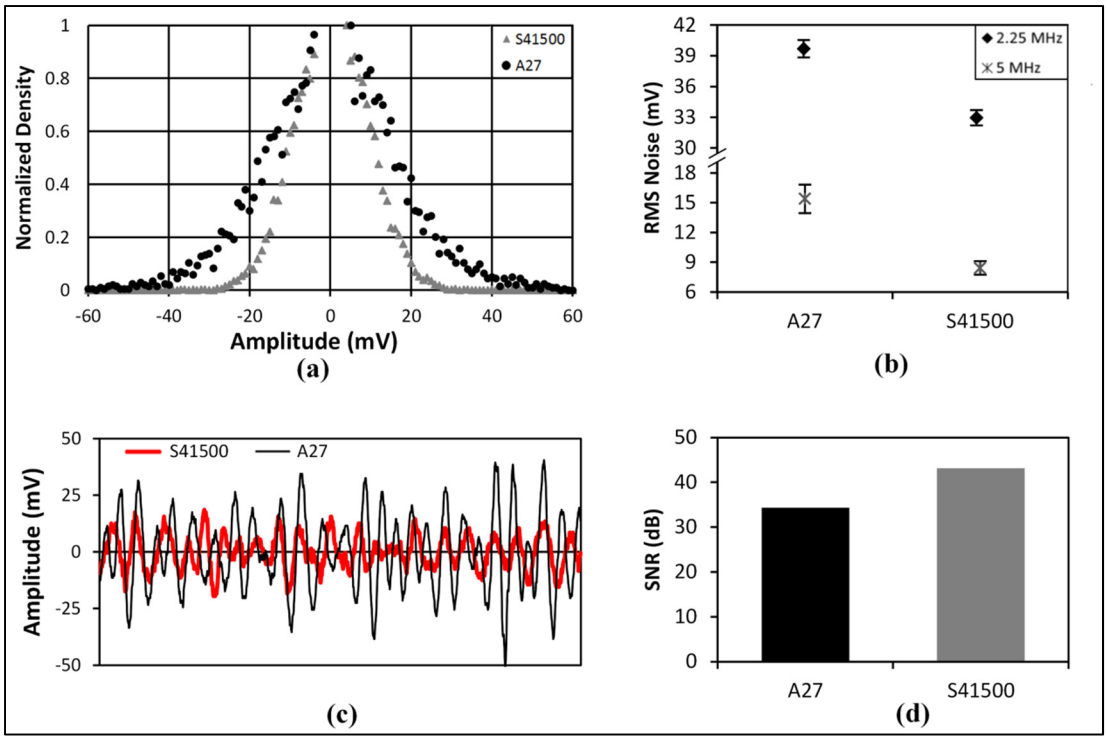

Figure 2.7 Ultrasonic noise characteristics; (a) Normalized distribution of noise amplitude at 5 MHz, (b) root mean square (RMS) of noise at 2.25 and 5 MHz, (c) 5 MHz A-scans from similar locations of A27 and S41500 blocks, and (d) Signal-to-noise ratio (SNR) at 5 MHz

2.4.1 Effect of acoustic parameters on the inspection reliability

As discussed earlier in this paper, ultrasonic attenuation and noise characteristics of materials are the dominant parameters affecting POD curves through displacing and changing the signal and noise distributions. Such a rational is presented in Figure 2.8 which illustrates the impact of ultrasonic behavior in A27 (Figure 2.8(b)) in comparison with S41500 (Figure 2.8(a)):

- Larger attenuation coefficient resulting in lower signal amplitude for a given reflector size ($A_2 < A_1$);
- Higher noise level ($N_2 > N_1$);
- Combination of signal amplitude and noise level results in lower signal-to-noise-ratio (SNR2 < SNR1);
- Wider noise distribution ($W_2 > W_1$).

From this comparison, it becomes obvious that the interference between the noise and the signal distributions occurs on a larger interval of ultrasonic amplitude in A27.

The acceptance of a part is usually based on the amplitude of a detected signal and on an accept/reject threshold criteria ($\hat{a}_{decision}$). This threshold is usually set at a level that results in a stringent quality control (high POD) without sacrificing noisy but defect free parts (low POFI). If someone wants to establish the $\hat{a}_{decision}$ criteria for A27 based on the one successfully used with S41500, three options could be envisaged:

- If a similar $\hat{a}_{decision}$ is used in both cases, the higher attenuation value and the wider noise distribution in A27 will yield lower POD and higher POFI;
- If the $\hat{a}_{decision}$ is set so as to have analogous POD for a specific flaw size (Figure 2.8(e)), a higher POFI value will result for the A27. In fact, the higher attenuation in A27, displacing the amplitude distribution for a specific flaw size and hence the

$\hat{a}_{decision}$ to lower values, combined with its wider backscattering noise distribution leads to a more significant noise distribution on the right of the $\hat{a}_{decision}$ cutoff.

- In some applications, noise distribution is used for the determination of $\hat{a}_{decision}$ in order to avoid high POFI (Kurz et al., 2013). In such a case, higher cutoff values should be set for A27 due to its wider noise distribution (Figure 2.8(d)). Accordingly, in this material, for a particular defect size having a given amplitude distribution, the POD value would drop. Moreover considering the effect of higher attenuation in A27, the distribution of signal amplitude for a similar defect size covers a lower interval of values as compared to S41500; therefore, the elevated $\hat{a}_{decision}$ for A27 causes a further decrease in the POD for this specific size.

In summary, regardless of the $\hat{a}_{decision}$ threshold used, A27 will always yield either inspection reliability reduction, larger probability of defect free part rejection, or even both. In comparison, the S41500 grade yields superior inspection effectiveness.

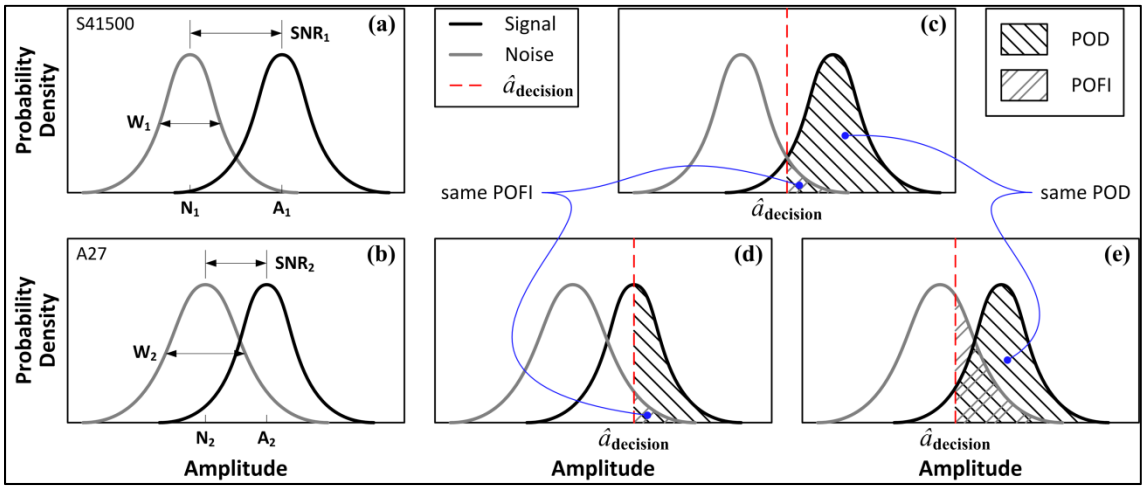

Figure 2.8 Effect of signal and noise distributions on POD and POFI; (a) represents low noise content and attenuation as compared to (b)

2.5 Conclusions

In the hydraulic turbine industry, runners are often manufactured using materials like ASTM A27 and UNS S41500 materials. In this study, the acoustic properties of these two grades of steel have been investigated and determined by a statistical evaluation of the obtained data using immersion ultrasonic inspections on the as-received materials. The obtained properties allow for more precise simulations to be carried out on the inspection of these materials by using observed acoustic properties. Furthermore, the evaluation of ultrasonic attenuation and backscattered noise characteristics shows that at 5 MHz frequency, the standard deviation of noise amplitude in ASTM A27 is 1.85 times of this parameter in UNS S41500 while the attenuation in the latter demonstrates 0.023 dB/cm lower value. Therefore, for a given flaw size, the interference between the noise and signal distribution is lower in UNS S41500 as compared to ASTM A27 (almost 9 dB higher SNR for UNS S41500 at 5 MHz). Accordingly, the reliability of ultrasonic inspection outcome in this material to be higher due to its superior POD and sensitivity. This in turn leads to a better knowledge of the integrity of S41500 runners, which can be translated to more realistic life estimations for these runners.

Acknowledgements

The authors gratefully acknowledge the financial support of the Fonds de recherche du Québec - Nature et technologies (FRQNT), the Natural Sciences and Engineering Research Council of Canada (NSERC), Institut de recherche d'Hydro-Québec (IREQ), and Andritz Hydro Inc. The authors also wish to acknowledge Dr. Samir Mourad Chentouf for many discussions and his technical assistance in the metallographic evaluations.

CHAPTER 3

ULTRASONIC INSPECTION OF MARTENSITIC STAINLESS STEELS IN HYDROELECTRIC TURBINE RUNNERS: REFORMED AUSTENITE EFFECT ON THE LONGITUDINAL WAVE INSPECTION

Hamid Habibzadeh Boukani[a], Martin Viens[a], Souheil Antoine Tahan[a], and Martin Gagnon[b]

[a] École de technologie supérieure (ÉTS), Montréal (Québec), H3C 1K3, Canada
[b] Institut de recherche d'Hydro-Québec (IREQ), Varennes (Québec), J3X 1S1, Canada

Paper submitted to the journal of NDT & E International, January 2018

Abstract

Due to the extensive use of martensitic stainless steels for the production of hydroelectric turbine runners, non-destructive evaluations, including ultrasonic inspection, of these steels is of importance in the hydropower industry. These steel grades are normally tempered after casting and welding in order to mitigate residual stresses and reduce hardness. Based on the material's thermal history, different amounts of reformed austenite will appear in the microstructure. The ultrasonic wave, during its travel, interacts with the reformed austenite particles and thus its properties are affected. In this study, four different tempering heat treatments have been applied on UNS S41500 material to generate variations in tempered austenite content. The outcome of experiments shows that the attenuation and backscattering noise increase with the reformed austenite content and hence the signal to noise ratio significantly diminishes. The results of the modelling phase demonstrate that the ultrasonic inspection reliability degrades with the increase of the austenite content.

3.1 Introduction

Low carbon martensitic stainless steel is generally used for the manufacturing of turbine runners in the hydropower industry due to its toughness and strength, as well as its superior corrosion and cavitation resistance (Habibzadeh Boukani *et al.*, 2015; Thibault *et al.*, 2014). Martensitic stainless steel grade is normally tempered after casting and welding so as to

decrease the amount of residual stresses and hardness, and to obtain greater toughness in the weld zone (Bilmes *et al.*, 2001). During the tempering process, finely distributed austenite (γ) precipitates in the microstructure and remains untransformed after cooling down to room temperature; after tempering (reformed) austenite content is a function of several parameters including the tempering temperature and duration as well as the chemical composition of the alloy (Bilmes *et al.*, 2001; Thibault *et al.*, 2014).

Hydroelectric turbine runners are subjected to different degradation mechanisms limiting their service life. Fatigue is considered to be one of the most important mechanisms threatening the reliability of the equipment. This phenomenon can be accounted for by using fatigue reliability model enabling plant operators to estimate turbine runners remaining life and avoid the risk of unplanned failure during service. According to previous studies (Gagnon, Tahan, Bocher, & Thibault, 2013; Gagnon *et al.*, 2014; Thibault *et al.*, 2014), these models use the Kitagawa diagram as a limit state combined with Linear Elastic Fracture Mechanics (LEFM). The main inputs to the aforementioned model are loading conditions, material properties, and flaw size distribution. In order to have reliable fatigue life estimations, accurate inputs are required. Flaw size can be characterized using nondestructive inspection methods; ultrasonic inspection is one of the methods that can be used for this goal. Therefore, in order to have robust knowledge on this input, evaluating the key parameters in the ultrasonic properties of martensitic steel material becomes critical for proper assessment of inspection results (Habibzadeh Boukani *et al.*, 2014).

At different stages (e.g. as part of manufacturing process or for in-service maintenance, etc.), hydroelectric turbine runners are ultrasonically inspected in order to verify their integrity. In ultrasonic inspection method, ultrasonic waves are transmitted into the material and then scattered at the points where acoustic impedance discontinuities occur. The reliability and outcome of inspections are subjected to uncertainties due to changes in the ultrasonic signal attenuation and noise. In polycrystalline materials, there are several microstructural features directly affecting the ultrasonic properties including backscattering noise and ultrasonic velocity and attenuation (Feuilly *et al.*, 2009; Nagy & Adler, 1988; Papadakis, 1981; Saniie,

Wang, & Bilgutay, 1988). According to Stella et al. (Stella *et al.*, 2009), ultrasonic properties in austenitic stainless steel is remarkably affected by the heat treatment processes. They have shown that the ultrasonic wave attenuation is a function of sensitization and the amount of chromium-carbide precipitation; however, no clear correlation between the ultrasonic velocity and the applied heat treatments were found. The results obtained by Freitas et al. (Freitas *et al.*, 2010) also show the influence of different phases, formed as a result of various heat treatments, on wave velocity and attenuation. Using an ultrasonic immersion technique, Lin et al. (Lin, Li, & Tan, 2004) demonstrated that relative ultrasonic attenuation of low alloy steels varies as a function of quenching and tempering state. Another study (Kruger & Damm, 2006) reveals that the γ-content in low alloy steel microstructure has an observable effect on longitudinal wave velocity which is attributed to the remarkable difference between the sound velocity in austenite and other steel phases such as martensite and ferrite. Grain size also has a significant impact on the ultrasonic velocity and attenuation in polycrystalline metals (Ensminger & Bond, 2011; Feuilly *et al.*, 2009; Hirone & Kamigaki, 1958; Mutlu *et al.*, 2009; Palanichamy *et al.*, 1995; Papadakis, 1981). In addition, sub-grains and carbides as well as their dispersion in the microstructure have an effect on ultrasonic properties (El Rayes *et al.*, 2015; Stella *et al.*, 2009). Backscattering noise characteristics are also a function of metal microstructure; the influence of different phases and grain size are discussed in (Feuilly *et al.*, 2009) and (Lin *et al.*, 2003). Saniie et al. (Saniie & Bilgutay, 1986; Saniie *et al.*, 1988) believe that, in the Rayleigh region of scattering, where the size of scatterers is much smaller than the wavelength, the effect of multiple scattering, which assumes that the wave is scattered several times by different scatterers, becomes negligible on the backscattering noise; therefore, the backscattering noise will depend on the combination of the contribution of each scatterer taken individually. In such case, the noise level is a function of the number of scatterers, their cross-section, and their acoustic impedance (Saniie & Bilgutay, 1986).

There are also several studies (Ensminger & Bond, 2011; Freitas *et al.*, 2010; Hirone & Kamigaki, 1958; Lin *et al.*, 2004; Palanichamy *et al.*, 1995; Stella *et al.*, 2009) mentioning that heat treatment processes affect acoustic properties of carbon steels, austenitic and duplex

stainless steels as a result of microstructural changes induced by these processes. However, martensitic stainless steels have been scarcely investigated in terms of acoustic properties of material and nondestructive inspection outcome. Moreover, previous studies have focused mostly on the correlation of ultrasonic properties with microstructures in a metallurgical perspective while the current study looks at the effect of reformed austenite on the outcome of ultrasonic inspection. More specifically, we investigate the influence of reformed austenite content on the probability of detection (POD) and the probability of false indication (POFI) resulting from ultrasonic inspection of martensitic stainless steels.

This paper is organized as follows: First, the experimental procedure is presented followed by an overview on the data processing method. Next, the results of metallurgical and ultrasonic evaluations are reported and discussed. Afterwards, the effect of variations of ultrasonic properties on the inspection reliability is evaluated. Finally, we conclude on the impact of tempering heat treatment on ultrasonic inspection of UNS S41500 martensitic stainless steel.

3.2 Experimental procedure

Four test samples were prepared from UNS S41500 martensitic stainless steel; all the samples were taken from a single production batch in order to reduce the effect of chemical composition variations on the outcome of heat treatments. The chemical composition of the samples is represented in Table 3.1.

Table 3.1 Chemical composition of the UNS S41500 samples (wt.%)

C	S	P	Mn	Si	Cr	Ni	Mo	Cu	V
0.03	0.001	0.013	0.68	0.41	12.58	3.78	0.59	0.08	0.06

First, the blocks were all austenitized at the same temperature (1100 °C) and for the same duration of time (60 minutes); as a result, the grain size of the parent austenite was kept constant in all the samples because prior austenite grain size would influence the acoustic

properties of material and the dimensions of martensite laths, blocks and packets (sub-grains) (Krauss, 2015; Papadakis, 1970). Next, the blocks were tempered for a duration of 90 minutes at four different temperatures ranging from 560 to 640 °C. Then, the tempered samples were machined to their final dimensions (95×60×35 mm^3) and subsequently side drilled holes (SDHs) of 3.18 mm in diameter were drilled and reamed in each of the blocks. The surfaces and SDHs were parallel with a tolerance of ±0.1 mm; moreover, the surface roughness was reduced to less than 0.8 μm in order to avoid any ultrasonic signal distortion and roughness induced scattering (Fowler, Elfbaum, Smith, & Nelligan, 1996; İşleyici, 2005) which could influence the ultrasonic attenuation measurements.

For the purpose of microstructural investigations, samples from each block were ground, polished and finally etched. In addition, X-ray diffraction (XRD) was used to measure the reformed austenite content in each tempered sample. Rockwell hardness was also obtained for each tempered samples in order to verify the γ-content results. Evaluations were done according to ASTM E18-03 standard and using a ZHU 250 Zwick and Roell hardness tester.

Ultrasonic evaluations were carried out on a TecScan immersion system using two different transducers in pulse-echo mode. The specifications of these transducers are presented in Table 3.2. Encoded immersion technique, provided by this system, presents more uniform probe manipulation; in addition, it eliminates the deviations which normally exist in manual contact ultrasonic measurements caused by variations in the thickness of coupling gel (Saniie *et al.*, 1988) and probe holding pressure. On the other hand, the noise generated by electrical circuits has a detrimental effect on the amplitude and frequency spectrum of received signals; therefore, an averaging of 30 records per data point was used to reduce this effect. The received signals were transferred to a computer for further processing using TecView software. An in-house code was also used to calculate the ultrasonic velocity and attenuation using the recorded data. In this code, the time at which the first positive zero crossing of each backwall reflection occurs was extracted so as to calculate the time of flight (TOF) between the successive backwall echoes. The TOF was used along with the wave path in order to determine the ultrasonic velocity in each sample.

For the attenuation calculation, high frequency noise was removed from the signal and envelopes of signals were generated using Hilbert transform (Bendat, 1991). Then, the effect of diffraction and reflection was compensated on the successive backwall reflections and hence the corrected peak amplitude of reflected signal at 10 different locations was plotted against the travelling distance; this allows finding the scattering induced attenuation which is an inherent parameter of the studied microstructures.

Table 3.2 Specifications of immersion transducers

Frequency (MHz)	**Nominal element diameter (mm)**	**-6 dB Bandwidth (%)**
2.25	13	49.47
5	10	51.7

For the Signal-to-noise ratio (SNR) measurements, the maximum amplitude of the reflected wave from analogous SDHs, located at a depth of 45 mm, is considered as the “signal”. The noise samples are taken from A-scans at the identical time interval as the signals when the transducer is located far from the SDHs in the blocks. Finally, the approach of Blitz and Simpson (Blitz & Simpson, 1995) was used to calculate the SNR values. In addition, the distribution of amplitudes of the backscattering noise within 55 mm of the material thickness was computed and evaluated. The standard deviation of the aforementioned distributions were calculated and then normalized by the standard deviation of the noise amplitude of the first sample.

3.3 Numerical Simulations and POD evaluation

With the use of semi-analytical models, the influence of heat treatment process on the ultrasonic inspection reliability of martensitic stainless steel grade is investigated. In this context, the scanning of a S41500 block in immersion was simulated in the CIVA software (Dib *et al.*, 2016) As depicted in Figure 3.1, the virtual block contains an ellipsoidal rutile (TiO_2) inclusion whose principal axis is perpendicular to the system *y*-axis. In order to evaluate the model-based POD of the inspection setup, the orientation of the flaw with

respect to *x*-axis is set as a normally distributed value with a mean of 0° and a standard deviation of 2°. In addition, to be able to plot the POD as a function of flaw size, the length of the inclusion along its principal axis is set as a uniformly distributed value ranging from 2 to 13 mm (typical size of inclusions found in such a structure) (Habibzadeh Boukani, 2018).

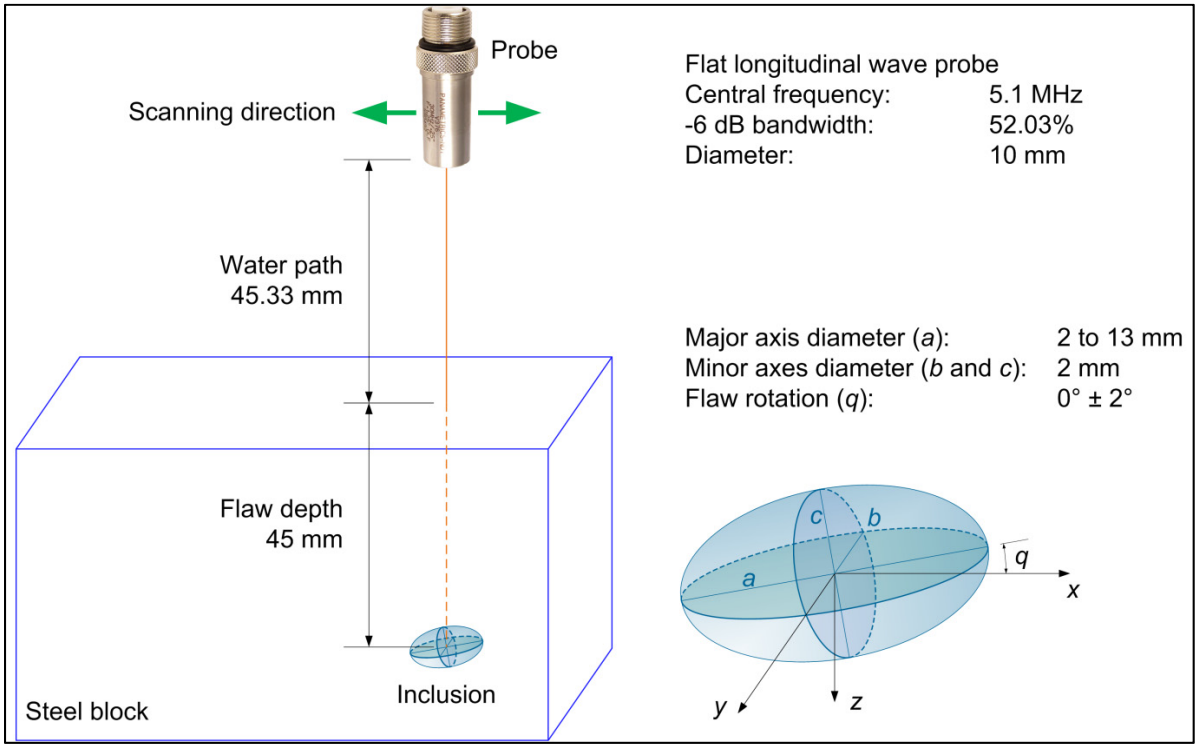

Figure 3.1 Configuration of the numerical model

The ultrasonic signal waveform (central frequency, bandwidth, and phase) provided in the product certificate of the physical 5 MHz probe was used as a reference to adjust the virtual probe input signal properties in CIVA. Two different sets of material properties have been compared: the first one corresponds to a S41500 block with 1% γ-content while the second one corresponds to the same material but with 20% γ-content. To do so, the findings of the experimental phase of this study on the observed ultrasonic attenuation and the collected backscattering noise were used.

In fact, the echo from a reference side drilled hole (SDH), similar to the SDH in the experimental samples, was calculated using the separation of variables (SOV) model for each

heat treated condition. Subsequently, the value of the signal-to-noise ratio (SNR), obtained in the experimental phase, was used to define the parameters of modelled backscattering noise. It is noteworthy that semi-analytical models cannot reliably estimate wave scattering over the entire range of flaw types and sizes. As an example, "Modified Born" approximation becomes inaccurate for high frequency applications. Nonetheless, this model has been used in the current POD study because the goal of simulations is to make a comparison between the POD of the two heat treated samples rather than to evaluate the absolute amplitude of flaw responses.

In order to mimic physical measurements, the virtual samples have been scanned along a line, parallel to the x-axis, and going through the center of the ellipsoidal flaw. Scanning steps of 1.5 mm have been selected with normal incident angle. For all the virtual scans performed, the maximum signal amplitude $\hat{a}$ has been recorded as a function of flaw size a. Finally, all collected data were analysed using a POD evaluation algorithm (signal response approach) provided in (Annis, 2015).

3.4 Results and discussion

As proposed in the literature (Lin *et al.*, 2004; Lin *et al.*, 2003), in order to investigate the impact of a specific microstructural feature without the interference of grain size effect, grain size should be kept constant. To ensure that, in the current study, the grain size did not have significant effect on the acoustic parameters of the samples, a statistical evaluation of the distribution of prior austenite grain size has been performed. For each sample, optical images taken at 200x magnification were analyzed using the Clemex image analysis software to measure the cross section of austenite grains. The box-plot diagram, depicted in Figure 3.2, presents the result of the measurements (on 150 grains). The median of grain size shows a maximum variation of 6% for the four samples. It is thus confirmed that the parent grain size in all 4 samples is quite similar and unaffected by the tempering process.

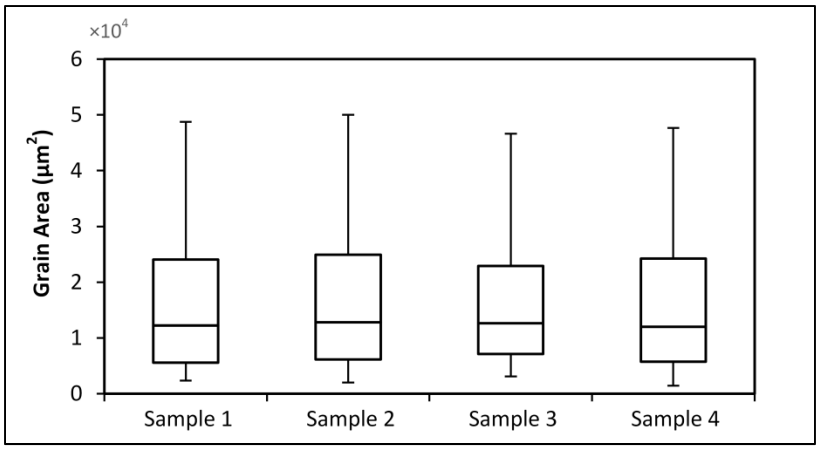

Figure 3.2 Box-plot diagram of parent austenite grain size of samples

Considering the data in Figure 3.2 and the applied ultrasonic frequencies (2.25 and 5 MHz), the ratio of mean grain size (d) to the longitudinal wavelength (λ) shows that the tests are carried out in the Rayleigh regime of scattering (λ > d) (Ensminger & Bond, 2011; Saniie *et al.*, 1988).

Tempering of martensitic stainless steel at temperatures above the Ac_1 (austenite transformation point) leads to decomposition of martensite and formation of austenite (Bilmes *et al.*, 2001). Therefore, due to diverse tempering temperatures applied to the samples, the volume fraction of austenite reformed in the microstructure after tempering is different. These reformed austenite particles are developed at the boundaries of the martensite laths, blocks and packets during the tempering heat treatment; therefore, their dimensions are similar to the dimensions of the martensite laths. By increasing the reformed austenite content, the size of particles grows and their distribution becomes more uniform. In other words, as the reformed austenite content increases in the microstructure, γ-particles tend to fuse together to form elongated austenite platelets (Amrei *et al.*, 2016). On the other hand, the tempering process mitigates the level of lattice distortion and residual stresses in the martensitic microstructure (Krauss, 2015). The reformed austenite content obtained by XRD evaluations, using the Rietveld method, on the samples are presented in Table 3.3.

Table 3.3 Tempering temperature and austenite content in samples

Sample	Heat Treatment	Temperature (°C)	Time (min)	Austenite Content (%)	Hardness (HRC)
1	Austenitization + tempering	1100+560	60+90	1	28.9
2	Austenitization + tempering	1100+600	60+90	5	26.7
3	Austenitization + tempering	1100+640	60+90	8	23.4
4	Austenitization + double tempering	1100+680+620	60+90 +90	20	22.2

As represented in Figure 3.3, the results of microhardness measurements are in accordance with the reformed austenite content. In other words, the tempering heat treatment mitigates the level of residual stresses and lattice distortion in the martensite phase and promotes the diffusion-based process of austenite formation which consequently decreases the hardness of the microstructure. Therefore, sample 4 possesses the lowest hardness while the highest value belongs to sample 1. This is in agreement with the results of Bilmes *et al*. (Bilmes *et al.*, 2000; Bilmes *et al.*, 2001) where the hardness is reported to be an inverse function of the γ-content. The hardness of each sample, provided in Figure 3.3, is the average of 20 readings taken at different points.

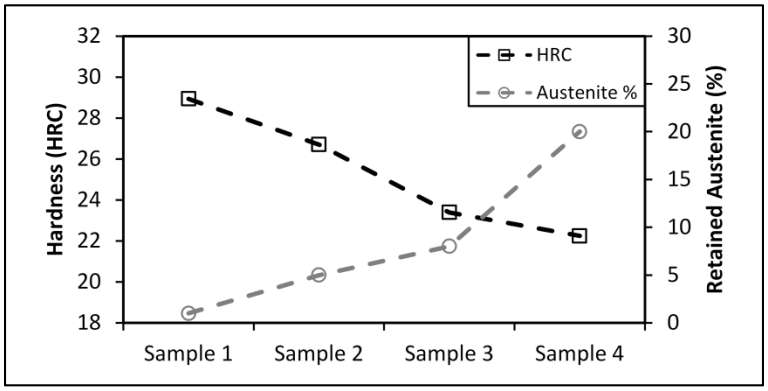

Figure 3.3 Microhardness measurements in HRC

3.4.1 Ultrasonic attenuation and backscattering noise

Ultrasonic wave attenuation is composed of three different contributors including scattering, absorption, and diffraction. The last phenomenon, which depends primarily on the geometry of the transducer and the wavelength of the ultrasonic perturbation, is accounted for and compensated in the following results using mathematical equations (Kino, 1987). On the other hand, the absorption coming from inelastic interactions in the material transforms ultrasonic wave into heat. In polycrystalline metals, absorption is a negligible contributor to the total attenuation as compared to the scattering (Feuilly *et al.*, 2009; Ploix, 2006; Saniie *et al.*, 1988), which is an inherent consequence of material microstructure. Scattering is generated because the ultrasonic energy is reoriented and mode converted at the multiple interfaces where acoustic impedance is discontinuous. This discontinuity could be the result of variations in the physical and mechanical properties of the adjacent media. The presence of γ-particles within the martensite (M) matrix creates scattering sites along the travelling path of the coherent ultrasonic wave. Even though, due to its extremely small size (nanometric scale), a single γ-particle is not expected to have a significant interaction with the travelling wave but the coalescence of these particles as a group as well as the large difference between the acoustic impedance of the austenite particles and martensite matrix are expected to be the source of the attenuation variation in the currently tested samples. This can be observed in the results presented in Figure 3.4. Contrary to Feuilly *et al*. (Feuilly *et al.*, 2009) who found the attenuation in an Inconel alloy to be independent of the precipitation presence, the more austenite precipitations are formed in UNS S41500, the higher the attenuation value becomes. The scattering attenuation further increases in sample 4 due to the higher γ-content and its more uniform distribution within the martensite matrix caused by the double tempering process (Bilmes *et al.*, 2009; Bilmes *et al.*, 2001). It is noteworthy that the amount of crystal distortion, residual stresses, and carbide and carbonitride content is inversely correlated with the tempering temperature and duration (Bilmes *et al.*, 2009); hence, it seems that their contribution to the attenuation is not comparable to the reformed austenite effect. As shown in Figure 3.4, at 5 MHz, the

attenuation rises with the γ-content at a greater rate due to shorter ultrasonic wavelength and accordingly more interaction with the extremely small γ-particles.

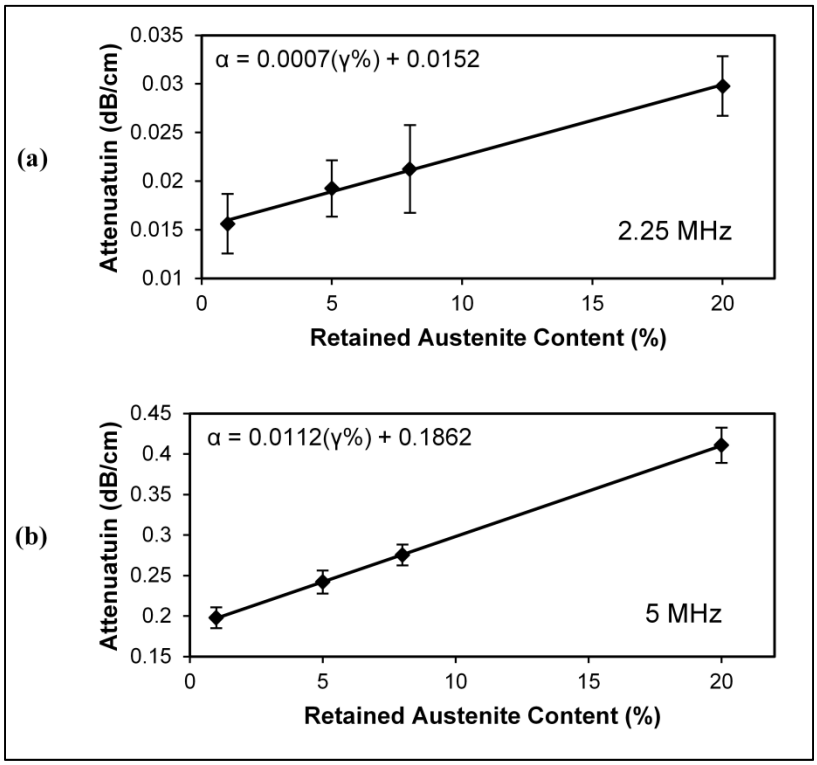

Figure 3.4 Longitudinal wave attenuation at (a) 2.25 MHz and (b) 5 MHz

To be specific, the coherent plane waves travelling in the material will be more attenuated due to the greater number of scatterers (γ-particles) and their larger cross-section (Amrei *et al.*, 2016; Bilmes *et al.*, 2001); this could be translated into an increase in the scattering induced attenuation. Freitas *et al*. (Freitas *et al.*, 2010) and Hsu *et al*. (Hsu *et al.*, 2004) reported that attenuation is directly correlated with the hardness in carbon and tempered martensitic stainless steels, respectively. Contrary to their results, the attenuation shows a negative correlation with the hardness in tempered UNS S41500 because the hardness is an inverse function of the reformed austenite (scatterer) amount which seems to be the main contributor to the rise of scattering induced attenuation in this study.

The backscattering noise level also increases with the reformed austenite content. The γ-particles reflect a portion of the wave in random directions and deviate the wave energy from its travelling path causing some part of this energy to return to the transducer as the backscattering noise. Considering the ultrasonic frequency and the size of scatterers, the experiments are in the Rayleigh region of scattering where there should be no effect of multiple scattering, as a contributor to the backscattering noise. In addition, the backscattering noise is the result of incoherent addition of the contribution of each scatterer; therefore, its amplitude does not increase significantly when the reformed austenite content increases. This is depicted in Figure 3.5 where the noise level for each sample is represented as the standard deviation (STD) of noise amplitude normalised with the one of sample 1.

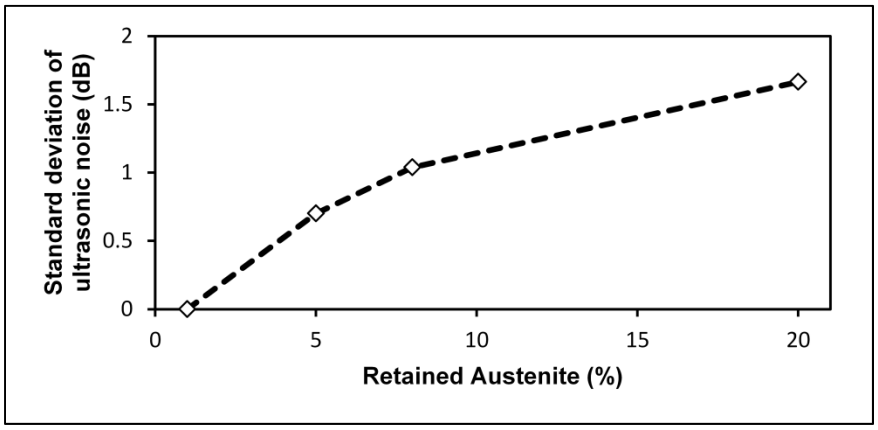

Figure 3.5 Standard deviation (SD) of the ultrasonic noise at 5 MHz

The result in Figure 3.6 shows the SNR average at the ultrasonic frequency of 5 MHz. SNR is a good metric to highlight the signal and noise amplitude change as a function of reformed austenite content. The backscattering noise level as well as the attenuation in the longitudinal wave inspection shows an increase with the reformed austenite content; however, the wave attenuation increases at a higher pace than the backscattering noise. This is to say that, in comparison with noise, attenuation is a greater contributor to the degradation of SNR with the growth of γ-content.

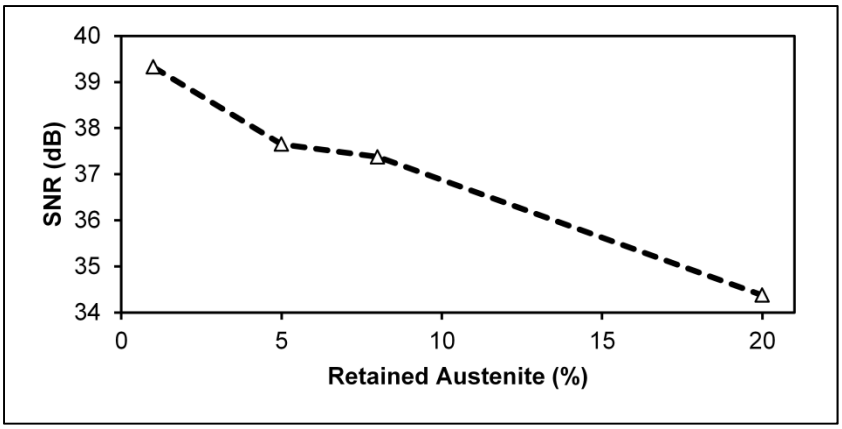

Figure 3.6 Signal-to-noise ratio (SNR) as a function of the reformed austenite content at 5 MHz

3.4.2 Ultrasonic velocity

As it can be seen in Figure 3.7, although a slightly decreasing correlation seems to appear between longitudinal wave velocity and reformed austenite amount, the significance of this correlation is dubious. According to Kruger *et al*. (Kruger & Damm, 2006), it was expected to observe a much larger reduction in the ultrasonic velocity with the formation of an increasing amount of reformed austenite (as much as 60 m/s over a 20% increase in retained austenite). This discrepancy could be attributed to the effect of tempering that relaxes residual stresses in the martensite matrix. In fact due to lower crystal distortion in the tempered martensite, ultrasonic waves will travel at higher velocities (Gür & Tuncer, 2004) so as to compensate velocity reduction caused by the presence of austenite phase.

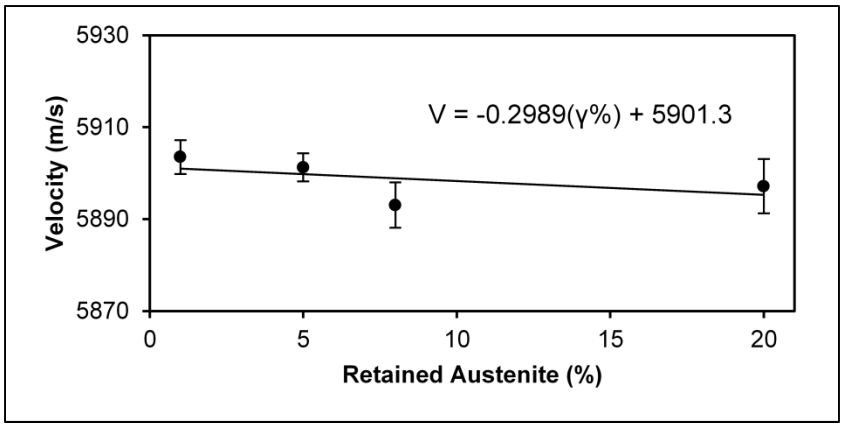

Figure 3.7 Longitudinal wave velocity at 5 MHz

3.4.3 Ultrasonic Inspection Reliability

The model-based POD evaluation was carried out for samples #1 and #4 which contain the lowest and the highest reformed austenite, respectively. Generally, signal response amplitude ($\hat{a}$) for a given defect size (a) is normally distributed around an average value ($\mu(a)$). Backscattering noise is also characterized by a probability density distribution. Any variation in the microstructure will most likely lead to a change in the average and standard deviation of both the signal amplitude and noise distributions. These two distributions are directly impacting the probability of detection (POD) and probability of false indication (POFI) values and hence to the inspection reliability.

As it can be seen in Figure 3.8, simulation results obtained with CIVA could be best fitted with a linear regression correlating $\hat{a}$ and a. Based on this, ultrasonic signal response amplitude could be described as:

$$\hat{a} = \mu(a) + \delta \tag{3.1}$$

where $\mu(a) = \beta_1 \cdot a + \beta_0$ is the mean of the distribution function for all a values, β_0 and β_1 are the linear correlation coefficients estimated by a maximum likelihood method, and

$\delta = \mathrm{N}\ (0, \sigma)$ is the random error which is considered to have a standard normal distribution (zero mean and constant standard deviation σ). This random error includes the effect of all the random factors making the inspection of a particular defect of size different from the average of all defects of the same size.

In order to limit the rejection of good components due to a higher microstructural noise, the decision threshold $\hat{a}_{decision}$ shall be adjusted accordingly (Annis, 2009). In the current work, POD curves have been computed using a decision threshold $\hat{a}_{decision}$ that results in a POFI value of 1%. Because the noise amplitude is slightly higher in sample #4, $\hat{a}_{decision}$ is somewhat higher in this case. Since POD is the probability that $\hat{a} > \hat{a}_{decision}$, it could be shown that:

$$POD(a) = \int_{\hat{a}_{decision}}^{\infty} [\mu(a) + \delta]\, d\hat{a} = 1 - \Phi\left(\frac{\hat{a}_{decision} - \mu(a)}{\sigma}\right) = \Phi\left(\frac{a - a_{50}}{\sigma / \beta_1}\right) \qquad (3.2)$$

Adapted from Georgiou (2006)

where $\Phi(x)$ is the cumulative normal distribution function and $a_{50} = (\hat{a}_{decision} - \beta_0)/\beta_1$ is the defect size that results in a POD of 50%.

As it can be seen in Figure 3.8, due to the higher γ-content of sample #4, the corresponding POD curve is displaced toward larger defect sizes. In fact, the $a_{90/95}$ value for an ellipsoidal inclusion in sample #4 shows an increase of 55.5% as compared to sample #1. This increase is principally caused by higher attenuation and noise content in sample #4. In conclusion, an increase in the backscattering noise level and in the attenuation, caused by higher reformed austenite content, has adverse effects on the reliability of ultrasonic inspection of runners' joints. The modelling phase of this research is still under progress in order to improve the semi-analytical models to increase the accuracy of the simulated POD and POFI.

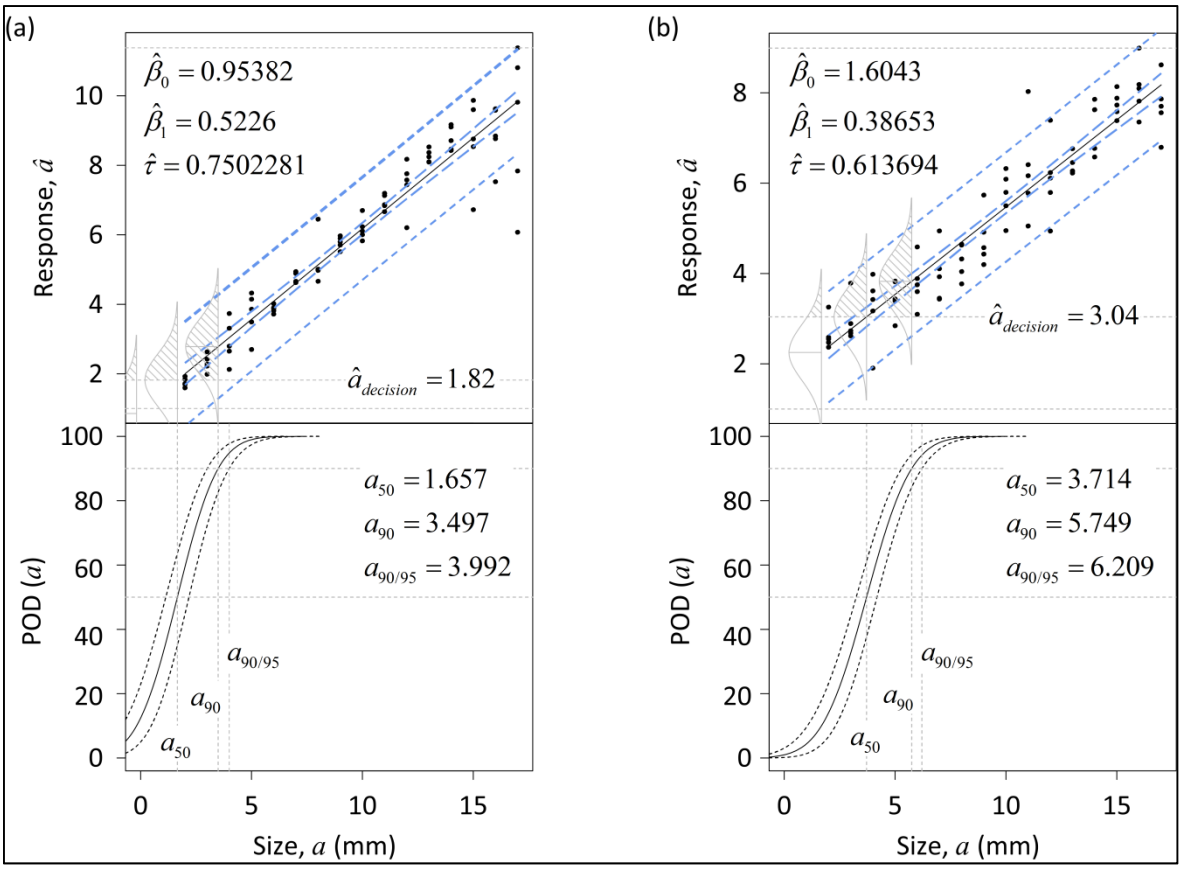

Figure 3.8 POD curves for an ellipsoidal rutile inclusion in samples with (a) 1% and (b) 20% austenite content

3.5 Conclusions

The aim of this paper was to establish a correlation between tempering heat treatment of UNS S41500 martensitic stainless steel and the outcome of ultrasonic inspections on hydroelectric turbine runners. Based on the results, the following conclusions can be drawn:

- Ultrasonic attenuation shows an increase with the volume fraction of reformed austenite in the tempered UNS S41500 martensitic stainless steel. The γ-particles cause the coherent ultrasonic amplitude to decay as a consequence of being scattered at the martensite/austenite interfaces.
- Considering the sensitivity of attenuation to the reformed austenite content, this acoustic parameter could be employed as a means for characterizing the products of tempering heat treatment in UNS S41500 martensitic stainless steels.

- Backscattering noise is directly correlated with the volume fraction of reformed austenite. However, the increase rate for the backscattering noise level is lower than the attenuation due to the fact that the noise is the result of incoherent addition of the contribution of each scatterer.
- Signal-to-noise ratio (SNR) shows an inverse correlation with the reformed austenite content. A significant 5 dB reduction in SNR was observed when the γ-content increased from 1 to 20%.
- Although ultrasonic velocity shows irregular decreasing correlation with the γ-content, the significance of this correlation is dubious. This irregularity could emanate from the competition between the tempering process of martensite phase (increases ultrasonic velocity) and the formation of γ-particles (decreases ultrasonic velocity).
- Probability of detection (POD) declines as the reformed austenite content rises. In other words, the distribution of signal and backscattering noise amplitude (the key parameters of POD and POFI) change as a function of the volume fraction of reformed austenite. The tendency of the model-based POD shows a significant increase (55.5%) in the $a_{90/95}$ with the growth of γ-content (from 1 to 20%).

Acknowledgements

This work was supported by the Fonds de recherche du Québec - Nature et technologies (FRQNT) and the Natural Sciences and Engineering Research Council of Canada (NSERC). The authors gratefully acknowledge the support of Institut de recherche d'Hydro-Québec (IREQ) and Andritz Hydro Inc. The authors would also like to express their gratitude to Demartonne Ramos França, Stéphane Godin, Étienne Dallaire, and Alexandre Lapointe for many discussions and their technical assistance. The POD statistical analysis performed in this work made use of mh1823 package developed by Charles Annis.

CHAPTER 4

CASE STUDY ON THE INTEGRITY AND NONDESTRUCTIVE INSPECTION OF FLUX-CORED ARC WELDED JOINTS OF FRANCIS TURBINE RUNNERS

Hamid Habibzadeh Boukani[a], Martin Viens[a], Souheil-Antoine Tahan[a], and Martin Gagnon[b]

[a] Department of Mechanical Engineering, École de technologie supérieure (ÉTS), Montréal (Québec), H3C 1K3, Canada
[b] Institut de recherche d'Hydro-Québec (IREQ), Varennes (Québec), J3X 1S1, Canada

Paper submitted to the International Journal of Advanced Manufacturing Technology, November 2017

Abstract

The welded joints of hydraulic turbine runners have a higher failure probability than other runner regions due to the inevitable presence of welding flaws and dynamic stress concentrations. Welding processes are always associated with flaws caused by technical or metallurgical factors. In order to lower the failure probability, critical welding flaws should be detected and removed before the runner commissioning; otherwise, they will propagate under dynamic stresses and endanger the structure before it reaches its expected life. In such a case, the electricity production process should be halted and a mandatory unplanned maintenance should be applied. The production halt and the maintenance process (or runner replacement) impose high costs to the utility owner. A remedy to this is to have prior knowledge of potential welding flaws so as to select proper nondestructive testing (NDT) methods to detect and characterize them. In addition, better characterization of the potential flaws and their dimensions leads to more precise life estimations. In this study, different NDT methods are used on a series of T-joints designed to be representative in scale of real turbine runner joints. The outcomes of these methods are compared and used to characterize some of the detected indications. In order to confirm NDT results, part of the joint containing a targeted indication has been extracted to undergo detailed evaluations. The objective is to provide detailed information on some common welding flaws in hydraulic turbine runners and to discuss the capability of different NDT methods used to characterize such flaws.

4.1 Introduction

In some applications, flux cored arc welding (FCAW) is preferred as compared to gas metal arc welding (GMAW) and shielded metal arc welding (SMAW) due to its high deposition rate. In addition, FCAW has the flexibility of using shielding gasses and fluxing materials with continuous metal wires (Kou, 2003; Starling *et al.*, 2011; Tümer & Yılmaz, 2016). FCAW is found to be a very efficient and productive method because it allows the deposition of the high volume of filler material required for joining the thick sections of hydraulic turbine runners in non-flat welding positions.. However, as with other welding methods, FCAW is susceptible to welding imperfections originating from several sources including welding thermal cycles, impurities in the weld zone, and technical and human factors. Even though a shielding gas protects the weld pool in the FCAW process, the oxidation phenomena in the arc is not completely eliminated because the shielding gas commonly contains a certain amount of CO_2 mixed with Argon to achieve higher arc stability, welding speed, and penetration as well as a desired mode of metal transfer (spray transfer) (Bauné *et al.*, 2000; Tümer & Yılmaz, 2016). Therefore, as a result of CO_2 dissociation in the arc, oxygen is always present, reacts with some of the elements in the welding zone, and forms oxide compounds. Additionally, the FCAW wire electrodes contain a flux core which is composed of several metallic and non-metallic compounds including oxides of silicon, titanium, zirconium, etc. These two groups of oxides form slag floating on the molten metal and protecting the hot weld metal from the air during cooling; however, the oxides may be driven into the weld metal by the arc force and get entrapped creating inclusions (Bauné *et al.*, 2000; Pamnani *et al.*, 2016; Quintana *et al.*, 2001; Tümer & Yılmaz, 2016; Zhu *et al.*, 2016). Furthermore, in multipass welds, the slag covering a weld bead should be completely removed after cooling through an interpass cleaning process so as to avoid contamination of the subsequent weld passes with non-metallic inclusions. Generally, in multipass welded joints, (1) inadequate accessibility (for cleaning) at weld toes due to inappropriate weld overlap and (2) insufficient heat input of subsequent pass to melt the remaining slag could induce interpass slag inclusions (Caron & Sowards, 2014; Habibzadeh Boukani *et al.*, 2014; Salvador & Antunes, 2016).

The life of martensitic stainless steel runners is mainly limited by the fatigue phenomena due to the dynamic mechanical stresses experienced during service. Fatigue life models, based on the fracture mechanics concept, have been developed to estimate the service life of in-service runners (Gagnon *et al.*, 2013). In these models, the damage tolerance approach is used to determine the maximum imperfection size which could be tolerated in the structure without causing failure during the planned service life. In such an approach, the classical accept/reject criteria of NDT methods are not that useful; instead, flaws in the critical regions should be detected and characterized in more quantitative rather than qualitative manner (Habibzadeh Boukani *et al.*, 2014; Thompson & Thompson, 1985). Flaw characteristics including size, position and geometry and their associated uncertainties are considered to be of high importance for fatigue reliability models (Gagnon *et al.*, 2014). With a more accurate estimation of flaw size, a more precise estimation on the remaining life could be obtained leading to less unexpected failure and unnecessary downtime, both of which impose high costs to the utility owner. Moreover, knowing the type of common flaws also helps to optimize the welding process parameters in order to avoid those flaws in the first place (Song, 1991).

For Francis runners, the welded joints at the blade/crown and blade/band interfaces are the most critical zones where the highest stress concentration occurs (Coutu *et al.*, 2004; Frunzăverde *et al.*, 2010; Huth, 2005; Saeed & Galybin, 2009). Due to the preceding fact and the susceptibility of joints to contain welding flaws, it is crucial to meticulously investigate the integrity of these zones using NDT methods. Prior knowledge of the positions and characteristics of welding flaws helps to select the most proper and reliable NDT methods for specific locations.

In hydraulic turbine runners, NDT techniques for surface and near-surface inspection such as visual, penetrant and magnetic particle testing are normally used. As a complement, manufacturers also use conventional ultrasonic testing (UT), involving a series of different beam angles, and radiographic inspection to target internal flaws (Adamkowski, 2009; Xiao *et al.*, 2013). These two methods are prone to have detection difficulties as a result of

complex surface contour and variable thickness of runner joints (Yicheng *et al.*, 2011). On the other hand, inspired by its capabilities in the inspection of complex shape structures, phased-array ultrasonic testing (PAUT) has attracted the experts' attention in the hydraulic turbine field (Yicheng *et al.*, 2011). This method offers several advantages in thick-section welds by electronically sweeping the beam angles in a quick and repeated manner; this in turn leads to covering a larger weld area, enhancing the detectability of randomly oriented flaws, and decreasing the inspection time (Ditchburn & Ibrahim, 2009).

Even though some investigations have been carried out on the application of NDT on hydraulic turbine runners (Xiao *et al.*, 2013; Yicheng *et al.*, 2011; Zhang *et al.*, 2014), the researchers mainly used intentionally seeded defects in their samples and inspection models. These defects are not always based on representatives of real welding flaws. This study aims at investigating some real welding defects in runner joints so as to evaluate their characteristics and detectability.

4.2 Experimental procedure

4.2.1 Complete T-joint sample – Manufacturing and nondestructive inspection

A series of T-joint specimens (as shown in Figure 4.1) was manufactured in martensitic stainless steel (UNS S41500) according to the requirements of turbine runners. The welding was made using a multipass FCAW process with a mixture of Ar- CO_2 as the shielding gas. Moreover, specific requirements for preheating, interpass, and post-weld heat treatment were considered to decrease the hardness of the welded joint and to improve its toughness. The chemical composition of both base metal and filler material is given in Table 4.1.

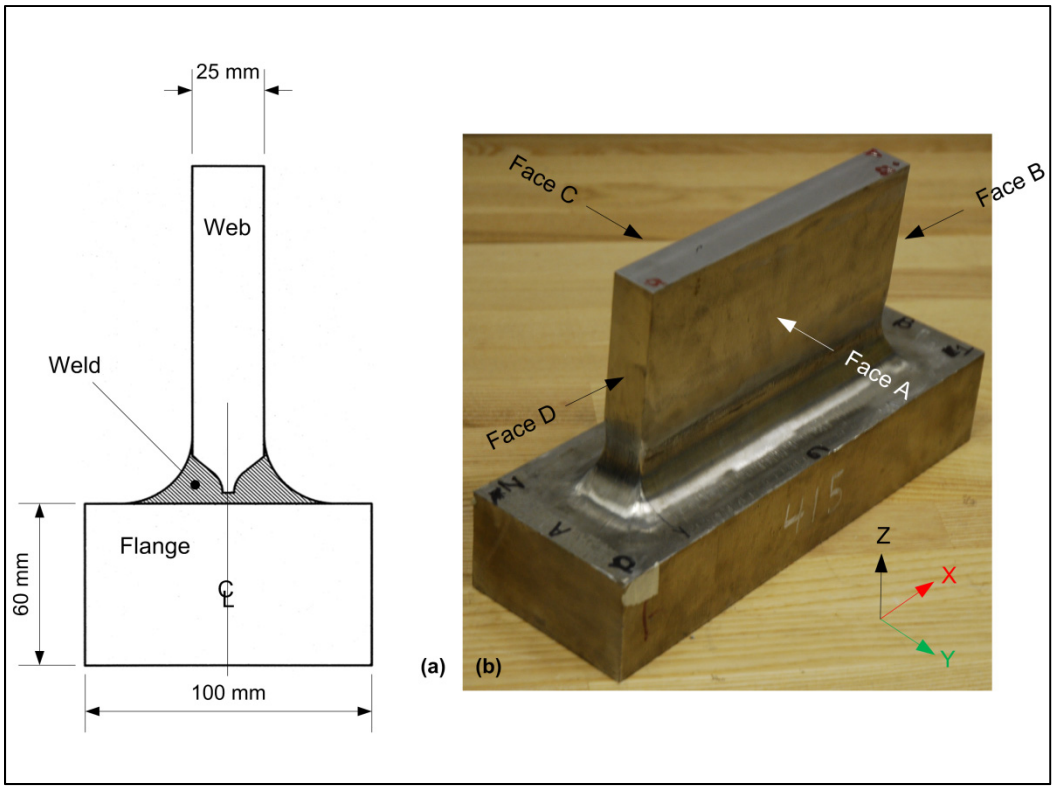

Figure 4.1 (a) Schematic representation of the T-joint and (b) designation of its faces

Table 4.1 Chemical composition of the base metal and the filler material

	Fe	C	Cr	Ni	Mo	Mn	Si	P	Cu
Base metal	Balanced	0.03	12.5-12.9	3.6-4.0	0.4-0.5	0.7	0.4	0.02	0.09
E410NiMo	Balanced	0.06	11.0-12.5	4.0-5.0	0.4-0.7	1.00	0.9	0.04	0.75

Once the specimens were manufactured according to the requirements, they were inspected using NDT methods to verify their integrity. First, magnetic particle inspection (method T in Table 4.2) was applied to the specimens. This was followed by conventional ultrasonic inspection using 45°, 60°, and 70° refracted shear waves (method U in Table 4.2); the inspection was carried out by scanning over the web of the T-joint, which represents the accessible surface in turbine runner for UT. Once the aforementioned inspections were followed as requested by the production procedure, some supplementary NDT methods - including conventional and computed radiography (method V in Table 4.2) as well as phased-array ultrasonic testing (method W in Table 4.2) - were applied.

Table 4.2 NDT methods applied on the T-joints

#	**Inspection method**	**Scanned surface**
T	Magnetic particles (MPI)	--
U	Conventional refracted ultrasonic shear waves	Web
V	Conventional and computed radiography	--
W	Manual phased-array ultrasonic (industrial standards)	Web
X	Manual phased-array ultrasonic (in-house method)	Web
Y	Immersion ultrasonic (in-house method)	Flange
Z	Manual phased-array ultrasonic (in-house method)	Flange

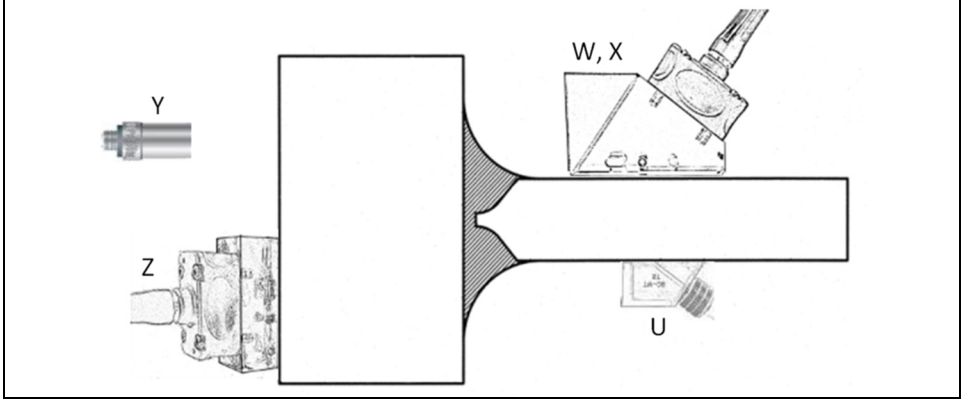

In our study, phased-array (methods X and Z in Table 4.2) and immersion ultrasonic (method Y in Table 4.2) tests were carried out using procedures developed in-house. These methods were mostly planned (1) to characterize the previously detected indications in more details and (2) to look for further potential flaws which may have been missed using the previous methods.

4.2.2 Extracted sample – Destructive inspection of a specific flaw

In order to correlate nondestructive inspection results with macro and micro scale flaw properties, a specific indication was investigated using a destructive slicing process. Because of the limited capacity of the slicing machine, part of the flange and the web were removed. To avoid machining through the corresponding discontinuity, cutting locations were

determined using the results of the NDT methods. According to this intent, a 25 mm-long sample containing the targeted indication was extracted from the T-joint. The selected sample is shown as #1 in Figure 4.2(a). Afterwards, a precision slicing was used to make slices out of this sample with a nominal thickness of 1.5 mm, as depicted in Figure 4.2(b). Both faces of the precision slices were used to characterize the geometry and the type of flaw that produced the aforementioned indication.

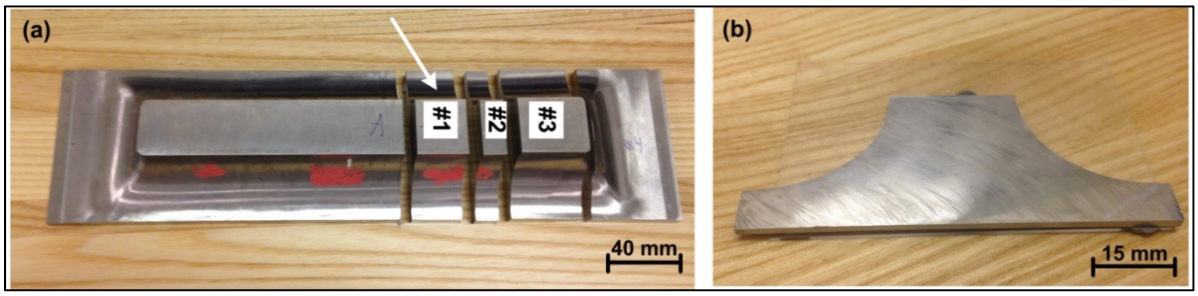

Figure 4.2 Principal cuts on the machined T-joint showing extracted samples used for destructive inspection and (b) one of the 1.5 mm thick slices cut-off from sample #1

Metallographic evaluations in macro and micro scales were applied on the as-sliced, sliced/polished, and sliced/polished/etched samples using optical microscopy (OM) and scanning electron microscopy (SEM). The samples were evaluated at different stages to make sure that the destructive mechanical processes would not change the discontinuity's properties. Furthermore, energy-dispersive X-ray spectroscopy (EDS) was used to reveal the principal constituent elements of the flaw. Finally, X-ray microtomography (CT) was applied on three of the slices, through which the indication is completely contained, to reconstruct the flaw geometry and dimensions.

4.3 Results

4.3.1 Nondestructive inspections

A group of applied NDT methods (including X, Y, and Z) reports the presence of a flaw on the centreline of the T-joint at the flange/weld interface. The outcome of the immersion

ultrasonic inspection (method Y) which is carried out using a 5 MHz flat transducer (∅10 mm) scanning the weld from the flange face is shown in Figure 4.3. The C-scan representation in Figure 4.3(a) provides a view from the bottom face of the flange; the vertical box indicates sample #1 which was extracted from the T-joint. According to these results, a series of discontinuities more or less aligned with the joint centreline at a depth approximately equal to the flange thickness is observed. Due to its features (including size, position and orientation), the indication pointed out by the arrow is not detected by the standard NDT methods (T to W). However, the better accessibility to the welded joint from the flange face enables method Y to reveal the presence of a clear discontinuity in the aforementioned location.

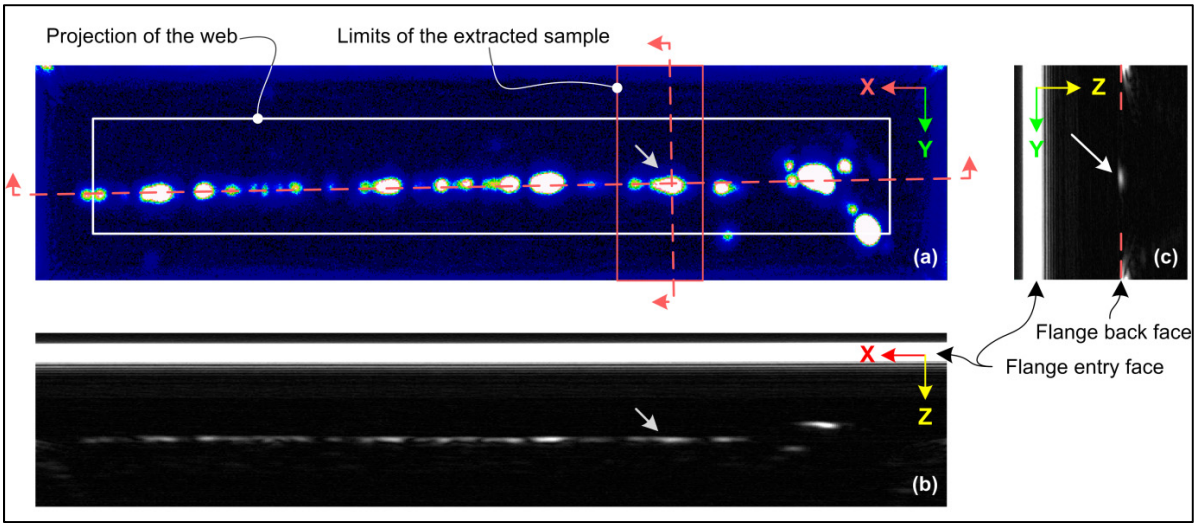

Figure 4.3 Results of method Y (a) C-scan representation; (b) and (c) B-scan representation on a plane passing through the selected indication parallel and normal to the x-axis, respectively

For method Z, two different scanning configurations have been considered: E-scan and S-scan. In the first one, longitudinal waves (L-waves), focused at the welded zone, are linearly swept under the probe footprint while the probe is located on the flange. Probe orientation is selected to sequentially align the sweeping direction at 0° and 90° with respect to the weld axis. As depicted in Figure 4.4(a), the first direction yields an image similar to the B-scan obtained by method Y around the selected discontinuity (Figure 4.3(b)). Using the

perpendicular direction (Figure 4.4(b)), the position of the indication center relative to the T-joint centreline is found to be in accordance with the immersion results from Figure 4.3(c). In addition, as shown in the refracted shear waves sectorial scan (S-scan) of Figure 4.4(c), the flaw indication is maximized at an angle of 52° relative to the normal of flange face.

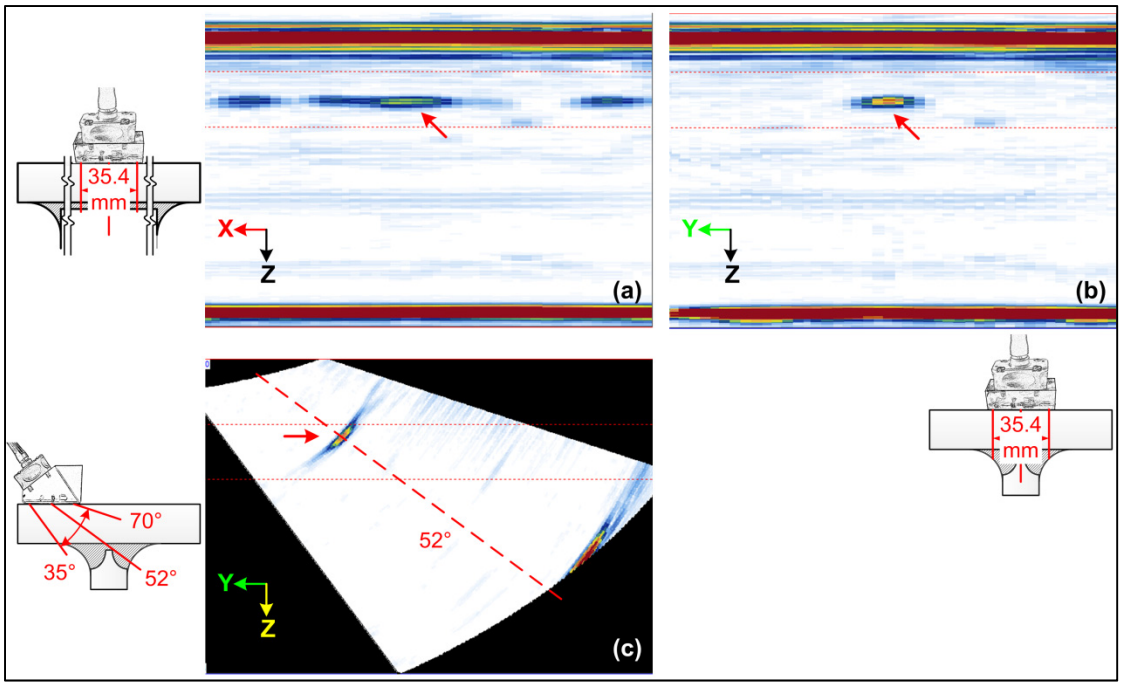

Figure 4.4 (a) and (b) E-scan and (c) S-scan results obtained with method Z in the vicinity of the selected flaw. The arrows point out the flaw indications

Method X is a phased-array ultrasonic testing (PAUT) inspection within which a 64 elements transducer of 5 MHz scans the weld over the web faces. With this method, refracted shear waves are swept from 35° to 70° as shown in Figure 4.5. On face C (Figure 4.5(a)), an indication was observed on the first half-skip at a refracted angle ranging from 65° to 69° with respect to normal. However, on face A (Figure 4.5(b)), a much smaller signal is received on the first half-skip at a refracted angle of 70°. On the second half-skip, while on face A (Figure 4.5(d)), a clear indication is found at a 55° refracted angle. On the contrary, from face C (Figure 4.5(c)), the flaw's signal is not resolvable from the noise.

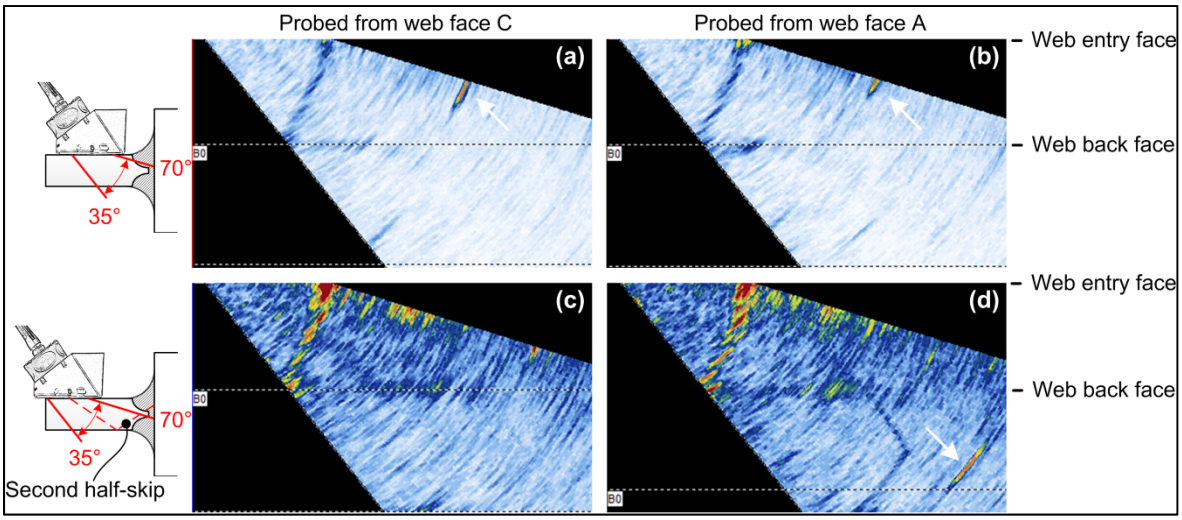

Figure 4.5 PAUT results at two different distances from the weld axis on web faces. The arrows point out the flaw's indication

Based on the outcome of NDT inspections around the selected indication, it is suspected to be due to an inclined lack of penetration (LOP) at the flange/weld interface on the centreline of the T-joint where lack of appropriate accessibility during welding could promote the formation of LOP. In order to validate such a hypothesis, a planar flaw representing the LOP is inserted at the flange/weld interface of a CIVA simulation model (Dib *et al.*, 2016). The semi-analytical results, provided in Figure 4.6, yield similar signals to the experimental PAUT results shown in Figure 4.3. Since the LOP is not perpendicularly oriented relatively to the incident waves direction, it won't reflect the shear waves back to the transducer; however, signals diffracted by the extremity of the planar flaw (tip diffracted signals) could be received by the transducer because they are spherical waves.

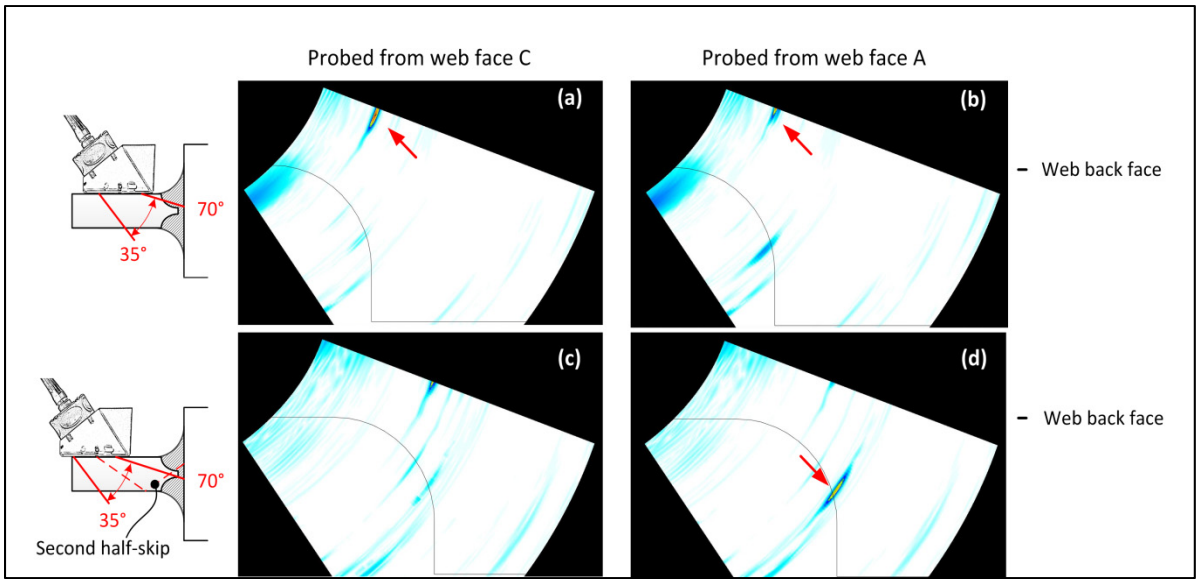

Figure 4.6 Simulation of PAUT results at two different distances from the weld axis on web faces; the gain for images (c) and (d) is higher than for images (a) and (b)

4.3.2 Destructive tests

After the principal cutting, optical microscope (OM) images on both faces of sample #1 show no indication of welding flaws. This confirms that the initial cut do not pass through any observable welding flaws.

As depicted in Figure 4.7, following the precision slicing process, the targeted flaw could be clearly observed on three consecutive slices at the flange/weld interface. This flaw, which is labelled as D1, seems to be a semicylindrical void partly filled with inclusion. Its boundary offers a roughly planar surface aligned with the one revealed after gouging. Microtomography evaluations of the three consecutive slices reveal that D1 forms a wormhole shape aligned with the weld axis and that its bottom boundary keeps a roughly planar surface through the thickness of the slices, as represented in Figure 4.7. The distance between the adjacent slices represents the part of material lost due to the thickness of the cutting wheel used for precision slicing. In addition, on the face of the slice depicted on Figure 4.7, another flaw (D2) is observed. As compared to D1, D2 is smaller in size and closer to the weld surface. Etching process reveals that this discontinuity occurs at the

boundary between two adjacent weld beads where the columnar grains of the new weld bead is separated from the fine microstructure of the high temperature heat affected zone (HT HAZ) which is located in the previous weld bead (Amrei *et al.*, 2015). Since D2 was not detectable through the different NDT inspections performed previously, there was no preplanned slicing program to study this discontinuity.

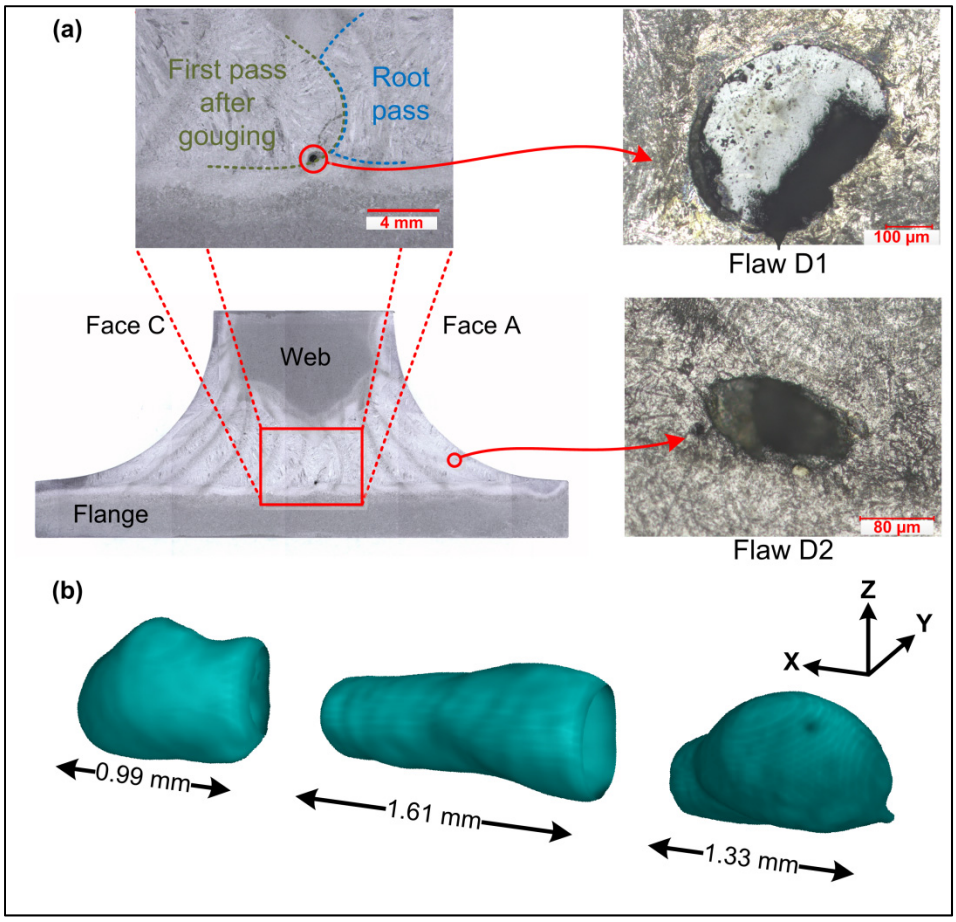

Figure 4.7 (a) Macrograph of a typical slice on which the targeted flaw (D1) and a previously undetected flaw (D2) could be observed; (b) 3D representation of CT results showing the shape of D1 in three consecutive slices

Further investigations, including EDS and microtomography, were carried out on D1 and D2 in order to determine their characteristics. According to the EDS results on D1 (Figure 4.8), the inclusion is found to be rich in titanium and oxygen and it also contains zirconium and

silicon. Moreover, almost no iron and nickel content is detected in the inclusion; however, these two elements are easily found in the base and weld metal adjacent to the inclusion. It is useful to note that elements detected in the inclusion (Ti, Zr, Si, and O) are all constitutive of the core flux of rutile FCAW electrodes (Quintana *et al.*, 2001).

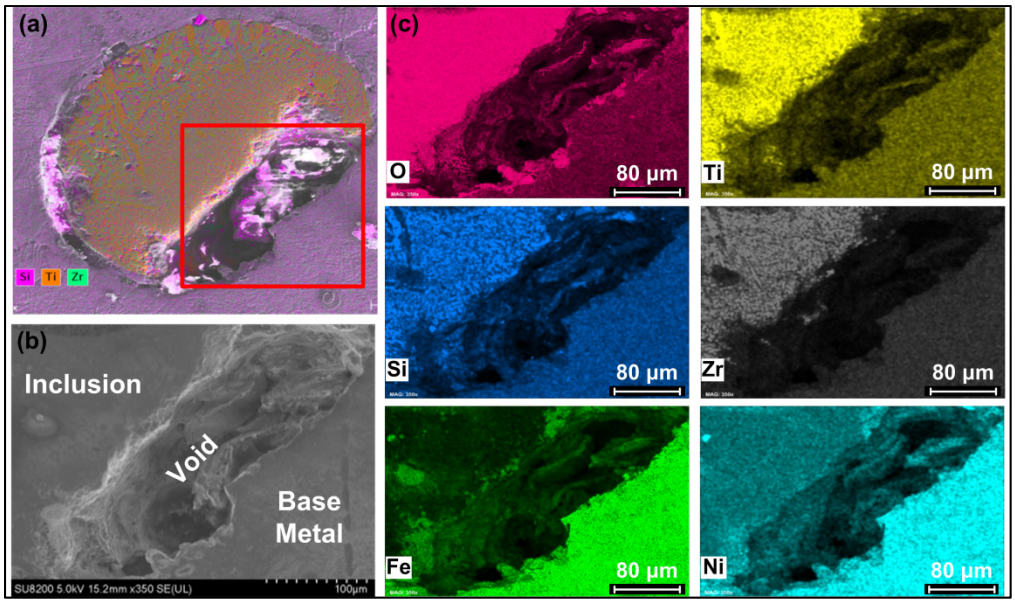

Figure 4.8 SEM image of (a) the D1 flaw and (b) the area determined by the red square in (a); and (c) EDS results showing the concentration of different elements in the inclusion

4.4 Discussion

Rather than being a LOP, the OM (see Figure 4.7) and SEM (see Figure 4.8) images reveal that D1 is an inclusion combined with a void at the interface of the back gouged groove. This inclusion which mainly contains titanium, oxygen, zirconium, and silicon is believed to originate from an external source because neither Ti nor Zr content is reported in the chemical composition of the base and filler (E410NiMo) metals (see Table 4.1). Furthermore, any Ti content in the chemical composition of martensitic stainless steels has a strong tendency to form carbides, carbonitrides Ti(C, N), or intermetallic compounds in the microstructure (Quintana *et al.*, 2001; Rodrigues, Lorenzo, Sokolowski, Barbosa, & Rollo, 2007). Generally, silicon, titanium and zirconium are added to the electrode flux to mainly

play a deoxidizing role and reduce the oxygen content in the weld metal by forming oxide compounds floating on top of the weld pool (Bauné *et al.*, 2000; Quintana *et al.*, 2001; Svensson, 1993). The oxidation occurs predominantly in the droplet stage leading to transfer of the aforementioned elements to the slag (Bauné *et al.*, 2000; Iwamoto, 1983; Kou, 2003; Tümer & Yılmaz, 2016). Moreover, Zr and Ti are very strong oxide formers with very stable oxides, even at high temperatures, that do not easily decompose in the weld metal (Howard, 2006; Iwamoto, 1983; Lu, Fujii, Sugiyama, Tanaka, & Nogi, 2002). Accordingly, since no trace of either intermetallic compound between titanium and nickel or titanium carbides is found in D1 inclusion, it could be concluded that D1 originates from the molten slag/flux entrapped in the weld pool (Zhu *et al.*, 2016). As also mentioned by Boukani *et al.* (Habibzadeh Boukani et al., 2014), in the multi-pass welded joints of martensitic stainless steel turbine runners, slag inclusion is one of the most expected flaws that could be formed from either entrapment of slag or incomplete interpass cleaning. In the latter case, the slag is not transferred to the surface of the new weld pass unless the heat input is high enough to partially melt the previous pass.

Due to its higher melting point, the entrapped molten slag composed of Si, Ti ,and Zr oxides solidifies earlier than the rest of the weld pool (Kim, Kim, Kim, Lee, & Yang, 1996). Based on the flaw's semi-cylindrical shape and its bottom planar boundary, it could be assumed that the molten slag started its solidification from the back gouged surface (see Figure 4.9). The tendency to form this type of flaw is higher in the first weld bead after the back gouging due to the following: high solidification rate of the weld metal, inappropriate back gouged groove geometry, and particular direction of weld pool flows. Indeed, the large "combined thickness" (heat sink effect) at the T-joint root and large depth-to-width ratio of the weld bead caused by the small back gouged groove dimensions promotes high heat transfer rate and hence fast solidification (Kou, 2003; Lancaster, 1997). It should also be noted that the presence of sulfur and oxygen, as surface-active agents, in the weld pool causes the Marangoni convection to become inward and downward. Therefore, the combined effect of the direction of Marangoni convection with higher solidification rate does not allow the inclusion to move to the top of the weld bead (Kou, 2003; Lu *et al.*, 2002). In short, the

preceding facts strengthen the hypothesis that the slag in the welding puddle gets entrapped in the inadequately prepared back gouging groove. Similar observations for the FCAW process are reported by other researchers (Arivazhagan & Kamaraj, 2011; Arivazhagan, Sundaresan, & Kamaraj, 2008; Matos; Salvador & Antunes, 2016).

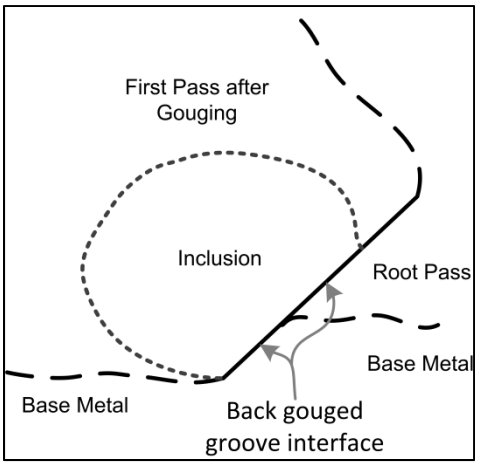

Figure 4.9 Schematic identifying structures surrounding the inclusion

As a consequence of the solidification and cooling contractions in the weld region, D1 loses its bonding with the metal at the back gouged interface and creates shrinkage induced void which appears as a lack of fusion. Figure 4.10 shows that the aforementioned void is in the form of an inclined plane at an angle of 35° to 40° relative to the web faces.

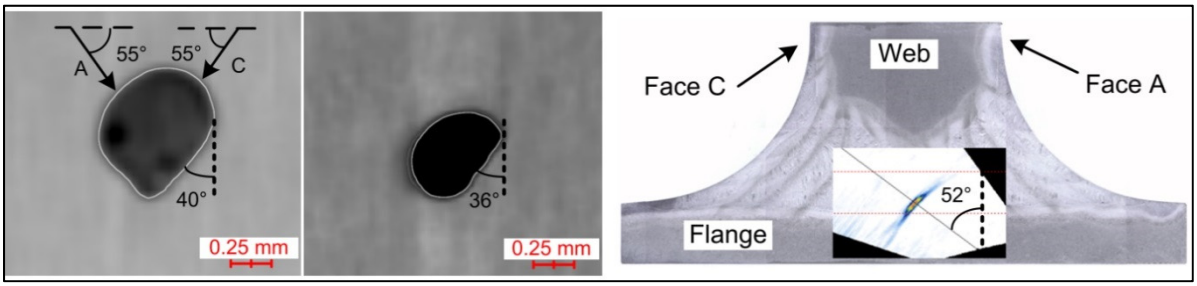

Figure 4.10 (a) and (b) CT results representing D1 shape on two different cross sections inside the slices; the arrows in (a) show the second half-skip access to D1 from A and C faces; (c) results of method Z superimposed on a slice of the T-joint

Similar investigations were carried out on D2. According to (1) the presence of the particles rich in Si, Zr, Ti, and oxygen in D2, (2) its position at the boundary of two adjacent weld passes, and (3) its non-spherical geometry, as depicted in Figure 4.7(a), this flaw is most likely a slag inclusion emanated from inadequate interpass cleaning process.

Not surprisingly, MPI (method T), which is a surface and near-surface inspection method, is not capable of detecting D1 due to its small cross section as well as its substantial depth (almost 20 mm) from the surface. In addition, method V (radiography) does not reveal any indications as a result of a very small contrast (ratio of defect size over the sample thickness) and the varying thickness of the joint which results in a significant film density gradient. As depicted in Figure 4.11, although the flaw position is accessible through the first half-skip of the 70° beam as well as the second half-skip of the 60° beam, methods U and W do not find either recordable nor rejectable indications. This seems to be due to the set-up sensitivity of the methods that was too low to get a large enough signal level. Indeed, based on the standard used, ultrasonic inspection gain was adjusted at +6 dB over the reference gain that is required to bring the signal reflected by a ∅2.38 mm side drilled hole to 80% FSH (Full Screen Height). It is noted that D1 size is thus less than one fifth of the diameter of the calibration reflector used to adjust system gain.

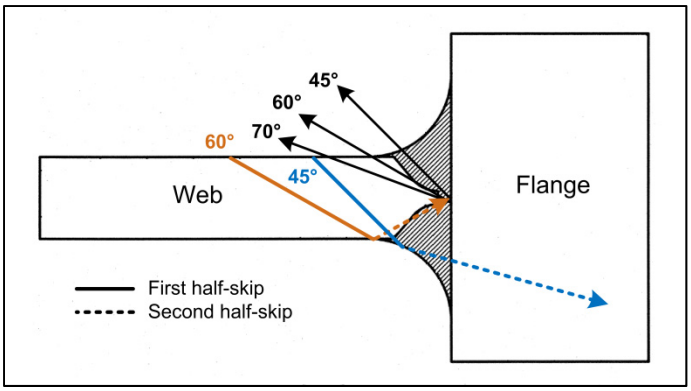

Figure 4.11 Access to the position of D1 on the first and second half-skip of 45°, 60°, and 70°

Similar to method W, method X is a PAUT inspection using an interval of refracted S-waves ranging from 35° to 70°. However, larger inspection gains are used in order to lead to higher sensitivity. Because of this, the reflection from D1 is now detectable from both A and C web faces. The gain required to bring the indication at 80% FSH is 5.1 dB lower when the inspection is carried out on the first half-skip from face C which shows that D1 has better accessibility from face C and it possesses larger cross section normal to the beam coming from this face (see Figure 4.10(a)). It is noteworthy that due to the constraints imposed by the size of the employed PAUT wedge, the lowest refracted angles cannot access the flaw position on their first half-skip because, to do that, the transducer would require to be seated on the curved surface of the weld joint. This makes D1 accessible only to the very last focal laws of the applied configuration from face C. The general orientation of D1 could be better estimated by comparing the results of the second half-skip scans (see Figure 4.5(c) and (d)); while scanning from face C yields almost no detectable indication, a clear indication is received at 55° beam from face A. Such a result indicates that a rather large cross section blocks the ultrasonic beam in this direction, as shown in Figure 4.10(a).

Additional information about D1 could be deduced from method Z results. Indeed, as depicted in Figure 4.4, the peak amplitude of ultrasonic signal was obtained for an angle of 52° which is the complementary angle of 38°. This is completely in accordance with the

outcome of destructive tests reporting an inclination of 35° to 40° for D1 relative to the web faces, as shown in Figure 4.10(c).

4.5 Conclusions

- Due to the FCAW process used to manufacture hydro turbine runners, slag inclusions are expected to happen as a result of (a) incomplete interpass cleaning and (b) entrapment of the slag in the weld bead.
- The presence of silicon, titanium, zirconium, and oxygen in the EDS results of D1 supports that the detected inclusion is an entrapped slag.
- The weld passes with elevated depth-to-width ratio are more prone to entrapped slag inclusion due to (a) higher heat transfer to the neighbouring metal and hence faster cooling rate and (b) interruption of welding flows.
- The back gouging process could create tiny grooves where the slag is entrapped and hence a slag inclusion at the weld/base metal interface can be formed. As a consequence of cooling contractions, the entrapped slag could lose its bonding with the metal and creates planar voids which are more dangerous flaws in terms of fatigue. Besides, excessive interpass grinding could also lead to a similar phenomenon.
- The semi-planar interface and particular orientation of D1 indicate that the inclusion remains in contact with the surface of the back gouged groove during the solidification of the weld metal. The tomography results reveal that D1 keeps the aforementioned shape and orientation along its length parallel to the weld axis.
- It is probable that lack of knowledge on the common flaw types in a given structure yields erroneous interpretation of their severity in terms of fatigue induced structure degradation.
- Conventional UT methods applied on the runners according to the requirements of current standards are not capable of detecting D1. In addition, D2 is not detectable by any of the NDT methods due to its size, position, and orientation. Changing the

calibration process and the inspection gain of conventional ultrasonic testing would help to detect D1.

- The in-house PAUT methods are capable of revealing the presence of D1 and, furthermore, they successfully characterize the orientation of this class of welding flaw.
- Although, a conventional method with a modified calibration process could detect D1, the inspection time would be significantly longer compared to PAUT. This is due to the time required for changing the wedges to achieve different beam angles and for recalibrating the inspection system.

Acknowledgements

The authors gratefully acknowledge the financial support of the Fonds de recherche du Québec - Nature et technologies (FRQNT), the Natural Sciences and Engineering Research Council of Canada (NSERC), the MITACS accelerate program, Institut de recherche d'Hydro-Québec (IREQ), and Andritz Hydro Inc. The authors also wish to acknowledge Ehsan Mohseni, Stéphane Godin, and Alexandre Lapointe for many discussions and their technical assistance.

CONCLUSION

In this thesis, we have tried to study the capability of different NDT methods in detection and characterization of welding flaws in hydro-turbine runner joints. The fatigue model developed by the Institut de Recherche d'Hydro-Québec (IREQ) requires accurate input values, including the initial flaw characteristics in critical zones, in order to yield reliable estimations of the remaining life of runners. In order to accurately define the flaw characteristics in the welded joints of runners, the following questions should be answered:

- How reliable are different NDT methods in characterization of common welding flaws located in runner joints?
- What are the influencing parameters on the reliability of NDT methods in this application?
- Where are the blind zones of inspection located? How is the role of these zones incorporated in the life estimation models?

Considering the aforementioned problems, we have helped to answer the following questions in this thesis:

- Chapter 2: How do the different microstructures of the mostly used steel grades in runner production, ASTM A27 and UNS S41500, affect the ultrasonic inspection?
- Chapter 3: What is the effect of tempering heat treatment on the acoustic properties of UNS S41500 martensitic steel and the resulting POD curve of ultrasonic inspection?
- Chapter 4: How are different NDT methods compared in terms of detecting welding flaws in runner joints? What are the most common welding flaws in runners?

Contributions

Chapter 2 devoted to the evaluation of two steel grades, widely used for the manufacturing of hydro-turbine runners, in terms of their acoustic properties as one of the influencing parameters on the ultrasonic inspection of runners. The goals were to make a comparison between the reliability of ultrasonic inspection of these grades and to have more realistic

values for the ultrasonic inspection simulations, as well. The results showed that the pearlitic-ferritic microstructure of A27 grade is more attenuating than the martensitic microstructure of S41500 since, in the former grade, more elevated amount of energy is removed from the ultrasonic beam by the scattering effect occurring at the interface of ferrite/pearlite phases.

The backscattering ultrasonic noise was also found to have higher values in the A27 grade which is due to the large acoustic impedance mismatch between the pearlite and ferrite grains. In other words, the high mismatch between the neighbouring grains contributes to the increase of scattered energy at each grain interface and they will add up together to make a larger backscattering noise. The two aforementioned phenomena, growth of attenuation and noise content, will displace the signal distribution toward lower values and increase the standard deviation of noise distribution, respectively. Therefore, our major contribution was to show that the signal to noise ratio (SNR) in the A27 material is degraded and hence the probability of false indication (POFI) and the probability of detection (POD) of flaws in this material are directly impacted. In fact based on the approach used for the reliability assessment, the degradation of SNR in the A27 grade could yield the followings:

- if a similar $\hat{a}_{decision}$ is used for both materials, POD will drop and POFI will raise for the A27 material;
- if $\hat{a}_{decision}$ is set so as to keep the POFI constant, a lower value will be set for S41500 resulting in higher sensitivity and also higher POD for a given flaw size in this material; at the same time POD decreases for the A27 material allowing for larger flaws to remain in the runner structure;
- if $\hat{a}_{decision}$ is set so as to keep POD constant for a given flaw size, POFI drastically increases for the A27 grade resulting in a higher rate of rejection of runners with noncritical flaws which in turn imposes an increase in the cost of repair and maintenance.

In chapter 3, we succeeded in creating a link between the ultrasonic inspection reliability and the tempering heat treatment of UNS S41500 martensitic stainless steel. In fact, we proved that increasing the reformed austenite content in UNS S41500 through specific tempering

processes, causes the coherent ultrasonic energy to decay more quickly since it is more significantly scattered at the martensite/austenite interfaces. The increase in scattering lowers the amplitude of the ultrasound pulse and increases the backscattering noise amplitude. In turn, this decreases the SNR of echoes from flaws and reduces the POD. This undesirable effect was demonstrated to increase with an increase in reformed austenite volume fraction.

Afterwards, in chapter 4, we improved the knowledge on the characteristics of common flaws in the welded joints of Francis runners through an experimental study on the integrity and nondestructive inspection of joints made with the same scale and the same manufacturing process as real runner joints. According to the experience of our industrial partners, slag inclusions are most likely to occur in the flux-core arc welded joints of these runners. The weld passes with elevated depth-to-width ratio are more prone to contain this flaw type. Moreover, it most likely occurs as a result of slag entrapment at the weld/base metal interface in the tiny grooves created by back gouging process. During the solidification process, planar voids which are more dangerous flaws in terms of fatigue could form due the bonding loss at the interface of solidified inclusion/metal caused by cooling contractions. Lack of knowledge on the common flaw types in a given structure could yield erroneous interpretation because dissimilar flaws with different flaw severity, in terms of fatigue, may generate similar NDT signals. Some flaws may not be detectable by any of the applied NDT methods due to their size, position, and orientation, the calibration process, and the NDT method limitations. The results showed that PAUT is one of the most efficient techniques in detecting the observed flaws due to the better access to the weld joint, the lower time amount required for the calibration and inspection (no wedge change), and its capability to better characterize the flaw orientation.

Originality of the thesis

Due to the originality of the thesis, several publications related to the research work have been produced. The following part lists the aforementioned papers in a chronological order:

- Habibzadeh Boukani, H, M Viens, SA Tahan et M Gagnon. 2014. « On the performance of nondestructive testing methods in the hydroelectric turbine industry ». In *IOP Conference Series: Earth and Environmental Science*. (Montreal, Canada). Vol. 22, p. 012018. IOP Publishing.
- Habibzadeh Boukani, Hamid, Samir Mourad Chentouf, Martin Viens, Antoine Tahan et Martin Gagnon. 2015. « The effect of martensitic stainless steel microstructure on the ultrasonic inspection of turbine runner joints ». In *AIP Conference Proceedings*. Vol. 1650, p. 909-916. AIP Publishing.
- Habibzadeh Boukani, Hamid, Demartonne Ramos França, Martin Viens, Antoine Tahan et Martin Gagnon. 2017. « Influence of the microstructure of hydraulic turbine runner on ultrasonic inspection ». *submitted to the International Journal of Microstructure and Materials Properties*.
- Habibzadeh Boukani, Hamid, Martin Viens, Antoine Tahan et Martin Gagnon. 2017. « Ultrasonic inspection of martensitic stainless steels in hydroelectric turbine runners: tempering austenite effect on the longitudinal wave inspection ». *submitted to the journal of NDT & E International*.
- Habibzadeh Boukani, Hamid, Martin Viens, Antoine Tahan et Martin Gagnon. 2017. « Case study on the integrity and nondestructive inspection of flux-cored arc welded joints of Francis turbine runners ». *submitted to the International Journal of Advanced Manufacturing Technology*.

RECOMMENDATIONS

The following paragraphs summarize some perspectives for the continuation of the current study and future research topics. These perspectives are classified in two categories including short-term and long term perspectives.

Short-term plans could be summarized as follows:

- By studying the currently applied NDT methods, it was found that due to some constraints, imposed by the runner geometry and inspection limitations, there are blind zones of inspection where the welded joint is not accessible to the inspection method. Therefore, in order to cover a larger zone in the weld region and to obtain a higher sensitivity, it is required to either develop new inspection methods or add some complementary NDT methods. As a matter of fact, since risk assessment programs are migrating from the conventional safe-life criteria toward the damage tolerant criteria, acquisition of more accurate data on the flaw characteristics in a larger zone in the material seems to be essential.
- The study on the blind zones of inspection could proceed by discretizing the runner joint and verifying if there is any overlap between these blind zones and the joint hot spots where the dynamic service loads are significantly high. A clear knowledge about the overlapped zones is desirable in order to determine which blind zones are worth additional investment in terms of time and money.
- Notwithstanding the findings of the current study, we have not, however, been able to answer all the questions generated during the fulfilment of this research. In chapter 2 and 3, the correlation between the microstructure and the acoustic properties of the two widely used steel grades were characterized. However in order to generate the POD data at lower time and labour prices, the findings of this study should be combined with complementary data on the characteristics and POO of common flaws in runner joints and consequently they should be inserted in commercially available modelling software to obtain model-based reliability data.

- Another important challenge to be addressed in future works is the detection of potential cold cracks located normal to the weld axis. According to the previous studies (Thibault *et al.*, 2009; Thibault *et al.*, 2010), the direction of the highest tensile residual stresses in the welded joint of martensitic stainless steel runners could promote the occurrence of such cold cracks. However, since our nondestructive and destructive tests have not revealed the presence of such transversal cracks, it is strongly recommended to carry out further investigations on a larger number of samples.
- Concerning the detectability of the aforementioned cold cracks, the currently used NDT methods are not appropriately designed for an optimized detection. However, using 2D linear PA transducers could be a solution since by electronically rotating the beam relative to the central axis of the probe, the cracks oriented normal to the weld axis could be more optimally targeted.

The subsequent paragraphs provide a summary of the long-term perspectives:

- In the design phase of hydraulic turbine runners, some more fundamental steps may be accounted for in order to improve the accessibility of NDT methods to the joints. In other words, apart from all the requirements already considered for the design of runners, it might also be necessary to take into account "design for inspection". Erhard and Otremba (Erhard & Otremba, 2014) emphasized on the importance of appropriate component design in fracture mechanics-based assessments in order to guarantee optimized inspections. In fact, since the fracture mechanics methods are more extensively adopted in the hydraulic turbine industry, more accurate inspection results are required to be incorporated in the life estimation models; thus, if all the critical flaws are not reliably detected and characterized due to the lack of access, either a nonessential production halt or a catastrophic failure may occur as a result of disregarding the real integrity conditions in the inaccessible area.
- Some ultrasonic inspection configurations (e.g. welded joints of austenitic stainless steel pipes, joints with single-sided access, etc.) suffer from significant limitations on their second half-skip access due to either high ultrasonic attenuation coefficient or

particular orientation of targeted flaws. For such applications, dual matrix array probes with transmission/reception longitudinal configuration (DMA TRL) have been previously recommended particularly to target the near surface flaws (Dheeraj, Khaja, & Mohsin, 2016; Lamarre, 2016). This configuration with special design for the runner geometry could be evaluated since the complex geometry of the blades could cause difficulties in accessing runner's joint on the second half-skip. Moreover, this configuration provides the possibility of focusing at different depths and electronically skewing the ultrasonic beam.

- Despite all the aforementioned actions, some blind zones in the runner welded joints may still be inaccessible to the NDT methods. Therefore, it is essential to initiate a large-scale quantitative study on the POO of different flaws in the welded joints of runners. In fact in the life estimation models, the zones covered by NDT will be evaluated using the combination of POD and POO data whereas the blind zones of inspection are assessed using only POO data. The latter is attributed to the fact that flaw detection is not possible in the blind zones and hence the POD concept is not anymore valid in these zones. This approach will estimate the remaining life based on the real condition of each zone.
- Moreover, it should be noted that the acoustic properties of materials in any part of the weld zone (including heat affected zone and fusion zone) would be differently affected since the joint undergoes complex thermal cycles during the welding process. It is recommended to investigate how the resulting inhomogeneity in ultrasonic attenuation, velocity, and backscattering noise could influence the capability of ultrasonic methods in flaw detection and localization.
- Once the preceding is done, a significant improvement could be achieved in the modelling approach through optimizing the noise modelled in CIVA. In other words, in future works the material could be defined as different zones possessing different acoustic characteristics and thus a more realistic inspection model could be obtained.
- If manual inspections are replaced with automated ones, more improvement could be introduced in the localization and sizing capability of ultrasonic methods. This could be achieved by developing post-processing techniques, such as synthetic aperture

focusing technique (SAFT), for the analysis of the automated inspection outcome. These post-processing techniques can significantly increase the resolution (not sensitivity) of acquired results (Nanekar, Jothilakshmi, Kumar, & Jayakumar, 2017; Zerbst, Heckel, & Carboni, 2016).

APPENDIX I

THE EFFECT OF MARTENSITIC STAINLESS STEEL MICROSTRUCTURE ON THE ULTRASONIC INSPECTION OF TURBINE RUNNER JOINTS

41st Annual Review of Progress in Quantitative Nondestructive Evaluation (QNDE) 2014
July 20-25, 2014, Boise, Idaho
AIP Conference Proceedings, Vol. 1650, No. 1, pp. 909-916, edited by Dale E. Chimenti, and Leonard J. Bond, American Institute of Physics, AIP Publishing

H. Habibzadeh Boukani [a], S. Mourad Chentouf [a], M. Viens [a], A. Tahan [a], M. Gagnon [b]

[a]École de technologie supérieure (ÉTS); Montréal, Québec, Canada
[b]Institut de recherche d'Hydro-Québec (IREQ); Varennes, Québec, Canada.

Abstract. Martensitic stainless steel runners are widely used in the hydroelectric turbine industry because of their good mechanical properties, cavitation and corrosion resistance. The high downtime cost and limited in-service inspection possibility of these turbine runners increase the need for accurate fatigue models to estimate the life of these equipment. One of the key inputs of these models is the distribution of flaw size and their location near highly stressed area. The critical area is generally located near the welded joint and flaw sizes are estimated using the outcome of nondestructive inspection. In such case, more reliable NDT results will lead to less uncertainty in the life estimation and hence unfavorable consequences, such as unexpected failure during service or non-essential down time for unnecessary inspections, are avoided. Turbine runner welded joints are inspected using ultrasonic refracted shear waves. Considering the dependence of the refracted angle to the shear wave velocity in the material as well as the role of this angle in the precision of defects' localization, the martensitic microstructure effect on sound wave velocity needs to be accurately known. Furthermore, attenuation coefficient, which affects reflected signal amplitude, is an essential data for the evaluation of defect size which is also dependent on microstructure. In this context, dependence of ultrasonic shear wave properties on

metallurgical characteristics of martensitic stainless steel was studied. Our objective is to obtain better POD from a more accurate characterization of received indications.

APPENDIX II

ON THE PERFORMANCE OF NONDESTRUCTIVE TESTING METHODS IN THE HYDROELECTRIC TURBINE INDUSTRY

27th IAHR Symposium Hydraulic Machinery and Systems
September 22-26, 2014, Montréal, Canada
IOP Conference Series: Earth and Environmental Science, Vol. 22, No. 1, p. 012018, IOP Publishing

H Habibzadeh Boukani [a], M Viens [a], S A Tahan [a] and M Gagnon [b]

[a] École de technologie supérieure (ÉTS), Montréal, Québec, Canada
[b] Institut de recherche d'Hydro-Québec (IREQ), Varennes, Québec, Canada

Abstract. Welded joints of turbine runners are one of the most critical parts of Francis turbines due to the presence of welding discontinuity and high stress. Because of thermal cycles, solidification, cooling distortion and residual stresses, welded joints always include discontinuities of different types and sizes. Some specific parameters will limit welding flaw dimensions in some or all direction based on the joint geometry, material and welding procedure. If discontinuities of critical size remain undetected, fatigue cracks might initiate and propagate in these zones because of dynamic in-service stresses leading to high repair costs and long down times. Therefore, reliable NDT methods and good knowledge of the probability of occurrence of welding flaws is important for fatigue life estimations. Every NDT method has its weaknesses; therefore, even after meticulous inspections it is likely for some discontinuities of critical sizes to remain in the welded joint. Our objective is to clarify the probability of detection and occurrence of different types of welding flaws in hydroelectric turbine runners. Furthermore, an overview of current nondestructive inspection methods and their capability in characterizing flaw dimensions will be discussed. Finally, advanced NDT techniques, for the characterization of welded joints integrity, will be proposed.

BIBLIOGRAPHY

Achenbach, J. (2000). « Quantitative nondestructive evaluation ». *International Journal of Solids and Structures,* vol. 37, nº 1, p. 13-27. doi: 10.1016/S0020-7683(99)00074-8

Adamkowski, A. (2009). « Problems of assessing technical state, strength and lifetime of hydraulic turbine flow system components ». In *R&D Actors Network Meeting*. (Gdansk, Poland, September 10-11th, 2009).

Altamura, A., & Beretta, S. (2012). « Reliability assessment of hydraulic cylinders considering service loads and flaw distribution ». *International Journal of Pressure Vessels and Piping,* vol. 96, p. 76-88. doi: 10.1016/j.ijpvp.2012.07.006

Amrei, M. M., Monajati, H., Thibault, D., Verreman, Y. & Bocher, P. (2016). « Effects of various post-weld heat treatments on austenite and carbide formation in a 13Cr4Ni steel multipass weld ». *Metallography, Microstructure, and Analysis,* vol. 5, nº 1, p. 50-61. doi: 10.1007/s13632-015-0251-z

Amrei, M. M., Verreman, Y., Bridier, F., Thibault, D. & Bocher, P. (2015). « Microstructure characterization of single and multipass 13Cr4Ni steel welded joints ». *Metallography, Microstructure, and Analysis,* vol. 4, nº 3, p. 207-218. doi: 10.1007/s13632-015-0202-8

Annis, C. (2009). *Nondestructive evaluation system reliability assessment, MIL-HDBK-1823A*. U.S. Department of Defense.

Annis, C. (2015). *Statistical best-practices for building Probability of Detection (POD) models.*(Version 4.2.6). < http://StatisticalEngineering.com/mh1823/ >.

Arivazhagan, B., & Kamaraj, M. (2011). « A study on factors influencing toughness of basic flux-cored weld of modified 9Cr-1Mo steel ». *Journal of materials engineering and performance,* vol. 20, nº 7, p. 1188-1195. doi: 10.1007/s11665-010-9757-3

Arivazhagan, B., Sundaresan, S. & Kamaraj, M. (2008). « Effect of TIG arc surface melting process on weld metal toughness of modified 9Cr-1Mo (P91) steel ». *Materials Letters,* vol. 62, nº 17, p. 2817-2820. doi: 10.1016/j.matlet.2008.01.054

Arpin-Pont, J., Gagnon, M., Tahan, S., Coutu, A. & Thibault, D. (2012). « Strain gauge measurement uncertainties on hydraulic turbine runner blade ». In *IOP Conference Series: Earth and Environmental Science*. (Beijing, China) Vol. 15, p. 062042. IOP Publishing.

Bagaviev, A., & Ulbrich, A. (2004). « Life assessment of turbine components based on deterministic and probabilistic procedures ». *International Journal of Pressure Vessels and Piping,* vol. 81, nº 10-11, p. 855-859. doi: 10.1016/j.ijpvp.2004.07.003

Bauné, E., Bonnet, C. & Liu, S. (2000). « Reconsidering the basicity of a FCAW consumable-part 1: Solidified slag composition of a FCAW consumable as a basicity indicator ». *Welding Journal-New York-,* vol. 79, nº 3, p. 57-65

Bendat, J. S. (1991). *The Hilbert transform and applications to correlation measurements*. Bruel and Kjaer.

Bhadeshia, H., & Honeycombe, R. (2006). *Steels: microstructure and properties (3rd Edition)*. Elsevier, 360 p.

Bilmes, P., Llorente, C. & Ipiña, J. P. (2000). « Toughness and microstructure of 13Cr4NiMo high-strength steel welds ». *Journal of materials engineering and performance,* vol. 9, nº 6, p. 609-615. doi: 10.1361/105994900770345458

Bilmes, P., Llorente, C., Méndez, C. & Gervasi, C. (2009). « Microstructure, heat treatment and pitting corrosion of 13CrNiMo plate and weld metals ». *Corrosion Science,* vol. 51, nº 4, p. 876-881. doi: 10.1016/j.corsci.2009.01.018

Bilmes, P., Solari, M. & Llorente, C. (2001). « Characteristics and effects of austenite resulting from tempering of 13Cr–NiMo martensitic steel weld metals ». *Materials characterization,* vol. 46, nº 4, p. 285-296. doi: 10.1016/S1044-5803(00)00099-1

Blitz, J., & Simpson, G. (1995). *Ultrasonic methods of non-destructive testing*, 2. Coll. « Non-Destructive Evaluation ». Springer Science & Business Media, 264 p.

Bouda, A. B., Benchaala, A. & Alem, K. (2000). « Ultrasonic characterization of materials hardness ». *Ultrasonics,* vol. 38, nº 1, p. 224-227. doi: 10.1016/S0041-624X(99)00081-5

Boyd-Lee, A., Harrison, G. & Henderson, M. (2001). « Evaluation of standard life assessment procedures and life extension methodologies for fracture-critical components ». *International Journal of Fatigue,* vol. 23, p. 11-19. doi: 10.1016/S0142-1123(01)00116-5

Bray, D. E., & Stanley, R. K. (1997). *Nondestructive evaluation: a tool in design, manufacturing and service*, Revised Edition. Boca Raton: CRC Press, 586 p. doi: 10.1016/S0963-8695(97)00037-6

Calmon, P., Mahaut, S., Chatillon, S. & Raillon, R. (2006). « CIVA: An expertise platform for simulation and processing NDT data ». *Ultrasonics,* vol. 44, p. e975-e979. doi: 10.1016/j.ultras.2006.05.218

Caron, J. L., & Sowards, J. W. (2014). « Weldability of nickel-base alloys ». In *Comprehensive Materials Processing*. Vol. 6, p. 151-179. Elsevier Ltd. doi: 10.1016/B978-0-08-096532-1.00615-4

Carreón, H., Barrera, G., Natividad, C., Salazar, M. & Contreras, A. (2016). « Relation between hardness and ultrasonic velocity on pipeline steel welded joints ». *Nondestructive Testing and Evaluation,* vol. 31, nº 2, p. 97-108. doi: 10.1080/10589759.2015.1074231

Carvalho, A., Rebello, J., Silva, R. & Sagrilo, L. (2006). « Reliability of the manual and automatic ultrasonic technique in the detection of pipe weld defects ». *Insight-Non-Destructive Testing and Condition Monitoring,* vol. 48, nº 11, p. 649-654. doi: 10.1784/insi.2006.48.11.649

Carvalho, A., Rebello, J., Souza, M., Sagrilo, L. & Soares, S. (2008). « Reliability of non-destructive test techniques in the inspection of pipelines used in the oil industry ». *International Journal of Pressure Vessels and Piping,* vol. 85, nº 11, p. 745-751. doi: 10.1016/j.ijpvp.2008.05.001

Chatillon, S., Poidevin, C., Gengembre, N. & Lhémery, A. (2003). « Simplified modeling of backscattered noise and attenuation phenomena for quantitative performance demonstration of UT methods ». In *AIP Conference Proceedings*. p. 93-100. IOP Institute of Physics Publishing LTD.

Coutu, A., Proulx, D., Coulson, S. & Demers, A. (2004). « Dynamic assessment of hydraulic turbines ». In *Proceedings of HydroVision*. p. 16-20.

da Silva, R. R., & de Padua, G. X. (2012). « Nondestructive Inspection Reliability: State of the Art ». In *Nondestructive Testing Methods and New Applications*. InTech. doi: 10.5772/37112

Dheeraj, P., Khaja, M. & Mohsin, I. (2016). « Advanced phased array technology application for single-sided access weld inspection ». *Insight-Non-Destructive Testing and Condition Monitoring,* vol. 58, nº 11, p. 585-595. doi: 10.1784/insi.2016.58.11.585

Dib, G., Larche, M., Diaz, A. A., Crawford, S. L., Prowant, M. S., Anderson, M. T., . . . Bond, L. J. (2016). « Experimental validation of ultrasonic NDE simulation software ». In *AIP Conference Proceedings*. Vol. 1706, p. 170004. AIP Publishing.

Ditchburn, R., & Ibrahim, M. (2009). *Ultrasonic phased arrays for the inspection of thick-section welds*. Victoria, Australia Australian Department of Defense Science and Technology Organization. < http://www.dtic.mil/dtic/tr/fulltext/u2/a510070.pdf >.

El Rayes, M. M., El-Danaf, E. A. & Almajid, A. A. (2015). « Characterization and correlation of mechanical, microstructural and ultrasonic properties of power plant steel ». *Materials characterization,* vol. 100, p. 120-134. doi: 10.1016/j.matchar.2014.11.034

Ensminger, D., & Bond, L. J. (2011). *Ultrasonics: fundamentals, technologies, and applications*, 3rd Edition. CRC press, 765 p. doi: 10.1201/b11173

Erhard, A., & Otremba, F. (2014). « Nondestructive testing and fracture mechanics ». In *5th International CANDU In-Service Inspection Workshop in conjunction with the NDT in Canada 2014 Conference (Hrsg.)*. (Toronto, Canada).

Feuilly, N., Dupond, O., Chassignole, B., Moysan, J. & Comeloup, G. (2009). « Relation between ultrasonic backscattering and microstructure for polycrystalline materials ». In *35th Annual Review of Progress in Quantitative Nondestructive Evaluation*. (Chicago, USA). Vol. 1096, p. 1216-1223. AIP Publishing.

Fowler, K. A., Elfbaum, G. M., Smith, K. A. & Nelligan, T. J. (1996). « Theory and application of precision ultrasonic thickness gauging ». *Insight,* vol. 38, n^{o} 8, p. 582-587

Freitas, V. L. d. A., Albuquerque, V. H. C. d., Silva, E. d. M., Silva, A. A. & Tavares, J. M. R. (2010). « Nondestructive characterization of microstructures and determination of elastic properties in plain carbon steel using ultrasonic measurements ». *Materials Science and Engineering: A,* vol. 527, n^{o} 16, p. 4431-4437. doi: 10.1016/j.msea.2010.03.090

Frunzăverde, D., Muntean, S., Mărginean, G., Campian, V., Marşavina, L., Terzi, R. & Şerban, V. (2010). « Failure analysis of a Francis turbine runner ». In *IOP Conference Series: Earth and Environmental Science*. (Timişoara, Romania) Vol. 12, p. 012115. IOP Publishing.

Gagnon, M., Tahan, A., Bocher, P. & Thibault, D. (2012a). « A probabilistic model for the onset of High Cycle Fatigue (HCF) crack propagation: application to hydroelectric turbine runner ». *International Journal of Fatigue*. doi: 10.1016/j.ijfatigue.2012.09.011

Gagnon, M., Tahan, A., Bocher, P. & Thibault, D. (2013). « On the fatigue reliability of hydroelectric Francis runners ». *Procedia Engineering,* vol. 66, p. 565-574. doi: 10.1016/j.proeng.2013.12.108

Gagnon, M., Tahan, A., Bocher, P. & Thibault, D. (2014). « Influence of load spectrum assumptions on the expected reliability of hydroelectric turbines: A case study ». *Structural Safety,* vol. 50, p. 1-8. doi: 10.1016/j.strusafe.2014.03.008

Gagnon, M., Tahan, S., Bocher, P. & Thibault, D. (2010). « Impact of startup scheme on Francis runner life expectancy ». In *IOP Conference Series: Earth and Environmental Science*. (Timisoara, Romania) Vol. 12, p. 012107. IOP Publishing.

Gagnon, M., Tahan, S., Bocher, P. & Thibault, D. (2012b). « The role of high cycle fatigue (HCF) onset in Francis runner reliability ». In *IOP Conference Series: Earth and Environmental Science*. (Beijing, China) Vol. 15, p. 022005. IOP Publishing.

Gagnon, M., Tahan, S. A. & Coutu, A. (2009). « Uncertainty in operational modal analysis of hydraulic turbine components ». *International Journal of Fluid Machinery and Systems,* vol. 2, nº 4, p. 278-285. doi: 10.5293/IJFMS.2009.2.4.278

Georgiou, G. A. (2006). *Probability of Detection (POD) curves: derivation, applications and limitations*. Coll. « Jacobi Consulting Limited Health and Safety Executive Research Report ». < http://www.hse.gov.uk/research/rrpdf/rr454.pdf >.

Ginzel, E. A., Thomson, R. & Ginzel, R. K. (2011). « A qualification process for phased-array UT using DNV RP-F118 guidelines ».

Godin, S. (2014). « Effet d'un enrichissement en nickel sur la stabilité mécanique de l'austénite de réversion lorsque soumise à de la fatigue oligocyclique ». École de technologie supérieure. < http://espace.etsmtl.ca/id/eprint/1305 >.

Guo, N., Lin, S., Gao, C., Fan, C. & Yang, C. (2013). « Study on elimination of interlayer defects in horizontal joints made by rotating arc narrow gap welding ». *Science and Technology of Welding & Joining,* vol. 14, nº 6, p. 584-588. doi: 10.1179/136217109X456942

Guo, Y. (2003). « Effects of material microstructure and surface geometry on ultrasonic scattering and flaw detection ». PhD Thesis. Iowa State University, 160 p. < http://lib.dr.iastate.edu/rtd/1435/ >.

Gür, C., & Tuncer, B. (2004). « Investigating the microstructure-ultrasonic property relationships in steels ». In *16th World Conference on Nondestructive Testing*. (Montreal, Canada).

Gür, C. H., & Cam, I. (2007). « Comparison of magnetic Barkhausen noise and ultrasonic velocity measurements for microstructure evaluation of SAE 1040 and SAE 4140 steels ». *Materials characterization,* vol. 58, nº 5, p. 447-454. doi: 10.1016/j.matchar.2006.06.008

Gür, C. H., & Tuncer, B. O. (2005). « Characterization of microstructural phases of steels by sound velocity measurement ». *Materials characterization,* vol. 55, nº 2, p. 160-166. doi: 10.1016/j.matchar.2005.05.002

Habibzadeh Boukani, H., Chentouf, S. M., Viens, M., Tahan, A. & Gagnon, M. (2015). « The effect of martensitic stainless steel microstructure on the ultrasonic inspection of turbine runner joints ». In *41st Annual Review of Progress in Quantitative Nondestructive Evaluation*. (Boise, Idaho). Vol. 1650, p. 909-916. AIP Publishing.

Habibzadeh Boukani, H., Viens, M., Tahan, S. & Gagnon, M. (2014). « On the performance of nondestructive testing methods in the hydroelectric turbine industry ». In *IOP Conference Series: Earth and Environmental Science*. (Montreal, Canada). Vol. 22, p. 012018. IOP Publishing.

Habibzadeh Boukani, H. V., Martin
Tahan, Souheil-Antoine
Gagnon, Martin. (2018). « Case study on the integrity and nondestructive inspection of flux-cored arc welded joints of Francis turbine runners ». doi: Manuscript submitted for publication

Hakl, J., Bielak, O. & Vlasák, T. (2001). « Residual life assessment of steam turbine casing containing crack defect ». *International Journal of Pressure Vessels and Piping,* vol. 78, nº 11-12, p. 977-984. doi: 10.1016/S0308-0161(01)00112-0

Hirone, T., & Kamigaki, K. (1958). *Attenuation of the ultrasonic waves in metals. II: Stainless steel*. Coll. « Ser. A, Physics, chemistry and metallurgy ». Science reports of the Research Institutes: Tohoku University, 276-282 p.

Howard, P., Copley, D. & Gilmore, R. (1995). « A Signal-to-noise ratio comparison of ultrasonic transducers for C-scan imaging in titanium ». In *Review of Progress in Quantitative Nondestructive Evaluation*. p. 2113-2120. Springer.

Howard, S. M. (2006). « Ellingham diagrams ». *SD School of Mines and Technology,*

Hsu, C.-H., Teng, H.-Y. & Chen, Y.-J. (2004). « Relationship between ultrasonic characteristics and mechanical properties of tempered martensitic stainless steel ». *Journal of materials engineering and performance,* vol. 13, nº 5, p. 593-599. doi: 10.1361/15477020420828

Huth, H. J. (2005). « Fatigue design of hydraulic turbine runners ». Norwegian University of Science and Technology. < http://hdl.handle.net/11250/241313 >.

İşleyici, U. (2005). « Effect of surface roughness on ultrasonic testing ». Middle East Technical University, 115 p.

Iwamoto, N. (1983). « Structure of slag (XI): Role of TiO_2 in slag ». *Transactions of JWRI,* vol. 12, nº 1, p. 131-141

Jenson, F., Mahaut, S., Calmon, P. & Poidevin, C. (2010). « Simulation based POD evaluation of NDI techniques ». In *10 th European conference on non-destructive testing*. (Moscow, Russia).

Katchadjian, P. (2004). « Practical applications of ultrasonic testing in nuclear and conventional industry ». *Insight-Non-Destructive Testing and Condition Monitoring,* vol. 46, nº 12, p. 754-757. doi: 10.1784/insi.46.12.754.54494

Kim, J. W., Kim, S. k., Kim, D. s., Lee, Y. d. & Yang, P. k. (1996). « Formation mechanism of Ca-Si-Al-Mg-Ti-O inclusions in type 304 stainless steel ». *ISIJ International,* vol. 36, nº Suppl, p. S140-S143. doi: 10.2355/isijinternational.36.Suppl_S140

Kino, G. S. (1987). *Acoustic waves: devices, imaging, and analog signal processing*, 107. Prentice-Hall Englewood Cliffs N.J.

Kou, S. (2003). *Welding metallurgy*. John Wiley & Sons. doi: 10.1002/0471434027

Krauss, G. (2015). *Steels: processing, structure, and performance*, 2nd Edition. ASM International, 704 p.

Kruger, S. E., & Damm, E. B. (2006). « Monitoring austenite decomposition by ultrasonic velocity ». *Materials Science and Engineering: A,* vol. 425, nº 1, p. 238-243. doi: 10.1016/j.msea.2006.03.056

Kumar, A., Laha, K., Jayakumar, T., Rao, K. B. S. & Raj, B. (2002). « Comprehensive microstructural characterization in modified 9Cr-1Mo ferritic steel by ultrasonic measurements ». *Metallurgical and Materials Transactions A,* vol. 33, nº 6, p. 1617-1626. doi: 10.1007/s11661-002-0171-9

Kupperman, D. S., & Reimann, K. J. (1980). « Ultrasonic wave propagation and anisotropy in austenitic stainless steel weld metal ». *IEEE Transactions on Sonics and Ultrasonics,* vol. 27, nº 1, p. 7-14. doi: 10.1109/T-SU.1980.31137

Lamarre, A. (2016). « Improved inspection of CRA-clad pipe welds with accessible advanced ultrasonic phased-array technology ». In *19th World Conference on Non-Destructive Testing*. (Munich, Germany).

Lancaster, J. F. (1997). *Handbook of structural welding: processes, materials and methods used in the welding of major structures, pipelines and process plant*. Coll. « Woodhead Publishing Series in Welding and Other Joining Technologies ». Elsevier, 448 p.

Lin, L., Li, X. & Tan, J. (2004). « Comparison among ultrasonic velocity, attenuation and power spectra of different heat treatment transformation products in 38crmoal steel ».

Key Engineering Materials, vol. 270, p. 346-352. doi: 10.4028/www.scientific.net/KEM.270-273.346

Lin, L., Li, X. & Zhang, J. (2003). « Nondestructive differentiation of three transformation products in low alloy steel using two ultrasonic methods ». *Materials evaluation,* vol. 61, nº 4, p. 512-516

Lu, S., Fujii, H., Sugiyama, H., Tanaka, M. & Nogi, K. (2002). « Weld penetration and Marangoni convection with oxide fluxes in GTA welding ». *Materials Transactions,* vol. 43, nº 11, p. 2926-2931. doi: 10.2320/matertrans.43.2926

Ma, X., Wang, L., Liu, C. & Subramanian, S. (2012). « Microstructure and properties of 13Cr5Ni1Mo0. 025Nb0. 09V0. 06N super martensitic stainless steel ». *Materials Science and Engineering: A,* vol. 539, p. 271-279. doi: 10.1016/j.msea.2012.01.093

Matos, N. (2012). « Welding procedures specification for FCAW of wind towers ». Tecnico Lisboa.

Matzkanin, G. A., & Yolken, H. (2001). *Probability of detection (POD) for Nondestructive Evaluation (NDE)*. Austin TX: Nondestructive Testing Information Analysis Center. < http://www.dtic.mil/dtic/tr/fulltext/u2/a398282.pdf >.

Mirakhorli, F., Cao, X., Pham, X.-T., Wanjara, P. & Fihey, J.-L. (2016). « Hybrid laser-arc welding of 10-mm-thick cast martensitic stainless steel CA6NM: As-welded microstructure and mechanical properties ». *Metallurgical and Materials Transactions A*, p. 1-19. doi: 10.1007/s11661-016-3523-6

Mutlu, I., Oktay, E. & Ekinci, S. (2009). « Effect of grain size on the ultrasonic parameters in stainless steels ». *International Journal of Microstructure and Materials Properties,* vol. 4, nº 4, p. 423-435. doi: 10.1504/IJMMP.2009.031397

Mutlu, I., Oktay, E. & Ekinci, S. (2013). « Characterization of microstructure of H13 tool steel using ultrasonic measurements ». *Russian Journal of Nondestructive Testing,* vol. 49, nº 2, p. 112-120. doi: 10.1134/S106183091302006X

Nagy, P. B., & Adler, L. (1988). « Scattering induced attenuation of ultrasonic backscattering ». In *Review of Progress in Quantitative Nondestructive Evaluation*. Vol. 7B, p. 1263-1271. Springer.

Nanekar, P., Jothilakshmi, N., Kumar, A. & Jayakumar, T. (2017). « Sound beam focusing using phased array–SAFT technique ». *Insight-Non-Destructive Testing and Condition Monitoring,* vol. 59, nº 3, p. 129-137. doi: 10.1784/insi.2017.59.3.129

Nishiyama, Z. (2012). *Martensitic transformation*. Elsevier, 480 p.

Palanichamy, P., Joseph, A., Jayakumar, T. & Raj, B. (1995). « Ultrasonic velocity measurements for estimation of grain size in austenitic stainless steel ». *NDT & E International,* vol. 28, nº 3, p. 179-185. doi: 10.1016/0963-8695(95)00011-L

Palanichamy, P., Vasudevan, M., Jayakumar, T., Venugopal, S. & Raj, B. (2000). « Ultrasonic velocity measurements for characterizing the annealing behaviour of cold worked austenitic stainless steel ». *NDT & E International,* vol. 33, nº 4, p. 253-259. doi: 10.1016/S0963-8695(99)00047-X

Pamnani, R., Jayakumar, T., Vasudevan, M. & Sakthivel, T. (2016). « Investigations on the impact toughness of HSLA steel arc welded joints ». *Journal of Manufacturing Processes,* vol. 21, p. 75-86. doi: 10.1016/j.jmapro.2015.11.007

Papadakis, E. P. (1965). « Ultrasonic attenuation caused by scattering in polycrystalline metals ». *The Journal of the Acoustical Society of America,* vol. 37, nº 4, p. 711-717. doi: 10.1121/1.1909401

Papadakis, E. P. (1970). « Ultrasonic attenuation and velocity in SAE 52100 steel quenched from various temperatures ». *Metallurgical and Materials Transactions B,* vol. 1, nº 4, p. 1053-1057. doi: 10.1007/BF02811803

Papadakis, E. P. (1981). « Scattering in polycrystalline media ». In *Methods in Experimental Physics*. Vol. 19, p. 237-298. doi: 10.1016/S0076-695X(08)60336-1

Ploix, M.-A. (2006). « Étude de l'atténuation des ondes ultrasonores. Application au contrôle non destructif des soudures en acier inoxydable austénitique ». PhD Thesis. Institut National des Sciences Appliquées de Lyon, 144 p.

Quintana, M., McLane, J., Babu, S. & David, S. (2001). « Inclusion formation in self-shielded flux cored arc welds ». *Welding Journal-New York-,* vol. 80, nº 4, p. 98S-105S

Renshaw, J., Thigpen, B. & Breza, J. (2013). « MRP-227/228 component inspections supporting nuclear power plant license renewal ». *Energy Conversion and Management,* vol. 74, p. 569-573. doi: 10.1016/j.enconman.2013.03.042

Rihar, G., & Uran, M. (2006). « Lack of fusion characterisation of indications ». *Welding in the World,* vol. 50, nº 1-2, p. 35-39. doi: 10.1007/BF03266513

Rodrigues, C., Lorenzo, P., Sokolowski, A., Barbosa, C. & Rollo, J. (2007). « Titanium and molybdenum content in supermartensitic stainless steel ». *Materials Science and Engineering: A,* vol. 460-461, p. 149-152. doi: 10.1016/j.msea.2007.01.016

Sabourin, M., Thibault, D., Bouffard, D. A. & Levesque, M. (2010). « Hydraulic runner design method for lifetime ». *International Journal of Fluid Machinery and Systems,* vol. 3, nº 4, p. 301-308. doi: 10.5293/IJFMS.2010.3.4.301

Saeed, R., & Galybin, A. (2009). « Simplified model of the turbine runner blade ». *Engineering Failure Analysis,* vol. 16, nº 7, p. 2473-2484. doi: 10.1016/j.engfailanal.2009.04.012

Salvador, C., & Antunes, R. (2016). « FCAW repair welding cycles, HAZ microstructure and corrosion resistance of 2304 duplex stainless steel ». *Corrosion Engineering, Science and Technology,* vol. 51, nº 8, p. 573-580. doi: 10.1080/1478422X.2016.1166706

Saniie, J., & Bilgutay, N. M. (1986). « Quantitative grain size evaluation using ultrasonic backscattered echoes ». *The Journal of the Acoustical Society of America,* vol. 80, nº 6, p. 1816-1824. doi: 10.1121/1.394296

Saniie, J., Wang, T. & Bilgutay, N. M. (1988). « Statistical evaluation of backscattered ultrasonic grain signals ». *The Journal of the Acoustical Society of America,* vol. 84, nº 1, p. 400-408. doi: 10.1121/1.396944

Sarafan, S., Wanjara, P., Champliaud, H. & Thibault, D. (2015). « Characteristics of an autogenous single pass electron beam weld in thick gage CA6NM steel ». *The International Journal of Advanced Manufacturing Technology,* vol. 78, nº 9-12, p. 1523-1535. doi: 10.1007/s00170-014-6713-7

Sarkar, P., Meeker, W. Q., Thompson, R. B., Gray, T. A. & Junker, W. (1998). « Probability of Detection modeling for ultrasonic testing ». In *Review of Progress in Quantitative Nondestructive Evaluation*. Vol. 17b, p. 2045-2052. Springer. doi: 10.1007/978-1-4615-5339-7_265

Shull, P. J. (2002). *Nondestructive evaluation: theory, techniques, and applications*, 142. Coll. « Dekker Mechanical Engineering ». CRC Press. doi: 10.1201/9780203911068

Song, S.-J. (1991). « Ultrasonic flaw classification and sizing ». PhD Thesis. Iowa State University, Iowa State University, 199 p.

Starling, C. M. D., Modenesi, P. J. & Borba, T. M. D. (2011). « Bead characterization of FCAW of a rutilic fluxed core wire ». *Welding International,* vol. 25, nº 11, p. 825-837. doi: 10.1080/09507116.2010.527479

Stella, J., Cerezo, J. & Rodríguez, E. (2009). « Characterization of the sensitization degree in the AISI 304 stainless steel using spectral analysis and conventional ultrasonic techniques ». *NDT & E International,* vol. 42, nº 4, p. 267-274. doi: 10.1016/j.ndteint.2008.11.005

Suresh, S. (1998). *Fatigue of materials*. Cambridge university press. doi: 10.1017/CBO9780511806575

Svensson, L.-E. (1993). *Control of microstructures and properties in steel arc welds*, 1. Coll. « Materials Science & Technology ». CRC press, 256 p.

Thibault, D., Bocher, P. & Thomas, M. (2009). « Residual stress and microstructure in welds of 13% Cr–4% Ni martensitic stainless steel ». *Journal of Materials Processing Technology,* vol. 209, nº 4, p. 2195-2202. doi: 10.1016/j.jmatprotec.2008.05.005

Thibault, D., Bocher, P., Thomas, M., Gharghouri, M. & Côté, M. (2010). « Residual stress characterization in low transformation temperature 13% Cr–4% Ni stainless steel weld by neutron diffraction and the contour method ». *Materials Science and Engineering: A,* vol. 527, nº 23, p. 6205-6210. doi: 10.1016/j.msea.2010.06.035

Thibault, D., Bocher, P., Thomas, M., Lanteigne, J., Hovington, P. & Robichaud, P. (2011). « Reformed austenite transformation during fatigue crack propagation of 13% Cr–4% Ni stainless steel ». *Materials Science and Engineering: A,* vol. 528, nº 21, p. 6519-6526. doi: 10.1016/j.msea.2011.04.089

Thibault, D., Gagnon, M. & Godin, S. (2014). « Bridging the gap between metallurgy and fatigue reliability of hydraulic turbine runners ». In *IOP Conference Series: Earth and Environmental Science*. (Montreal, Canada). Vol. 22, p. 012019. IOP Publishing.

Thompson, R. B., & Thompson, D. O. (1985). « Ultrasonics in nondestructive evaluation ». *Proceedings of the IEEE,* vol. 73, nº 12, p. 1716-1755. doi: 10.1109/PROC.1985.13367

Tryon, R. G., Cruse, T. A. & Mahadevan, S. (1996). « Development of a reliability-based fatigue life model for gas turbine engine structures ». *Engineering fracture mechanics,* vol. 53, nº 5, p. 807-828. doi: 10.1016/0013-7944(95)00138-7

Tümer, M., & Yılmaz, R. (2016). « Characterization of microstructure, chemical composition, and toughness of a multipass welded joint of austenitic stainless steel AISI316L ». *The International Journal of Advanced Manufacturing Technology,* vol. 87, nº 9-12, p. 2567-2579. doi: 10.1007/s00170-016-8614-4

Vijayalakshmi, K., Muthupandi, V. & Jayachitra, R. (2011). « Influence of heat treatment on the microstructure, ultrasonic attenuation and hardness of SAF 2205 duplex stainless steel ». *Materials Science and Engineering: A,* vol. 529, nº 0, p. 447-451. doi: 10.1016/j.msea.2011.09.059

Wall, M., & Burch, S. (2000). « Worth of modelling for assessing the intrinsic capability of NDT ». In *15th World Conference on Nondestructive Testing*. (Roma, Italy, October 15-21).

Wall, M., Burch, S. & Lilley, J. (2009). « Human factors in POD modelling and use of trial data ». *Insight-Non-Destructive Testing and Condition Monitoring,* vol. 51, nº 10, p. 553-561. doi: 10.1784/insi.2009.51.10.553

Wang, Y. (2006). « Advanced statistical methods for analysis of NDE data ». PhD Thesis. Iowa State University.

Xiao, K., Shi, Y. K., Ma, Q. Z., Zhang, J. & Li, X. H. (2013). « The intelligent ultrasonic system for quality testing of weld connections in turbine runners ». *Advanced Materials Research,* vol. 774-776, p. 1543-1546. doi: 10.4028/www.scientific.net/AMR.774-776.1543

Yicheng, Z., Xiaohong, L., Jun, Z. & Hui, D. (2011). « Model based reliability analysis of PA ultrasonic testing for weld of hydro turbine runner ». *Procedia Engineering,* vol. 16, p. 832-839. doi: 10.1016/j.proeng.2011.08.1162

Zerbst, U., Heckel, T. & Carboni, M. (2016). « Non-destructive testing and fracture mechanics: A short discussion ». In *42nd Annual Review of Progress in Quantitative Nondestructive Evaluation*. (Minneapolis, Minnesota) Vol. 1706, p. 150002. AIP Publishing.

Zhang, J., Li, X.-h., Shi, Y.-k. & Liang, L.-s. (2014). « Phased array ultrasonic inspection of embedded defects in hydropower turbine runner welds ». *Insight-Non-Destructive Testing and Condition Monitoring,* vol. 56, nº 7, p. 390-394. doi: 10.1784/insi.2014.56.7.390

Zhao, L., & Rudlin, J. (2014). « Development of an advanced ultrasonic inspection tool for rapid volumetric examination of aluminothermic rail welds ». In *IEEE Far East Forum on Nondestructive Evaluation/Testing (FENDT)*. p. 354-357. IEEE.

Zhu, Z., Fan, K., Liu, H. & Ma, G. (2016). « Characteristics of short-circuit behaviour and its influencing factors in self-shielded flux-cored arc welding ». *Science and Technology of Welding and Joining,* vol. 21, nº 2, p. 91-98. doi: 10.1179/1362171815Y.0000000069